School of Earth and Planetary Sciences

Undifferenced and Uncombined GNSS Time Transfer and its Space Applications

Xiaolong Mi

0000-0003-2950-3472

This thesis is presented for the Degree of
Doctor of Philosophy
of
Curtin University

July 2023

Declaration

To the best of my knowledge and belief this thesis contains no material previously published by any other person except where due acknowledgment has been made. This thesis contains no material which has been accepted for the award of any other degree or diploma in any university.

Xiaolong Mi

5 July 2023

Abstract

Time transfer is an essential element for a range of scientific research and industrial applications, including high-resolution radio astronomy, financial services, space missions, transport, precision measurement, and relativistic geodesy. Global Navigation Satellite System (GNSS) has emerged as a competitive solution for time transfer due to its low cost and high precision. However, with the emergence of optical clocks, the precision requirements of time transfer techniques have increased, posing a challenge for current GNSS techniques. Therefore, improving the performance of GNSS time transfer models and algorithms has become a current research focus. This thesis aims to develop new models and algorithms to assess the potential role of GNSS in future time transfer systems. To this end, new GNSS time transfer methods are developed in this research based on the undifferenced and uncombined (UDUC) observations, which offer several advantages. Special attention has been paid to the integer ambiguity resolution (IAR), the key to exploiting phase observation information in time transfer. UDUC GNSS time transfer with IAR is proposed for short-, medium-, and long-baselines considering different ionospheric constraints. The feasibility of the proposed model is supported by characterizing the role of IAR in improving the precision of time transfer. Furthermore, a UDUC time transfer model with satellite clocks estimated, not externally obtained, is proposed to address the impact of precise satellite clock products on time transfer. Validations demonstrate that the frequency stability in the low-mid 10^{-17} range for averaging times within one day is achievable with integer ambiguities resolved and satellite clocks estimated. The time-invariant assumption of receiver code bias is essential for accurately implementing of GNSS time transfer, but it is difficult to achieve in practice. The variation characteristics of the receiver code bias, which can reach the nanosecond level, have been proven, thereby highlighting the necessity of considering receiver code bias variations in time transfer. Accordingly, a UDUC GNSS time transfer method is proposed considering receiver code bias variations. This approach solves the impacts of receiver code bias variations on time transfer from the algorithm level rather than attempting to control the bias variations from the receiver, antenna, and the cables connecting them. Given that building a positioning, navigation, and timing (PNT) system based on low-orbit (LEO) satellites is a current development trend in space science, the proposed UDUC GNSS time transfer theory is extended to space applications. Since precise orbit determination (POD) is the premise of any space application, the UDUC method with IAR for absolute and relative POD is proposed. With the UDUC algorithm and IAR, the proposed model achieves a 2-4 cm consistency in 3D

compared to reference orbits. Consequently, the application of the UDUC GNSS time transfer in LEO satellites is explored, providing a preliminary verification for establishing of LEO-based space-time reference in the future.

Acknowledgements

I am overwhelmed with deep gratitude for my supervisor, Professor Ahmed El-Mowafy, for his unwavering support, scientific discussions, and motivation throughout my PhD research. He has been an exceptional mentor, providing invaluable guidance and teaching me how to effectively balance my research and personal life. With his unwavering assistance, my PhD work and stay in Australia surpassed my wildest expectations.

I am indebted to my supervisor, Professor Peter Teunissen, for his invaluable advice and stimulating discussions over the years. His remarkable scientific insights and expertise in geodesy and GNSS have been an inspiration to me. I deeply admire him for his unwavering dedication to scientific excellence and for being a source of motivation throughout my academic journey.

I would like to extend my heartfelt appreciation to Professor Kan Wang for her invaluable assistance and support. Her exceptional intellect, tireless work ethic, and warm demeanour have made our scientific discussions a pleasure. I am grateful to have had the privilege of working alongside such an exceptional scientist and person.

The funding received from the Australian Research Council (Discovery Project - Grant No: DP 190102444) and Curtin University to fund my PhD research program is acknowledged. I am deeply grateful for the unwavering support of my colleagues at the Curtin GNSS-SPAN, whose assistance has been invaluable. Furthermore, I would like to thank my friends from Curtin University for being my constant companions on this scientific research and life journey.

Special thanks are due to my friends and colleagues at the Chinese Academy of Sciences, particularly to Professor Yunbin Yuan and Professor Baocheng Zhang for their unwavering support and encouragement. Their kindness and unwavering support have been a beacon of hope throughout my academic journey.

Finally, I would like to express my heartfelt gratitude to my family for their constant encouragement and support throughout my life's various stages. Their unwavering love and support have been my greatest source of strength, and I cannot thank them enough for their selfless dedication and love.

Acknowledgement of Country

We acknowledge that Curtin University works across hundreds of traditional lands and custodial groups in Australia and with First Nations people around the globe. We wish to pay our deepest respects to their ancestors and members of their communities, past, and present, and to their emerging leaders. Our passion and commitment to working with all Australians and peoples from across the world, including our First Nations peoples, are at the core of the work we do, reflective of our institutions' values and commitment to our role as leaders in the reconciliation space in Australia.

List of Publications

This thesis by compilation comprises four first-author peer-reviewed papers and two chapters discussing the model modifications and applications during this PhD. The copyright authorizations, and author contribution declarations are provided in Appendix A, and B, respectively.

- **Mi, X.,** Zhang, B., El-Mowafy, A., Wang, K., & Yuan, Y. (2023). Undifferenced and uncombined GNSS time and frequency transfer with integer ambiguity resolution. Journal of Geodesy, 97(2), 13. https://doi.org/10.1007/s00190-022-01689-8
- **Mi, X.,** Zhang, B., El-Mowafy, A., Wang, K., & Yuan, Y. (2023). On the potential of undifferenced and uncombined GNSS time and frequency transfer with integer ambiguity resolution and satellite clocks estimated. GPS Solutions, 27(1), 25. https://doi.org/10.1007/s10291-022-01363-8
- **Mi, X.,** Sheng, C., El-Mowafy, A., & Zhang, B. (2021). Characteristics of receiver-related biases between BDS-3 and BDS-2 for five frequencies including inter-system biases, differential code biases, and differential phase biases. GPS Solutions, 25(3), 113. https://doi.org/10.1007/s10291-021-01151-w
- **Mi, X.,** Allahvirdi-Zadeh, A., El-Mowafy, A., Huang, Z., Wang, K., Zhang, B., & Yuan, Y. (2023). Absolute and relative POD of LEO satellites in formation flying: Undifferenced and uncombined approach. Advances in Space Research, 72(4), 1070-1080. https://doi.org/10.1016/j.asr.2023.05.024

Table of Contents

List of Figures

As the thesis primarily comprises of publications divided into chapters, with figure numbers commencing at 1 in each chapter, please find below the list of figures arranged by their respective chapters.

Chapter 1

Chapter 2

Chapter 3

Chapter 4

Chapter 5

Chapter 6

Chapter 7

List of Tables

As the thesis primarily comprises of publications divided into chapters, with table numbers commencing at 1 in each chapter, please find below the list of tables arranged by their respective chapters.

Chapter 2

Chapter 3

Chapter 4

Chapter 5

Chapter 6

List of Abbreviations

APM	Innovation Academy for Precision Measurement Science and Technology
AV	All in View
BDS	BeiDou Navigation Satellite System
BIPM	Bureau international des poids et mesures
CDMA	Code Division Multiple Access
CNES	Centre National d’Etudes Spatiales
CODE	Centre for Orbit Determination in Europe
CV	Common View
DCB	Differential Code Bias
DD	Double Differenced
DFT	Discrete Fourier Transform
DOY	Days of Year
DPB	Differential Phase Bias
DSC	Decoupled Satellite Clock
DIA	Detection, Identification, and Adaptation
FCB	Fractional Cycle Bias
FFT	Fast Fourier Transform
GEO	Geostationary Earth Orbit
GF	Geometry-Free
GLONASS	Globalnaya Navigatsionnaya Sputnikovaya Sistema
GNSS	Global Navigation Satellite System
GPS	Global Positioning System
GPST	GPS Time

LEO	Low-Earth Orbit
IAR	Integer Ambiguity Resolution
IF	Ionosphere-Free
IGS	International GNSS Service
IGSO	Inclined Geosynchronous Orbit
IPPP	Integer Precise Point Positioning
IRC	Integer Recovery Clock
ISB	Integer-System Bias
MDEV	Modified Allan Deviation
MEO	Medium Earth Orbit
PCO	Phase Centre Offset
PCV	Phase Centre Variations
PNT	Positioning, Navigation and Timing
POD	Precise Orbit Determination
PPP	Precise Point Positioning
PPP-AR	PPP Ambiguity Resolution
PPP-RTK	PPP Real-Time Kinematic
PTB	Physikalisch-Technische Bundesanstalt
RTK	Real-Time Kinematic
RMS	Root Mean Square
SCE	Satellite Clocks Estimated
SCF	Satellite Clocks Fixed
SD	Single Differenced
SPB	Satellite Phase Bias
STD	Standard Deviation
TAI	International Atomic Time

TVRCB	Time-Varying Receiver Code Biases
TWSTFT	Two-Way Satellite Time and Frequency Transfer
UDUC	Undifferenced and Uncombined
USNO	United States Naval Observatory
UPD	Uncalibrated Phase Delay
UTC	Coordinated Universal Time
ZWD	Zenith Wet Delay

1 Introduction

1.1 Background

Time is a fundamental parameter in our daily life, and precise timekeeping is critical for various applications, ranging from communication networks to scientific experiments (Adhikari et al., 2021; Arms et al., 2009; Chou et al., 2010; Cliche and Shillue, 2006; Lisdat et al., 2016). The requirement for accurate and stable time has led to the development of various time transfer techniques, each with its own advantages and limitations. Time transfer can be defined as the process of transmitting time information from one location to another, and it is essential for the formation and maintenance of a world time scale (Defraigne and Petit, 2003; Levine, 2008; Piester et al., 2008).

There are several methods for time transfer, including Two-Way Satellite Time and Frequency Transfer (TWSTFT), optical fibre, laser, and Global Navigation Satellite Systems (GNSS). TWSTFT is a widely used technique that relies on transmitting a timing signal between two ground stations via satellites (Jiang, 2008). Optical fibre and laser time transfer techniques involve transmitting the timing signal via a fibre-optic cable or a laser beam (Kodet et al., 2016; Samain et al., 2014), respectively. These methods can achieve sub-nanosecond accuracy, but they require specialized equipment and infrastructure and can be expensive to implement for some users.

GNSS, on the other hand, has emerged as a low-cost and widely available technology for time transfer (Defraigne and Petit, 2015). GNSS is a satellite-based navigation system that consists of a network of satellites orbiting the Earth and ground-based receivers that can determine the precise time and location of the receivers on the ground. GNSS signals contain a precise time stamp, which can be used for time transfer between different locations on the Earth's surface.

GNSS time transfer offers several advantages over other techniques. Firstly, it is a low-cost solution that does not require specialized equipment or infrastructure. GNSS signals are available globally, making it a universal and easily accessible technology. Secondly, GNSS provides high accuracy and precision, with sub-nanosecond level timing accuracy achievable with modern GNSS receivers. Furthermore, GNSS is a continuous and real-time technique that provides an immediate transfer of timing information.

In summary, GNSS time transfer has emerged as a low-cost and widely available technique for high-precision time transfer. Its advantages include global coverage, high accuracy, and real-time capabilities. However, there are still several challenges that need to be addressed to ensure its reliability and accuracy. Ongoing research in the field of GNSS time transfer is focused on improving the technique and addressing these challenges, which will enable the development of more robust and reliable time transfer systems.

1.2 Literature Review

GNSS time transfer has been widely used for Coordinated Universal Time (UTC) comparisons since the 1980s due to its precision and low cost (Allan and Weiss, 1980; Jiang, 2008; Petit and Defraigne, 2023). It is also used for providing time stamps and frequency calibration relative to national metrology institutes. With the advancement of GNSS algorithms and models, the commonly used method for GNSS time transfer has changed from the common-view (CV) to the all-in-view (AV) method, and then to the precise point positioning (PPP) method.

The CV method is a GNSS time transfer method that was proposed in the 1980s, which initially used code observations only (Lewandowski et al., 1993). The CV method constructs an inter-station single-differenced (SD) GNSS observation model that requires the two stations to track signals from the same satellites (Lee et al., 2008). The advantages of the CV method are as follows. Firstly, the CV method only needs broadcast ephemeris, which can easily achieve real-time time transfer. Secondly, GNSS satellite orbit and clock errors are eliminated during the SD process. Thirdly, ionospheric and tropospheric errors are also significantly mitigated during the differential process when the distance between the station is not large. However, the CV method has limitations for long-distance time transfer and is limited in accuracy due to using only code observations.

To overcome the limitations of the CV method, the AV method was developed for long-distance GNSS time transfer (Petit and Jiang, 2008). The AV method synchronizes the local clock and the reference time scale of GNSS at each of the considered stations based on visible GNSS satellites (Defraigne et al., 2013). The synchronization error is then differentiated between the two stations needing time transfer, eliminating the impact of GNSS time stamps. The AV method requires additional precise GNSS satellite products, especially precise satellite clock products. However, the time transfer accuracy of the AV method is limited, also because of the use of only code observations.

To overcome the limitations of both the CV and AV methods, the PPP method based on both code and carrier phase observations was introduced for time transfer (Bruyninx et al., 1999; Larson and Levine, 1999). The implementation of PPP and AV methods is the same in the previous methods, with the only difference being the introduction of higher precision carrier phase observations. The PPP method also requires precise satellite products to determine the synchronization error between the local clock and the GNSS reference time scale, thus supporting long-distance time transfer. The PPP based on the ionosphere-free (IF) combination was favoured by the time community because the ionosphere delay, which is of no interest in time transfer, is eliminated. However, time transfer with the IF PPP is limited to dual-frequency observations and wastes potential multi-frequency observation information (Khodabandeh and Teunissen, 2016; Tu et al., 2019). In multi-frequency scenarios, multiple IF observations can be constructed, but the correlation between them in IF will still limit the time transfer performance.

Considering the drawbacks of the IF combination, the GNSS community is now turning to undifferenced and uncombined (UDUC) observations. The advantages of working with the UDUC GNSS observations are already recognized in high-precision GNSS positioning (Lannes and Prieur, 2013; Odijk et al., 2016; Samain et al., 2014), which includes the following aspects. Firstly, UDUC observations preserve all parameters so that possible error-specific dynamic models can be applied to improve model strength. Secondly, the UDUC formulation fully uses the original observation information and is flexible in multi-frequency scenarios. Thirdly, the stochastic model is simplified, giving the simplest form of observational variance. Fourthly, quality control is more robust with the UDUC formulation, avoiding problems such as noise amplification and model error transfer caused by combination and difference. Of course, in the UDUC model, it is impossible to unbiased estimate each parameter separately, and possible rank deficiency appearing in the model needs to be considered, which can be solved by the *S*-system theory (Teunissen, 1985). When the full-rank UDUC model is constructed, it can serve different GNSS applications. However, so far, a few UDUC methods have been applied to GNSS time transfer.

When considering high-precision GNSS applications, integer ambiguity resolution (IAR) is critical, particularly in the context of time transfer. The Integer Recovery Clock (IRC) (Laurichesse et al., 2009), Decoupled Satellite Clock (DSC) (Collins, 2008), and Uncalibrated Phase Delay/Fractional Cycle Bias (UPD/FCB) models (Ge et al., 2008) are the three widely used methods to achieve IAR in Precise Point Positioning Ambiguity Resolution (PPP-AR) in theory. However, only one time transfer method that implements IAR currently exists, known as integer PPP (IPPP) (Petit et al., 2014; Petit et al., 2017), which is based on the PPP-AR of the IRC model. These models are based on IF observations, which have limitations (Mi et al., 2023).

Obtaining precise GNSS satellite clock products is vital for achieving synchronizing the receiver clock and the GNSS reference time scale in AV and PPP. In generating GNSS precise satellite products through GNSS network data processing, the rank deficiencies between the receiver clock and GNSS satellite clocks are always unavoidable and are challenging to separate entirely (Chen et al., 2018; Shi et al., 2019). Consequently, the accuracy and reliability of GNSS satellite clock products inevitably impact time transfer performance. At present, International GNSS Service (IGS) final GNSS satellite clock products can reach tens of picoseconds of accuracy (Guo and Geng, 2018), while real-time products only achieve sub-nanosecond levels (Huang et al., 2014). Hence, avoiding the influence of satellite clock products is a crucial problem in time transfer.

Hardware calibration is another essential aspect of GNSS time transfer since the estimable receiver clock absorbs the receiver hardware delays in any method (Defraigne et al., 2021). GNSS time transfer's hardware delay comprises the GNSS receiver, antenna, cable connecting the GNSS receiver and antenna, and indoor cable connecting the GNSS receiver to the time and frequency reference. For GNSS time transfer, hardware delay must be appropriately calibrated and remain constant over time. However, studies indicate that hardware delay can vary significantly and is closely related to the environment in which GNSS equipment are located (Mi et al., 2021; Rieck et al., 2003), particularly temperature. Time labs, therefore, often create a stable temperature environment to maintain the receiver hardware delay as constant as possible. However, short-term and long-term variations in hardware delay are challenging to avoid even under these conditions. Practical approaches to describing hardware delay variation and minimizing its impact on GNSS time transfer is thus an ongoing challenge that the time community is working to address.

Currently, thousands of Low Earth Orbit (LEO) satellites operate in space. With the launch of additional satellites in the future, a variety of space exploration and Positioning, Navigation and Timing (PNT) applications will benefit from the new LEO constellations (Li et al., 2019a; Li et al., 2019b). Achieving precise orbit determination (POD) and time synchronization is a prerequisite for any LEO constellation application (Montenbruck et al., 2009; Montenbruck et al., 2018). Furthermore, the space environment is more complex than the ground environment

(Allahvirdi-Zadeh et al., 2021), making time transfer more challenging. However, the theory and application of GNSS time transfer based on LEO satellites are limited, and its feasibility in maintaining space-time references remains to be explored.

1.3 Implementation of GNSS Time and Frequency Transfer

GNSS time and frequency transfer is a technique that utilizes GNSS satellite information to compare clocks at multiple spatially separated sites, enabling the creation and sharing of precise time or clock frequency. This method is commonly employed for establishing and distributing standard time scales like International Atomic Time (TAI) and UTC. The accuracy requirements for time transfer vary among different users. For instance, maintaining UTC necessitates achieving an accuracy of no less than nanoseconds of one day. To cater for the diverse needs of users, atomic clocks of varying precision levels are utilized. It is important to note that the accuracy of time and frequency transfer heavily relies on the performance of atomic clocks at the user end. The role of GNSS technology is to restore the performance of atomic clocks by calculating the clock difference between the considered receiver sites.

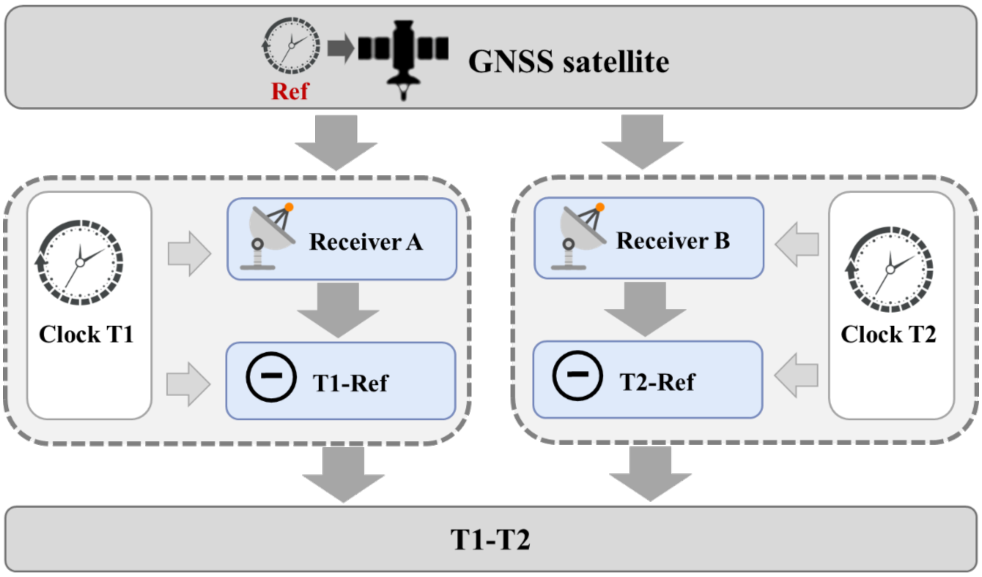

Figure 1 Schematic principle of GNSS time transfer

When utilizing GNSS technology for time and frequency transfer, the process typically involves two steps: time transfer and frequency transfer. Figure 1 illustrates the principle of GNSS time transfer. In the first step, the synchronization error between the local clock and the reference time scale is determined. The reference time scale depends on the satellite clock products used. If the GNSS clock information is obtained from the broadcast ephemeris, the time scale maintained by the GNSS constellation is used as the reference. Conversely, if a precise clock product is utilized, the time scale of that precise clock product serves as the reference. Each receiver is connected to an external clock, and its local time is provided by this external clock. By utilizing GNSS observations, T1-Ref and T2-Ref can be easily obtained. The second step involves calculating the difference between T1-Ref and T2-Ref, which are obtained from simultaneous observations of GNSS satellites at two stations, to obtain T1-T2. This represents the synchronization error between the two local clocks. The second step entails GNSS data processing, which can be performed using various methods such as PPP method.

Achieving accurate GNSS time transfer requires the calibration of the hardware delay of GNSS equipment. When working with GNSS observation equations, it is necessary to consider rank deficiencies, as not all unknown parameters can be estimated separately without including a bias. In constructing a full-rank GNSS time transfer model, parameter reconstruction is inevitably required. In this case, the synchronization error between the unbiased receiver clock and the reference time scale must account for the hardware delay (See subsequent chapters for details). This delay can originate from various sources, including the GNSS receiver, antenna, external clock, and connecting cables. Before conducting GNSS time transfer, the hardware delay of each signal in these instruments or cables should be precisely determined. Currently, absolute and relative calibration methods (Esteban et al., 2010; Overney et al., 1997) for hardware delay can meet the requirements for GNSS time transfer.

To implement GNSS frequency transfer, the results of GNSS time transfer need to be converted from the time domain to the frequency domain. This conversion can be achieved, for instance, through the use of the Fast Fourier Transform (FFT) (Nussbaumer et al., 1982), which computes the discrete Fourier Transform (DFT) of a sequence. Once the FFT is applied, the resulting frequency domain representation is used to calculate the power spectrum of the signal. The power spectrum represents the distribution of power across different frequencies and provides insights into the frequency stability of the GNSS frequency transfer. Analysing the frequency domain data involves identifying dominant frequencies by observing peaks in the power spectrum. The spread of power around these peak frequencies indicates the stability of the frequency, with a lesser spread indicating greater stability. Additionally, Modified Allan Deviation (MDEV) (Lesage and Ayi, 1984) can be evaluated to assess the stability of the frequency transfer data, which provides information about short-term and long-term stability, as well as the presence of frequency drift or noise. Software tools like Stable32 (Riley, 2008) can be used to convert time domain data into frequency domain data and perform frequency stability analysis.

1.4 Thesis Objectives

This research aims to establish a framework for developing the new state-of-the-art UDUC time transfer technique and extend it to space applications. Several GNSS time transfer challenges are addressed to achieve the research goal, including modelling with multi-frequency GNSS signals, IAR, satellite clocks estimation, and studying the impact of the variations in hardware delays. Special attention is paid to the space applications of GNSS time transfer where the POD of LEO satellites is an essential prerequisite. Therefore, the absolute and relative POD of LEO satellites based on UDUC observations is also discussed for future space applications of GNSS time transfer. The thesis is one of the first PhD dissertations concerning the UDUC approach for GNSS time transfer.

The thesis has six objectives to achieve its aim, which are:

1. Develop GNSS time transfer models with IAR applicable to multiple frequencies based on UDUC observations and explore the benefits of IAR for time transfer. In this process, GNSS time transfer models for short, medium, and long baselines will be constructed by considering different ionospheric constraints.
2. Develop GNSS time transfer models with satellite clocks estimated, not externally provided as currently done, based on UDUC observations and reveal the impact of precise satellite clock products on GNSS time transfer. This will include exploring the feasibility of serving future time references.
3. Study the short-term variations of different types of GNSS hardware delays and investigate whether they affect GNSS time transfer.
4. Develop GNSS time transfer models that consider hardware delay variations and quantify the impact of hardware delay variations on GNSS time transfer.
5. Develop absolute and relative POD methods for LEO satellite constellations and explore the advantages of the UDUC method in POD.
6. Explore the feasibility of LEO-based GNSS time transfer in maintaining space-time references.

1.5 Thesis Outline

The thesis comprises, after the introduction, of six chapters, each of which addresses a specific objective as discussed above. Four chapters are covered by published journal papers, where the conclusion for each publication is contained within itself. The thesis conclusions are given in a final chapter (Chapter 8) which summarises the findings of the whole thesis. The detailed structure of the thesis is as follows:

Chapter 2: UDUC GNSS Time Transfer with IAR for Short, Medium and Long Baselines

The first objective of the thesis listed above (Sec. 1.4) is addressed in the following publication forming Chapter 2 of the thesis:

- ***Mi, X.,*** *Zhang, B., El-Mowafy, A., Wang, K., & Yuan, Y. (2023). Undifferenced and uncombined GNSS time and frequency transfer with integer ambiguity resolution. Journal of Geodesy, 97(2), 13.* *https://doi.org/10.1007/s00190-022-01689-8*

This paper reviews the drawbacks of the existing GNSS time transfer methods and the advantages of the UDUC method in GNSS data processing, thus clarifying the necessity of introducing the UDUC method into GNSS time transfer. GNSS time transfer model with IAR (which is defined as the ionosphere-float model) that is suitable for multi-constellation and multi-frequency scenarios is derived first. Then, considering different ionospheric constraints, the ionosphere-fixed and ionosphere-weighted models suitable for short-baseline and medium-baseline time transfers are proposed, respectively. The time transfer performance of the UDUC models with IAR compared with the UDUC PPP is analysed, which shows the benefit of IAR for time transfer. This paper shows that the proposed model delivers comparable time transfer performance to the UDUC PPP model for long baselines. This is due to the impact of using precise satellite clocks, which will be studied in the next chapter.

Chapter 3: UDUC GNSS Time Transfer with Satellite Clocks Estimated

This chapter is covered by the following publication addressing the second objective of the thesis listed above:

- ***Mi, X.,*** *Zhang, B., El-Mowafy, A., Wang, K., & Yuan, Y. (2023). On the potential of undifferenced and uncombined GNSS time and frequency transfer with integer ambiguity resolution and satellite clocks estimated. GPS Solutions, 27(1), 25.* *https://doi.org/10.1007/s10291-022-01363-8*

This paper proposes the UDUC time transfer model with satellite clocks estimated, not provided externally, and investigates the effect of the estimated satellite clocks on time transfer. Based on the models in the previous chapter, the UDUC GNSS time transfer models with IAR and satellite clocks are constructed with the help of the *S*-system theory. The time transfer performance of the UDUC model with IAR and satellite clocks estimated is tested with GPS-only, and the effect of precise satellite clock products on time transfer is demonstrated in this research. In addition, it is found that GPS, Galileo, and BDS-3 all have the potential to achieve time transfer with picosecond level and frequency sstability in the low-mid 10^{-17} range for averaging times within one day. This paper proves that GNSS has the potential to serve optical clock time transfer and continue to play a role in future time reference maintenance.

Chapter 4: Characteristics of Multi-Frequency Multi-GNSS Receiver Biases

The following publication covers the third objective of the thesis addressed in this chapter:

- ***Mi, X.,*** *Sheng, C., El-Mowafy, A., & Zhang, B. (2021). Characteristics of receiver-related biases between BDS-3 and BDS-2 for five frequencies including inter-system biases, differential code biases, and differential phase biases. GPS Solutions, 25(3), 113. https://doi.org/10.1007/s10291-021-01151-w*

This paper systematically analyses GNSS receiver hardware delays and their short-term variations and influencing factors. The GNSS hardware delays involved are differential code bias (DCB), differential phase bias (DPB), and inter-system bias (ISB), which may affect high-precision positioning, time transfer and ionospheric studies. This study has three implications for the follow-up GNSS time transfer research. Firstly, the impact of different hardware delays must be considered when combining multi-constellation data. Secondly, there may be significant short-term variations in hardware delay, which should be accounted for in GNSS time transfer. Thirdly, the variations of hardware delay are closely related to the environment, especially the temperature, so the environment of the GNSS equipment should be paid attention to in the GNSS time transfer. This research lays the foundation for the next chapter to explore and quantify the impact of hardware delay variations on GNSS time transfer.

Chapter 5: UDUC GNSS Time Transfer considering Time-varying Receiver Code Biases

This chapter proposes a new UDUC GNSS time transfer model considering the variations of GNSS receiver hardware delay. It explores the variation characteristics of receiver hardware delay and its impact on time transfer. The specific idea is to select the hardware delay of the first epoch as a basis, so that the variations of hardware delay relative to the first epoch can be estimated. The advantage of this method is that the hardware delay variations of the GNSS equipment, including the GNSS receiver, antenna, and cable, are treated as a parameter instead of trying to control the variation of each part. This research reveals the variation characteristics and receiver hardware delay mechanism, enabling high-precision time transfer. This chapter addresses the fourth objective of the thesis.

Chapter 6: UDUC Precise Orbit Determination of LEO Satellites

The following publication addresses part of the fifth objective of the thesis:

- ***Mi, X.,*** *Allahvirdi-Zadeh, A., El-Mowafy, A., Huang, Z., Wang, K., Zhang, B., & Yuan, Y. (2023). Absolute and relative POD of LEO satellites in formation flying: Undifferenced and uncombined approach. Advances in Space Research, 72(4), 1070-1080. https://doi.org/10.1016/j.asr.2023.05.024*

The paper explores an essential prerequisite for space applications of GNSS time transfer: POD of LEO satellites. To ensure compatibility with the expansion of the UDUC GNSS time transfer, the POD model is established based on UDUC observations. A novel UDUC method suitable for absolute and relative POD in LEO satellite constellations is proposed. The estimated ambiguity is constructed into a double-differenced (DD) form for IAR with the help of common-view GNSS satellites. This approach can achieve real-time POD while simultaneously reducing the number of estimated parameters in LEO constellation processing, thereby improving computational efficiency. Therefore, this method aligns well with the developmental trajectory of future LEO constellations. The performance of the proposed method is verified based on two LEO satellites in formation flying. This study provides the basis for the next chapter of GNSS time transfer in space.

Chapter 7: LEO-Based GNSS Time Transfer Using the UDUC approach

This chapter explores the LEO-based GNSS time transfer performance in space based on UDUC observations. The development of LEO constellations is the future trend in satellite-based PNT. Achieving inter-satellite time synchronization and using LEO satellites for maintaining a time reference independent of the ground has become a current research hotspot. Therefore, this chapter explores the GNSS time transfer performance based on an LEO constellation, laying the foundation for the development of future space-time references. The research in this chapter achieves the last objective of the thesis.

Chapter 8: Conclusions and Recommendations

This last chapter of the thesis summarises the outcomes of this research and its contribution to the filed. It provides the potential direction of studies and future works related to achieving high accuracy and reliable GNSS time transfer and its applications.

2 UDUC GNSS Time Transfer with IAR for Short, Medium and Long Baselines

The present study unveils certain limitations of traditional methods of GNSS time transfer, such as inflexibility in multi-frequency scenarios and the inability to restore ambiguity integer characteristics, thereby restricting its overall performance. To address these concerns, GNSS time transfer models with integer ambiguity resolution (IAR) based on undifferenced and uncombined (UDUC) observations for short, medium and long baselines are proposed in this chapter. The performance of these models has been thoroughly examined and discussed. This chapter is presented in the following publication:

Mi, X., Zhang, B., El-Mowafy, A., Wang, K., & Yuan, Y. (2023). Undifferenced and uncombined GNSS time and frequency transfer with integer ambiguity resolution. Journal of Geodesy, 97(2), 13. https://doi.org/10.1007/s00190-022-01689-8

Journal of Geodesy (2023) 97:13
https://doi.org/10.1007/s00190-022-01689-8

ORIGINAL ARTICLE

Undifferenced and uncombined GNSS time and frequency transfer with integer ambiguity resolution

Xiaolong Mi[1] · **Baocheng Zhang**[2,5] · **Ahmed El-Mowafy**[1] · **Kan Wang**[3,4] · **Yunbin Yuan**[2]

Received: 20 October 2021 / Accepted: 25 November 2022 / Published online: 6 February 2023

Abstract

Precise point positioning (PPP) has been a competitive global navigation satellite system (GNSS) technique for time and frequency transfer. However, the classical PPP is usually based on the ionosphere-free combination of dual-frequency observations, which has limited flexibility in the multi-frequency scenario. More importantly, the unknown integer ambiguities are not restored to the integer nature, making the advantage of high-precision carrier phase observations underutilized. In this contribution, using the undifferenced and uncombined (UDUC) observations, we derive the time and frequency transfer model suitable for multi-constellation and multi-frequency scenarios. Notably, in short- and medium-baseline time and frequency transfer, the ionosphere-fixed and ionosphere-weighted UDUC models are derived, respectively, by making full use of the single-differenced (SD) ionospheric constraints. The proposed model can be applied to short-, medium- and long-baseline time and frequency transfer. The ambiguities are solved in a double-differenced (DD) form and can thus be restored to integers. To verify the feasibility of the model, GPS data from several time laboratories were collected, and the performance of the time and frequency transfer were analyzed with different baseline lengths. The results showed that the ionosphere-fixed and ionosphere-weighted UDUC models with integer ambiguity resolution could improve the frequency stability by 25–60% and 9–30% at an averaging time of several tens of seconds to 1 day for short- and medium-baseline, respectively. Concerning the long-baseline, the UDUC model is 10–25% more stable than PPP for averaging time below a few thousands second and over 1 day.

Keywords Time and frequency transfer · Global navigation satellite system (GNSS) · Integer ambiguity resolution (IAR) · Undifferenced and uncombined (UDUC) · Precise point positioning (PPP)

1 Introduction

Accurate time and frequency transfer are essential for relativistic geodesy, high-resolution radio astronomy, and precision measurement (He et al. 2018; Lisdat et al. 2016; Lopez et al. 2013; Milner et al. 2019; Roberts et al. 2017). In addition, time and frequency transfer is essential for many critical infrastructures such as financial services, space missions, transport, and defense applications (Davis et al. 2011). Compared with optical fiber, the global navigation satellite system (GNSS) is currently used as a more classical means of time and frequency transfer thanks to its simplicity and low cost (Defraigne and Baire 2011; Guyennon et al. 2009). Two major approaches, namely common view (CV) and precise point positioning (PPP) are widely used for time and frequency transfer in time laboratories.

The CV approach is based on the inter-station single-differenced (SD) model, requiring that the two stations track

---

✉ Baocheng Zhang
b.zhang@whigg.ac.cn

[1] School of Earth and Planetary Sciences, Curtin University, Perth, Australia

[2] State Key Laboratory of Geodesy and Earth's Dynamics, Innovation Academy for Precision Measurement Science and Technology, Chinese Academy of Sciences, Wuhan, China

[3] National Time Service Center, Chinese Academy of Sciences, Xi'an, China

[4] University of Chinese Academy of Sciences, Beijing, China

[5] State Key Laboratory of Satellite Navigation System and Equipment Technology, The 54th Research Institute of China Electronics Technology Group Corporation, Shijiazhuang 050081, China

signals from identical satellites (Lewandowski et al. 1993; Luna et al. 2017). The advantage of the CV approach is that only the broadcast ephemeris is needed, and the errors on satellite clocks and orbits are significantly mitigated during the SD process (Lee et al. 2008; Ray and Senior 2005). However, since the CV approach depends on the number of satellites in common-view, it is unsuitable for long-baseline time and frequency transfer (Ge et al. 2019).

With precise satellite orbits and clocks, PPP can provide the local time concerning the reference time scale of the satellite clock products (Defraigne et al. 2015; Zhang et al. 2020). Then, time and frequency transfer between the two stations can be accomplished by a simple difference between the two PPP local receiver time solutions. At this stage, the PPP approach is independent of the distance between the stations, which enables nanosecond time comparisons for intercontinental baselines. Traditional PPP is based on an ionosphere-free (IF) combination and is usually applied to dual-frequency observations (Ge et al. 2020; Khodabandeh and Teunissen 2016). However, in a multi-frequency scenario, although different IF combinations can be formed, this is not the optimal choice (Tu et al. 2019; Zhang et al. 2021). IF PPP does not take full advantage of all the observations because only one independent parameter, the ionospheric delay, gets eliminated, but more than one of the observables for both code and phase observations is sacrificed (Teunissen 2020). Instead of forming linear combinations of observables, some studies have implemented PPP based on the undifferenced and uncombined (UDUC) GNSS observations, namely UC PPP (Liu et al. 2017; Su and Jin 2019). The UC PPP contributes to strengthening the model to the best extent possible as it can flexibly impose dynamic constraints on all parameters (Zhang et al. 2019). In this case, ionospheric delays are no longer eliminated but estimated, making the model flexible in multi-frequency scenarios. In addition, the simplest observational variance matrix is used in the UC PPP (Odijk et al. 2016).

The ambiguity in the float form that exists in traditional PPP, limits the performance of the time and frequency transfer. Through theoretical deduction, Khodabandeh and Teunissen (2018) preliminarily demonstrates how integer ambiguity resolution benefits time and frequency transfer. Petit et al. (2015) have proposed the integer PPP (IPPP) method, which can recover the integer characteristic of ambiguities by considering the fractional-cycle biases (FCB) (Geng et al. 2012; Petit 2021). However, IPPP is still based on the IF combinations and is thus only suitable for dual-frequency scenarios. In addition, the IPPP solution is highly dependent on external FCB products, which may have a discrepancy in their timestamp that may affect the process of time transfer, and therefore requires consistent processing strategies at the user- and the network-end (Geng et al. 2020).

In this contribution, we propose a time and frequency transfer model that can achieve integer ambiguity resolution without external FCB products. The model is based on UDUC GNSS observations, which could benefit from several advantages (Odijk et al. 2016; Zhang et al. 2019). In this process, we present the method to eliminate the rank deficiencies from UDUC observations and then construct the full-rank time and frequency model with the ambiguities estimated in the double-differenced (DD) form.

The remainder of this paper proceeds as follows. Section 2 first develops a general UDUC model, namely the ionosphere-float model, without any ionospheric constraints. On this basis, the ionosphere-weighted and -fixed models suitable for medium and short baselines are derived. Then, how to implement time and frequency transfer using the UDUC models is given in Sect. 3. Section 4 presents the experimental results, including time and frequency transfer over short, medium, and long baselines. Finally, we summarize our findings and give our conclusions in Sect. 5.

2 UDUC models with different ionospheric constraints

This section first gives the ionosphere-float UDUC model without ionospheric constraints, which is compatible with time and frequency transfer from short to long baselines. Next, we propose two particular UDUC models, namely the ionosphere-fixed and -weighted models, over short and medium baselines, respectively, with a between-receiver SD ionospheric constraint.

2.1 Ionosphere-float UDUC model

The UDUC code and phase observation equations of two stations (*A* and *B*), in one GNSS constellation serving as a starting point of the proposed algorithm, are expressed as follows,

$$\begin{aligned}
p^s_{A,j} &= \rho^s_A + \tau^s_A + dt_A - dt^s + \mu_j I^s_A + d_{A,j} - d^s_{,j} + \varepsilon^s_{p,j}\\
\phi^s_{A,j} &= \rho^s_A + \tau^s_A + dt_A - dt^s - \mu_j I^s_A + \lambda_j N^s_{A,j} + \delta_{A,j} - \delta^s_{,j} + \varepsilon^s_{\phi,j}\\
p^s_{B,j} &= \rho^s_B + \tau^s_B + dt_B - dt^s + \mu_j I^s_B + d_{B,j} - d^s_{,j} + \varepsilon^s_{p,j}\\
\phi^s_{B,j} &= \rho^s_B + \tau^s_B + dt_B - dt^s - \mu_j I^s_B + \lambda_j N^s_{B,j} + \delta_{B,j} - \delta^s_{,j} + \varepsilon^s_{\phi,j}
\end{aligned} \tag{1}$$

where the description of the notations used is given in Table 1. However, Eq. (1) represents a rank deficient system, which indicates that not all unknowns can be estimated separately, but only their linear combinations. In this case, the *S*-system theory is used to identify the rank deficiencies, find the *S*-basis parameters, and construct a full-rank model (Odijk et al. 2017; Odolinski and Teunissen 2017).

Table 1 Symbol definitions used in Eq. (1) (The symbol r denotes stations A or B)

Symbol	Description
s, r, j	Satellite, receiver, and frequency
$p^s_{r,j}$ and $\phi^s_{r,j}$	Code and phase observations
ρ^s_r	Range between receiver r and satellite s
τ^s_r	Tropospheric delay
dt_r and dt^s	Receiver clock and satellite clock offsets
μ_j and I^s_r	Frequency-dependent coefficient ($\mu_j = f_1^2 \big/ f_j^2$) and slant ionospheric delays on the first frequency
$d_{r,j}$ and $d^s_{,j}$	Code biases of the receiver and satellite
$\delta_{r,j}$ and $\delta^s_{,j}$	Phase biases of the receiver and satellite
λ_j and $N^s_{r,j}$	Wavelength and undifferenced phase ambiguity
$\varepsilon^s_{p,j}$ and $\varepsilon^s_{\phi,j}$	Code and phase observation noise and miss-modeled random effects such as multipath

Table 2 The S-basis constraints for the ionosphere-float UDUC model, together with the types of rank deficiencies they eliminate, where $d_{r,GF} = \frac{1}{\mu_2-\mu_1}(d_{r,2} - d_{r,1})$, $d^s_{,GF} = \frac{1}{\mu_2-\mu_1}(d^s_{,2} - d^s_{,1})$ and $d_{r,IF} = \frac{\mu_2}{\mu_2-\mu_1} d_{r,1} - \frac{\mu_1}{\mu_2-\mu_1} d_{r,2}$

Rank deficiencies	S-basis constraints	Notation	Conditions
1	Pivot receiver code biases	$d_{r,j}$	$j \geq 1$
2	Pivot receiver phase biases	$\delta_{r,j}$	$j \geq 1$
3	IF receiver code biases	$d_{r,IF}$	
4	Phase ambiguities of pivot satellite	$N^1_{r,j}$	$j \geq 1$
5	Phase ambiguities of pivot receiver	$N^s_{r,j}$	$s \geq 1, j \geq 1$
6	Geometry-free (GF) receiver code biases	$d_{r,GF}$	
7	GF satellite code biases	$d^s_{,GF}$	

For high-precision time and frequency transfer, the procedure is conducted at stations where the ground-truth positions of the receivers are available. In addition, the precise satellite orbits that can be accessed by an external provider such as the International GNSS Service (IGS) allow the satellite-receiver ranges ρ^s_r to be computed accurately (Dow et al. 2009). The IF satellite clock offset ($d\tilde{t}^s = dt^s + d^s_{,IF}$) can also be provided by the IGS (Johnston et al. 2017), where $d^s_{,IF} = \frac{\mu_2}{\mu_2-\mu_1} d^s_{,1} - \frac{\mu_1}{\mu_2-\mu_1} d^s_{,2}$. In addition, the tropospheric delay τ^s_r is usually expressed as the sum of the dry and wet delays, $\tau^s_r = (\tau_d)^s_r + m^s_r \tau_r$, in which $(\tau_d)^s_r$ is the slant dry delay, which can be corrected a priori using empirical models. The wet delay is modeled as the product of the known elevation-dependent mapping function m^s_r and the unknown tropospheric wet zenith delay (ZWD)τ_r.

Assuming that m satellites are tracked, all are transmitting signals on f frequencies. For stations A and B, the model contains several types of rank deficiencies for each receiver as follows (Odijk et al. 2016):

1. Between the receiver and satellite code biases with the rank deficiency of size f;
2. Between the receiver and satellite phase biases with the rank deficiency of size f;
3. Between the receiver clock, code biases, and phase biases with the rank deficiency of size 1;
4. Between the receiver phase biases and ambiguities with the rank deficiency of size f;
5. Between the satellite phase biases and ambiguities with the rank deficiency of size $f \times m$;
6. Between the ionospheric delays and receiver code/phase biases with the rank deficiency of size 1;
7. Between the ionospheric delays and satellite code/phase biases with the rank deficiency of size m.

As mentioned before, to deal with these rank deficiencies, one can apply the S-system theory, which constrains the S-basis parameters and lumps the parameters from their original forms to estimable forms (Mi et al. 2020; Odolindski et al. 2015). Table 2 shows the S-basis constraints for the ionosphere-float UDUC model and their associated removed rank deficiencies.

Applying the S-basis constraints in Table 2, with the coordinates of points A and B known, the full-rank model can be expressed as follows,

$$\begin{aligned}
\tilde{p}^s_{A,j} &= \rho^s_A + m^s_A \tau_A + d\tilde{t}_A + \mu_j \tilde{I}^s_A - \tilde{d}^s_{A,j} + \varepsilon^s_{p,j} \\
\tilde{\phi}^s_{A,j} &= \rho^s_A + m^s_A \tau_A + d\tilde{t}_A - \mu_j \tilde{I}^s_A - \tilde{\delta}^s_{A,j} + \varepsilon^s_{\phi,j} \\
\tilde{p}^s_{B,j} &= \rho^s_B + m^s_B \tau_B + d\tilde{t}_B + \mu_j \tilde{I}^s_B - \tilde{d}^s_{B,j} + \varepsilon^s_{p,j} \\
\tilde{\phi}^s_{B,j} &= \rho^s_B + m^s_B \tau_B + d\tilde{t}_B - \mu_j \tilde{I}^s_B - \tilde{\delta}^s_{B,j} + \varepsilon^s_{\phi,j}
\end{aligned} \tag{2}$$

where $\tilde{p}^s_{r,j} = p^s_{r,j} + d\tilde{t}^s - (\tau_d)^s_r$ and $\tilde{\phi}^s_{r,j} = \phi^s_{r,j} + d\tilde{t}^s - (\tau_d)^s_r$. The estimable parameters and their interpretations are given in Table 3. Equation (2) is the UC PPP model, which is more flexible in multi-frequency scenarios than the classical IF PPP.

Table 3 Estimable parameters and their interpretation in the UDUC model using S-basis in Table 2 for stations A and B

Estimable parameter	Notation and interpretation	Conditions
Receiver clock offset	$d\tilde{t}_r = dt_r + d_{r,IF}$	
Satellite code bias	$\tilde{d}^s_{r,j} = d^s_{,j} - d^s_{,IF} - \mu_j d^s_{,GF} - d_{r,j} + d_{r,IF} + \mu_j d_{r,GF}$	$s \geq 1, j \geq 3$
Satellite phase bias	$\tilde{\delta}^s_{r,j} = \delta^s_{,j} - d^s_{,IF} + \mu_j d^s_{,GF} - \lambda_j N^s_{r,j} - \delta_{r,j} + d_{r,IF} - \mu_j d_{r,GF}$	$s \geq 1, j \geq 1$
Between-receiver code biases	$\tilde{d}_{AB,j} = d_{B,j} - d_{A,j} - d_{AB,IF} - \mu_j d_{AB,GF}$	$j \geq 3$
Between-receiver phase biases	$\tilde{\delta}_{AB,j} = \delta_{B,j} - \delta_{A,j} - d_{AB,IF} + \mu_j d_{AB,GF} + \lambda_j N^1_{AB,j}$	$j \geq 1$
Ionospheric delay	$\tilde{I}^s_r = I^s_r + d_{r,GF} - d^s_{,GF}$	$s \geq 1$
Phase ambiguity	$N^{1s}_{AB,j} = N^s_{AB,j} - N^1_{AB,j}$	$s \geq 1, j \geq 1$

There are satellites in common view for most of the baseline lengths used in the time and frequency transfer scenarios. Hence, it is expected to use the common-view satellites to resolve the integer ambiguities and obtain high precision in the time and frequency transfer. Note that the satellite code and phase biases ($d^s_{,j} - d^s_{,IF} - \mu_j d^s_{,GF}$ and $\delta^s_{,j} - d^s_{,IF} + \mu_j d^s_{,GF}$) are the same for different receivers tracking these satellites. Taking those of receiver A as the reference, the between-receiver code and phase biases are estimated instead of estimating those of receiver B. More importantly, the ambiguities of the common-view satellite are reformed into the DD form so that the integer property can be recovered. In this case, the ionosphere-float UDUC model can be formulated as follows:

$$
\begin{aligned}
\tilde{p}^s_{A,j} &= \rho^s_A + m^s_A \tau_A + d\tilde{t}_A + \mu_j \tilde{I}^s_A - \tilde{d}^s_{A,j} + \varepsilon^s_{p,j} \\
\tilde{\phi}^s_{A,j} &= \rho^s_A + m^s_A \tau_A + d\tilde{t}_A - \mu_j \tilde{I}^s_A - \tilde{\delta}^s_{A,j} + \varepsilon^s_{\phi,j} \\
\tilde{p}^s_{B,j} &= \rho^s_B + m^s_B \tau_B + d\tilde{t}_B + \mu_j \tilde{I}^s_B - \tilde{d}^s_{A,j} + \tilde{d}_{AB,j} + \varepsilon^s_{p,j} \\
\tilde{\phi}^s_{B,j} &= \rho^s_B + m^s_B \tau_B + d\tilde{t}_B - \mu_j \tilde{I}^s_B - \tilde{\delta}^s_{A,j} \\
&\quad + \tilde{\delta}_{AB,j} + \lambda_j N^{1s}_{AB,j} + \varepsilon^s_{\phi,j}
\end{aligned}
\tag{3}
$$

where $\tilde{d}_{AB,j}$ and $\tilde{\delta}_{AB,j}$ are the between-receiver code and phase biases,$N^{1s}_{AB,j}$ is the DD ambiguity (see Table 3).

The ionosphere-float UDUC model can be regarded as combining the advantages of the PPP and the real-time kinematic (RTK). On the one hand, the model utilizes the RTK principle, which integrates ambiguity into the DD form through the S-basis. The DD ambiguities can be fixed using integer ambiguity resolution theories, including integer rounding, integer bootstrapping and integer least-squares (Teunissen 1999), which improves the time and frequency transfer performance. On the other hand, when the baseline is long, there are no common-view satellites, the ionosphere-float UDUC model would be equivalent to the UC PPP one.

2.2 Ionosphere-weighted UDUC model

It is acceptable to use the model in Eq. (3) for time and frequency transfer over baselines of tens to hundreds of kilometers. However, the spatial correlation of the regional ionospheric delays from the same satellite is ignored in this process, which is assumed to be approximately equal for the different receivers at this distance (Mi et al. 2019a; Teunissen 1998). Therefore, the ionospheric delays are introduced as a third group of observables, aside from the code and phase observables. Their observation equation reads $\overline{I}^s_{AB} = I^s_{AB}$, where I^s_{AB} is the between-receiver SD ionospheric delays, and $\overline{I}^s_{AB}$ is the between-station SD ionospheric pseudo-observables (Interpolate by reference network or assume zero). Adding those observables and configuring the corresponding stochastic model makes it possible to provide a-priori reasonable information on the ionospheric delay (Mi et al. 2019b; Odijk and Teunissen 2008). The UDUC model becomes flexible for a wide range of baseline lengths, enabling fast integer ambiguity resolution. This ionosphere-weighted UDUC model can be written as

$$
\begin{aligned}
\tilde{p}^s_{A,j} &= \rho^s_A + m^s_A \tau_A + d\tilde{t}_A + \mu_j \tilde{I}^s_A - \tilde{d}^s_{A,j} + \varepsilon^s_{p,j} \\
\tilde{\phi}^s_{A,j} &= \rho^s_A + m^s_A \tau_A + d\tilde{t}_A - \mu_j \tilde{I}^s_A - \tilde{\delta}^s_{A,j} + \varepsilon^s_{\phi,j} \\
\tilde{p}^s_{B,j} &= \rho^s_B + m^s_B \tau_B + d\tilde{t}_B + \mu_j \tilde{I}^s_A + \mu_j I^s_{AB} \\
&\quad + \mu_j \tilde{d}_{AB} - \tilde{d}^s_{A,j} + \tilde{d}_{AB,j} + \varepsilon^s_{p,j} \\
\tilde{\phi}^s_{B,j} &= \rho^s_B + m^s_B \tau_B + d\tilde{t}_B - \mu_j \tilde{I}^s_A - \mu_j I^s_{AB} \\
&\quad + \mu_j \tilde{d}_{AB} - \tilde{\delta}^s_{A,j} + \tilde{\delta}_{AB,j} + \lambda_j N^{1s}_{AB,j} + \varepsilon^s_{\phi,j} \\
\overline{I}^s_{AB} &= I^s_{AB} + \varepsilon^s_{AB}
\end{aligned}
\tag{4}
$$

where ε^s_{AB} is random observation noise of between-receiver SD ionospheric delay. $\tilde{d}_{AB} = \frac{1}{\mu_2 - 1}((d_{B,2} - d_{B,1}) - (d_{A,2} - d_{A,1}))$ is the between-receiver differential code biases (DCB), which makes the separated ionospheric delay completely independent of receiver B and thus improves the model strength.

2.3 Ionosphere-fixed UDUC model

Provided that the distance between the two receivers involved is less than a few kilometers, one can assume that the ionospheric delays are the same for both receivers (Mi et al. 2021). With this knowledge, the ionosphere-fixed UDUC model can be constructed as,

$$
\begin{aligned}
\tilde{p}^s_{A,j} &= \rho^s_A + m^s_A \tau_A + d\tilde{t}_A + \mu_j \tilde{I}^s_A - \tilde{d}^s_{A,j} + \varepsilon^s_{p,j} \\
\tilde{\phi}^s_{A,j} &= \rho^s_A + m^s_A \tau_A + d\tilde{t}_A - \mu_j \tilde{I}^s_A - \tilde{\delta}^s_{A,j} + \varepsilon^s_{\phi,j} \\
\tilde{p}^s_{B,j} &= \rho^s_B + m^s_B \tau_B + d\tilde{t}_B + \mu_j \tilde{I}^s_A \\
&\quad + \mu_j \tilde{d}_{AB} - \tilde{d}^s_{A,j} + \tilde{d}_{AB,j} + \varepsilon^s_{p,j} \\
\tilde{\phi}^s_{B,j} &= \rho^s_B + m^s_B \tau_B + d\tilde{t}_B \\
&\quad - \mu_j \tilde{I}^s_A + \mu_j \tilde{d}_{AB} - \tilde{\delta}^s_{A,j} + \tilde{\delta}_{AB,j} + \lambda_j N^{1s}_{AB,j} + \varepsilon^s_{\phi,j}
\end{aligned}
\tag{5}
$$

where the forms of the estimable parameters are identical to those in the ionosphere-weighted model. The ionosphere-fixed UDUC model is a particular form of the ionosphere-weighted model: the weight of between-receiver SD ionospheric pseudo-observables ($\overline{I}^s_{AB} = 0$) is large enough and thus can be ignored in the model.

3 Implementation of time and frequency transfer with the UDUC models

This section details the implementation of time and frequency transfer with short-, medium- and long-baseline.

3.1 Time and frequency transfer over short-baseline

The ionospheric-fixed UDUC model is advantageous for time and frequency transfer over a short baseline as the zero between-receiver SD ionospheric delays at this distance are considered. Assuming a short baseline here, receiver A with a time and frequency standard and receiver B obtains the time difference with receiver A to adjust the local clock. From Eq. (5), the critical information $d\tilde{t}_A = dt_A + d_{A,IF}$ and $d\tilde{t}_B = dt_B + d_{B,IF}$ are estimated using the ionosphere-fixed UDUC model. Two concepts need to be clarified. First, the IF receiver code bias ($d_{r,IF}$) is contained in the receiver clock ($d\tilde{t}_r$); therefore $d\tilde{t}_r$ is the biased receiver clock. This bias is challenging to calibrate by true GNSS signals, and it is usually regularly corrected by absolute calibration means using simulated GNSS signals in the time laboratories (Defraigne 2017). Fortunately, previous studies have shown that this bias is stable for months under certain conditions in the time laboratories (Kanj et al. 2014). Second, for all timing applications using GNSS,dt_r is the synchronization error between the receiver and the reference of the precise satellite clock products (denoted as *ref*), where $dt_r = d\bar{t}_r - dt_{ref}.d\bar{t}_r$ is the true time of the receiver and dt_{ref} is the reference time of the satellite products. Then, we can get $d\tilde{t}_{AB}$ by a simple difference and eliminate the influence of the reference time, which can be expressed as $(d\bar{t}_B - dt_{ref} + d_{B,IF}) - (d\bar{t}_A - dt_{ref} + d_{A,IF}) = d\bar{t}_{AB} + d_{AB,IF}$. As we mentioned earlier,$d_{AB,IF}$ can be corrected by calibration means so that the time transfer from A to B can be achieved.

Furthermore, the short-baseline time transfer can also assist the receiver biases calibration. Assuming that A and B are receivers with the same frequency standard in the same time laboratory, A is the primary receiver used to maintain time. While bias calibration can also be done with code observations only, it is difficult to achieve high accuracy. However, this can be achieved using the ionosphere-fixed UDUC model with the common frequency standard. Thanks to the integer ambiguity resolution, this calibration is also guaranteed with high precision. This can be done as follows. First, since receiver A is pre-calibrated, using the ionosphere-fixed UDUC model, we can get $d\tilde{t}_A = d\bar{t}_A - dt_{ref}$ and $d\tilde{t}_B = d\bar{t}_B - dt_{ref} + d_{B,IF}$. Second, since the same frequency standard is connected,$d\bar{t}_A = d\bar{t}_B$. Then, the IF receiver code bias of receiver B can be obtained by the difference $(d\bar{t}_B - dt_{ref} + d_{B,IF}) - (d\bar{t}_A - dt_{ref}) = d_{B,IF}$. Compared with other calibration methods, this method has higher accuracy and is suitable for real-time calibration.

3.2 Time and frequency transfer over medium-baseline

The time transfer of medium baselines (tens to hundreds of kilometers) is of practical significance, especially the time synchronization within countries. In those cases, the ionosphere-weighted model is particularly significant by fully considering the characteristics of the between-receiver SD ionospheric delays. We assume receivers A and B form a medium baseline and apply time transfer between them, where A has the desired time and frequency standard. The synchronization error between the receiver and the reference time scale obtained by the ionosphere-weighted model (see Eq. (4) and Table 2) are identical to that by the ionosphere-fixed model, where $d\tilde{t}_A = dt_A + d_{A,IF}$ and $d\tilde{t}_B = dt_B + d_{B,IF}$. Then, time transfer can be realized through their difference ($d\tilde{t}_{AB}$), and here calibration of $d_{AB,IF}$ is required.

3.3 Time and frequency transfer over long-baseline

Theoretically, it is acceptable to realize long-baseline time and frequency transfer using the ionosphere-float UDUC model after reaching stable carrier-phase ambiguities. However, the limited number of common-view satellites makes it challenging to observe the improvement of the model relative to UC PPP. In addition, it is also challenging to achieve integer ambiguity resolution with the ionosphere-float model.

We consider the ionosphere-fixed and -weighted UDUC models to make the integer ambiguity resolution available. See Eqs. (4) and (5), the synchronization error between the receiver and the satellite products of two receivers can be obtained, just like PPP, respectively. Suppose a long-baseline

Table 4 An overview of GNSS data sets used in our analysis, including station name, institute, type of reference clock, receiver and antenna type, and observation period

Station ID	Institute	Reference clock	Receiver type	Antenna type	Observation period
USN7	USNO	H-maser	SEPT POLARX5TR	TPSCR.G5	2021, Days 325–331
USN8		H-maser	SEPT POLARX5TR	TPSCR.G5	
AMC4		H-maser	SEPT POLARX5TR	TPSCR.G5C	
NIST	NIST	H-maser	NOV OEM4-G2	NOV702	
BRUX	ROB	H-maser	SEPT POLARX4TR	JAVRINGANT_DM	
ROAG	ROA	H-maser	SEPT POLARX5TR	LEIAR25.R4	
SFER		Cesium	LEICA GR25	LEIAR25	
OP71	OP	H-maser	SEPT POLARX4TR	LEIAR25.R4	
OPMT		H-maser	ASHTECH Z-XII3T	3S-02-TSADM	
PTBB	PTB	H-maser	SEPT POLARX5TR	LEIAR25.R4	
PT11		H-maser	SEPT POLARX4TR	LEIAR25.R4	

time transfer between A and B needs to be implemented. Then, we choose one reference station C and D, near A and B, respectively. The distances requirement between A and C and between B and D are loose, which can be several to hundreds of kilometers. In the baseline formed between A and C, $d\tilde{t}_A = dt_A + d_{A,IF}$ can be obtained using the ionosphere-fixed or -weighted UDUC model. Similarly, $d\tilde{t}_B = dt_B + d_{B,IF}$ can be available in the baseline between B and D. In this case, $d\tilde{t}_A$ and $d\tilde{t}_B$ are the same as with the PPP approach, but the integer ambiguity resolution can be achieved. Finally, by computing the simple difference ($d\tilde{t}_{AB} = d\tilde{t}_B - d\tilde{t}_A$), the time transfer with integer ambiguity resolution between A and B can be achieved. It can be said that this is similar to IPPP, which is to achieve integer ambiguity resolution at both sides and then estimate the difference. Note that it does not concern whether the reference stations C and D have external time and frequency standards. Their role is to better estimate the satellite phase biases and constrain the ionospheric delays, thus enabling the integer ambiguity resolution and delivering a high precision for the estimable receiver clock offsets.

4 Results

This section provides the experimental results of applying time and frequency transfer based on the models developed earlier. First, the collected data and our processing strategies are introduced. Next, short-, medium- and long-baseline time and frequency transfer performances are assessed. In addition, the time and frequency transfer performance of the PPP with the same configuration is also given.

4.1 Experimental setup

To validate the feasibility and effectiveness of the proposed models, we select GPS data sets from several time laboratories, including USNO (USA), NIST (USA), ROB (Belgium), ROA (Spain), OP (France) and PTB (Germany). Our analysis uses observations of GPS dual-frequency (L1 and L2) to verify the model, which facilitates comparison with the traditional PPP. The relevant characteristics of the experimental data sets considered for this study are shown in Table 4. The H-maser clocks are high-performance atomic clocks whose intra-day stability (1×10^{-15}) is beyond what can be achieved with GNSS (Weinbach and Schön 2013). Therefore, we can evaluate the improvement of the UDUC model relative to the PPP from the analysis of the time difference noise and the corresponding frequency stability. The main processing strategies for the PPP and the UDUC model are summarized in Table 5.

4.2 Short-baseline time and frequency transfer

The first time and frequency transfer experiments were carried out at two time laboratories: (1) USN7 and USN8, operated with a common H-Maser clock at the USNO; and (2) ROAG and SFER, operated with an H-maser clock and

Table 5 Data processing strategies in this study for both the PPP and the UDUC models

Item	Strategy
Observation	GPS L1 + L2
Cut-off elevation	8°
Stochastic model	Elevation-dependent weighting (Shen et al. 2009) based on a priori standard deviations of 0.003 m and 0.6 m for phase and code observations (Banville et al. 2021), respectively
Tropospheric delays	Dry delay: corrected by UNB3m model (Leandro et al. 2008) Wet delay: estimated using a random-walk process with a spectral density of 0.1 mm/$\sqrt{s}$
Satellite phase biases	Estimated as a time-constant in a continuous arc
Float ambiguity	Estimated as a time-constant in a continuous arc
Between-receiver phase biases	Estimated as a time-constant
Between-receiver DCB	Estimated as white noise
Receiver clock offset	Estimated as white noise
Slant ionospheric delays	Estimated as white noise
Between-receiver SD ionospheric observable and weight	Observable: set to zero; Weight: expressed as $\frac{0.09\times\exp(0.005\times l_{AB})}{\sin^2(E^s)}$, where l_{AB} and E^s represent the base length and the satellite elevation angle (Zha et al. 2021)
Parameter estimator	Bidirectional Kalman filter
Integer ambiguity resolution and validation	Integer ambiguity resolution: LAMBDA (Teunissen 1995) Validation: Ratio test with a threshold of 3 (Teunissen and Verhagen 2009)
Outlier detection and elimination	DIA procedure (Teunissen 2018)
The discontinuity at the day boundaries	Extrapolation and bridge (Petit et al. 2015; Petit 2021)

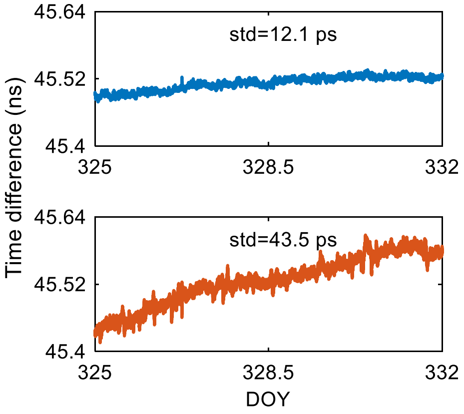

Fig. 1 A common-clock zero-baseline time link of the UNS7-UNS8 at the USNO computed with the ionosphere-fixed UDUC model (top) and the PPP (bottom) from 21 to 27 November 2021

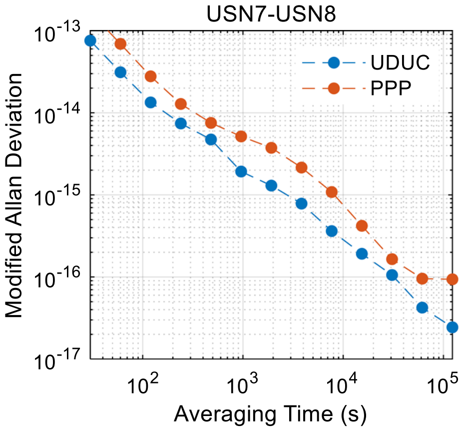

Fig. 2 Comparison of the MDEV between the ionosphere-fixed UDUC model and the PPP for the USN7-USN8 time-link

a Cesium clock at the ROA, respectively. The time link of USN7-USN8 is a zero-baseline connected to a common antenna, while the time link of ROAG-SFER is a short baseline of 124 m. As mentioned earlier, the ionospheric delays can be sufficiently eliminated at short baselines, so the ionosphere-fixed UDUC model was adopted in this case. With the ionospheric constraints, the instantaneous integer ambiguity resolution can be realized by the ionosphere-fixed UDUC model.

Figure 1 shows the time differences of the USN7-USN8 time link using the ionospheric-fixed UDUC model and the PPP. Since USN7 and USN8 are operated with the same H-maser clock, their time link directly reflects the noise and stability of the hardware delays with the same type of receivers. The gain of the ionosphere-fixed UDUC model with integer ambiguity resolution is that the noise of the time difference is effectively reduced compared with using the PPP. Results show that the standard deviation of the link values of time difference for the ionosphere-fixed UDUC model is 12.1 ps, 72.2% lower than the 43.5 ps for the PPP model. Figure 2 illustrates the modified Allan deviation (MDEV) of the USN7-USN8 time link over the week of the UDUC model and the PPP. It can be observed that the short-term and long-term frequency stability of the ionosphere-fixed UDUC model has improved compared to that of the PPP model. For example, the ionosphere-fixed UDUC model has frequency

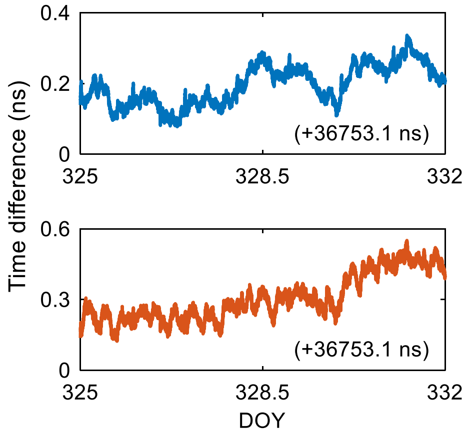

Fig. 3 A short-baseline time link of the ROAG-SFER at the ROA computed with the ionosphere-fixed UDUC model (top) and the PPP (bottom) from 21 to 27 November 2021

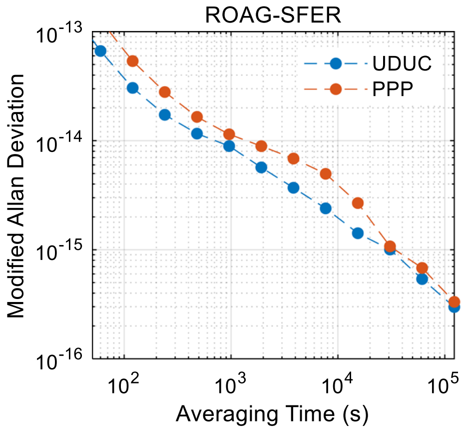

Fig. 4 Comparison of the MDEV between the ionosphere-fixed UDUC model and the PPP for the ROAG-SFER time-link

stability of 1.3×10^{-14} at 120 s average time, while the PPP it amounts to 2.8×10^{-14}, showing a 53.6% improvement. In addition, the frequency stability for an averaging time of 1 day of the ionosphere-fixed UDUC model is 64.9% higher than that of the PPP model, which is about 3.3×10^{-17} and 9.4×10^{-17}, respectively. Different from the conclusion of Petit et al. (2015), the UDUC model improves long-term stability and improves short-term one for the following reasons. First, the ionospheric constraints are considered; thus, the fast integer ambiguity resolution can be realized by the ionosphere-fixed UDUC model. Second, the satellite phase biases are estimated in the UDUC model, while the FCB in the IPPP is generated from a global network. Therefore, satellite phase biases are more consistent with the model, although also a product of auxiliary integer ambiguity resolution. Third, the UDUC model avoids the amplification of observation noise in the error propagation when differencing or using a measurement combination.

Another 124 m short baseline time link experiment is performed between ROAG and SFER at the ROA, equipped with H-maser and Cesium clocks. Like the USN7-USN8, we can also see the noise reduction of the time difference in Fig. 3. Since the time difference of the non-common-clock time link will be affected by atomic clocks themselves and is no longer constant, so the epoch difference is introduced. Epoch difference is a critical evaluation index in time and frequency transfer, reflecting the change of atomic clock per unit time and further the time transfer accuracy. The standard deviations in the following time difference results (Figs. 3, 5, 7, 9, 11) are the standard deviations of the epoch difference of the time difference. The epoch difference standard deviation of the ROAG-SFER link is 31.7% lower for the ionosphere-fixed UDUC model than that for the PPP over the test week, which is 5.65 ps and 8.27 ps, respectively. Figure 4 shows the MDEV of the ROAG-SFER time link over the week of the two models, from which the gain from the ionosphere-fixed UDUC model is visible. Taking the results at 3840 s average time as an example, the MDEV of the PPP and the ionosphere-fixed UDUC model is 6.9×10^{-15} and 3.7×10^{-15}, respectively, with an improvement of 46.4%. In addition, for an averaging time of 1 day for this time link, the improvement of the UDUC model over the PPP is 25.0% with 3.6×10^{-16} and 4.8×10^{-16}, respectively.

4.3 Medium-baseline time and frequency transfer

The next series of experiments have been carried out in four time laboratories, forming two medium baseline time links. One is the time link between NIST and AMC4, with a 146.8 km baseline length. The other, 262.3 km, is the time link between BRUX and OPMT. Based on the ionosphere-weighted UDUC model, 94.2% and 84.5% integer ambiguity resolutions are realized for the two time links, guaranteeing high-precision time and frequency transfer.

Figure 5 depicts the time difference of the NIST-AMC4 time link, from which the gain achieved from the ionosphere-weighted UDUC model compared to the PPP can be seen. The standard deviation of the epoch difference over the week of the link values concerning the mean is also 16.4% lower for the ionosphere-weighted UDUC model (5.61 ps) than for PPP (6.71 ps). Concerning the frequency stability in Fig. 6, we can see the improvement with the UDUC model for both the short- and long-term. For averaging times at a few 1000 s and below, the frequency stability of the ionosphere-weighted UDUC model is 15% to 30% better than that of the PPP. In addition, the frequency stability for an averaging time of 1 day of the UDUC model is 9.0% higher than that of the PPP model, which is not significant but demonstrates the improvement in long-term stability.

Similar to Figs. 5 and 6, 7 and 8 show the time and frequency transfer results but for the BRUX-OPMT time link.

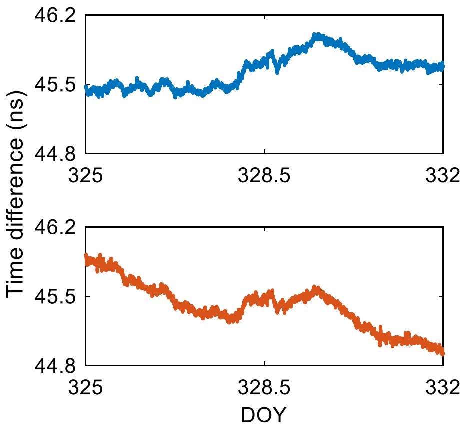

Fig. 5 A medium-baseline time link of the NIST-AMC4 at the NIST and the USNO computed with the ionosphere-weighted UDUC model (top) and the PPP (bottom) from 21 to 27 November 2021

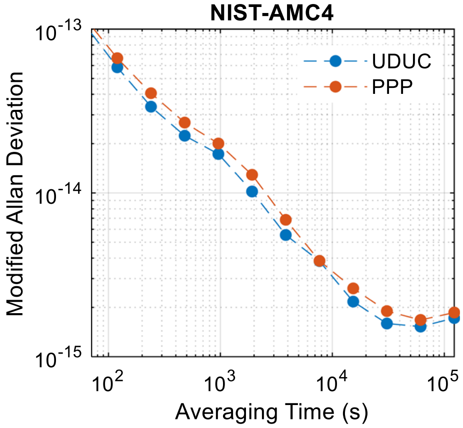

Fig. 6 Comparison of the MDEV between the ionosphere-weighted UDUC model and the PPP for the NIST-AMC4 time-link

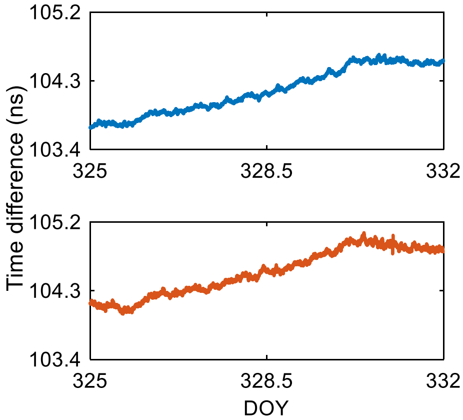

Fig. 7 A medium-baseline time link of the BRUX-OPMT at the ROB and the OP computed with the ionosphere-weighted UDUC model (top) and the PPP (bottom) from 21 to 27 November 2021

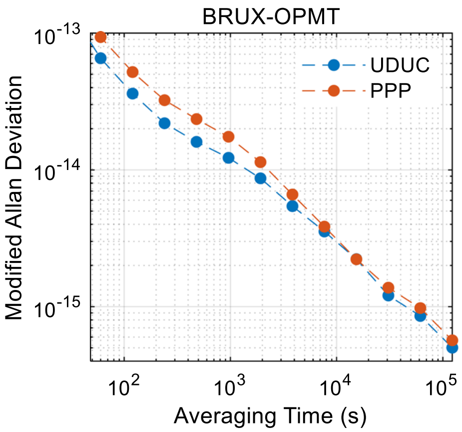

Fig. 8 Comparison of the MDEV between the ionosphere-weighted UDUC model and the PPP for the BRUX-OPMT time-link

It can be observed from Fig. 7 that the ionosphere-weighted UDUC model reduces the noise of time difference. The standard deviation over the test week of the epoch difference for the ionosphere-weighted UDUC model and the PPP is 4.37 ps and 5.94 ps, respectively. Figure 8 reflects the improvement of the ionosphere-weighted UDUC model in frequency stability compared with PPP, from which two phenomena are worth mentioning. First, the ionosphere-weighted UDUC model has 10–25% higher frequency stability than the PPP for averaging times at a few 1000 s and below. Second, at a few thousand to tens of thousands of seconds average time of frequency stability, the improvement of the ionosphere-weighted UDUC model became less noticeable (10–15%). This can be attributed to the weak ionospheric constraint due to the length of the BRUX-OPMT (262.3 km). Therefore, the contribution of this constraint becomes invalid in the later stage of filtering. Hence, the difference in long-term frequency stability between the ionosphere-weighted UDUC model and the PPP is smaller.

4.4 Long-baseline time and frequency transfer

In this scenario, the first time link is the PTBB-ROAG, a baseline length of 2182.3 km. In this situation, the number of common-view satellites is small, so it isn't easy to benefit from the ionosphere-float UDUC model. Therefore, two short baselines are used to calculate the time of PTBB and ROAG stations, respectively. Then a simple difference is performed to realize the long baseline time transfer between them. Both PTB and ROA time laboratories have multiple GNSS receivers available. Therefore, the clocks of PTBB and ROAG with ambiguity-fixed can be obtained by calculating PTBB-PT11 and ROAG-SFER, respectively, using the ionosphere-fixed UDUC model. Figure 9 shows the time differences of the time link, the variation of the time difference sequence of the UDUC model is smaller than that of PPP. The

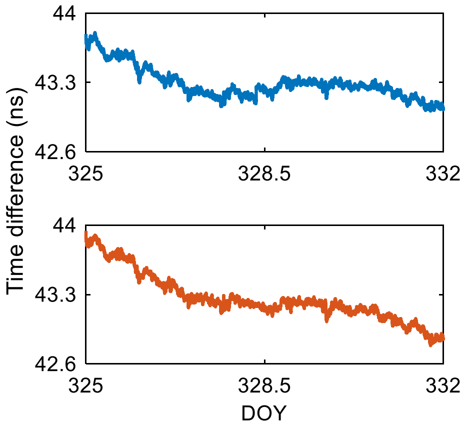

Fig. 9 A long-baseline time link of the PTBB-ROAG at the PTB and the ROA computed with the UDUC model (top) and the PPP (bottom) from 21 to 27 November 2021

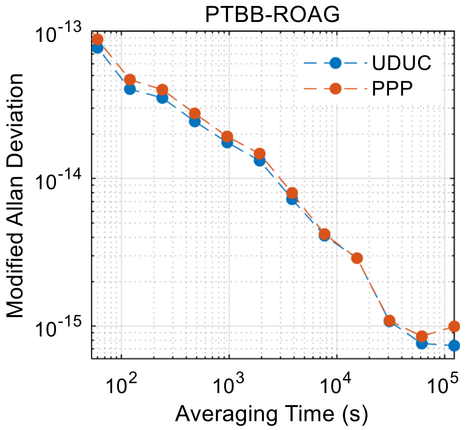

Fig. 10 Comparison of the MDEV between the UDUC model and the PPP for the PTBB-ROAG time-link

standard deviation of the epoch difference for the UDUC model is 4.72 ps, 9.40% lower than the 5.21 ps obtained using PPP. Figure 10 illustrates the frequency stability of the UDUC model and the PPP. The UDUC model improves frequency stability for averaging times at a few 1000 s and below. For averaging times within 4000 to 30,000 s, the performance of the UDUC model becomes close to that of the PPP. It can be seen that the frequency stability of the UDUC model performs better than the PPP at and over 1 day average time. The reasons can be explained as follows. First, the UDUC model can achieve fast integer ambiguity resolution with ionospheric constraints, thus improving the short-term stability. Second, at a few hours of averaging, the accuracy of the UDUC model is similar to that of the convergent PPP and IPPP, and the satellite clock products play the main influencing factor. Third, for the long-term frequency stability, the integer ambiguity resolution can maintain parameter estimation accuracy and perform better than PPP, which has also been verified in IPPP.

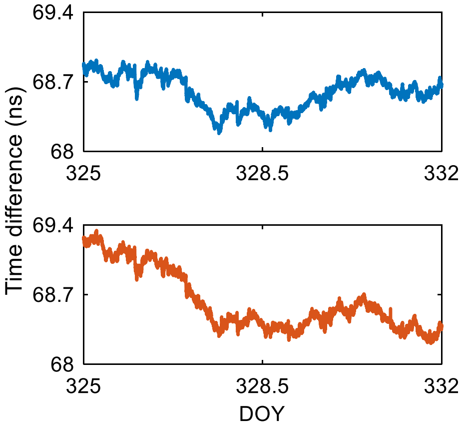

Fig. 11 A long-baseline time link of USN7-ROAG at the USNO and the ROA computed with the UDUC model (top) and the PPP (bottom) from 21 to 27 November 2021

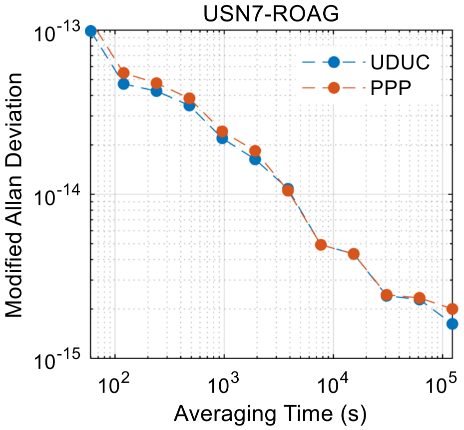

Fig. 12 Comparison of MDEV between the UDUC model and the PPP on USN7-ROAG time-link

Another long-baseline test is for the time link between USN7 and ROAG, with a length of 5863.3 km. Similarly, the clocks of USN7 and ROAG are obtained by calculating USN7-USN8 and ROAG-SFER using the ionosphere-fixed UDUC model so that the time and frequency transfer between USN7 and ROAG is realized. As we can see, this is exactly the time link involved in the two experiments of the short-baseline time and frequency transfer. As shown in Fig. 11, the standard deviation of the epoch difference for the PPP and the UDUC model is 6.06 ps and 6.91 ps, showing a 12.3% improvement. The frequency stability is depicted in Fig. 12, from which we can get a similar conclusion as in the PTBB-ROAG time link. Indeed, the UDUC model performed better at levels where the average time is below a few hours and over 1 day. Taking the result at 120 s, 3840 s and 1-day average time as an example, the frequency stability of the PPP model is 5.5×10^{-14}, 1.1×10^{-14} and 2.1×10^{-15}, and of the UDUC model is 4.7×10^{-14}, 1.1×10^{-14} and 1.8×10^{-15}, with 14.5%, 0% and 14.3% improvement, respectively (Fig. 12).

5 Conclusions

In this contribution, we presented a time and frequency transfer model with integer ambiguity resolution based on the UDUC observations. This model has the following characteristics, making it well suited for the time and frequency transfer in multi-constellation and multi-frequency scenarios. First, the UDUC model has flexibility that can easily be extended to any number of frequencies and constellations. Second, the UDUC model forms the DD ambiguities, enabling the integer ambiguity resolution, and thus recovers the high-precision of carrier phase observations. Third, there is a chance to apply ionospheric constraints for short and medium baselines, thus, further strengthening the observations model.

In short- and medium-baseline time and frequency transfer, with the ionosphere-fixed and ionosphere-weighted UDUC models applied and the integer ambiguities resolved, the time differences obtained by the ionosphere-fixed and ionosphere-weighted UDUC model have shown smaller noise than that by using PPP. Consequently, in terms of frequency stability, the improvement of the ionosphere-fixed (25–60%) and ionosphere-weighted (9–30%) models over the PPP for averaging time from several tens of seconds to 1 day can be observed. These experiments fully illustrate the advantages of the UDUC model with ionospheric constraints and integer ambiguity resolution in improving time and frequency transfer performance over short and medium baselines.

In long-baseline time and frequency transfer, the number of common-view satellites is small, and the realization of integer ambiguity resolution is difficult. Hence, the ionospheric-float UDUC model is similar to the PPP. In this case, we introduced a reference station at each end of the time comparison to utilize the advantages of the ionospheric constraints and obtain integer ambiguity resolution. The results show that the frequency stability of the UDUC model performs better than the PPP for averaging time below a few thousands second and over 1 day, which fully demonstrates the advantages of the proposed models.

This study provides experience in the implementation of time and frequency transfer at the UDUC level. It facilitates our understanding of the advantages of integer ambiguity resolution in time and frequency transfer. The performance of the UDUC model in time and frequency transfer within the framework of multi-frequency multi-constellation will be the focus of our future work.

Acknowledgements This work was partially funded by the Australian Research Council Discovery Project (Grant No. DP 190102444), the National Natural Science Foundation of China (Grant No. 42022025), the Open Fund of Hubei Luojia Laboratory Project (Grant No. 2201000061), and the National Time Service Center, Chinese Academy of Sciences (No. E167SC14). We thank the time laboratories for providing GNSS data, including the PTB, the OP, the ROA, the ROB, the NIST and the USNO. We also thank the IGS for providing precise orbit, clock products and data. The corresponding author is supported by the CAS Pioneer Hundred Talents Program.

Author contributions XM and BZ proposed the method and designed the research, developed the software, processed the data, and wrote the manuscript. AE, KW and YY revised the manuscript and shared in the discussions related to the proposed methods.

Data availability The RINEX data and precise products acquired from the IGS network can be downloaded at https://cddis.nasa.gov/archive/gnss/.

Declarations

Conflict of interest The authors declare that they have no conflict of interest.

References

1. Banville S, Hassen E, Lamothe P, Farinaccio J, Donahue B, Mireault Y, Goudarzi M, Collins P, Ghoddousi-Fard R, Kamali O (2021) Enabling ambiguity resolution in CSRS-PPP. Navig J Inst Navig 68(2):433–451. https://doi.org/10.1002/navi.423
2. Davis J, Shemar S, Whibberley P (2011) A Kalman filter UTC(k) prediction and steering algorithm. In: 2011 Joint Conference of the IEEE International Frequency Control Symposium/European Frequency and Time Forum Proceedings, pp 779–784. https://doi.org/10.1109/FCS.2011.5977793
3. Defraigne P (2017) GNSS time and frequency transfer. In: Teunissen PJ, Montenbruck O (eds) Springer handbook of global navigation satellite systems. Springer handbooks. Springer, Cham. https://doi.org/10.1007/978-3-319-42928-1_41
4. Defraigne P, Baire Q (2011) Combining GPS and GLONASS for time and frequency transfer. Adv Space Res 47(2):265–275. https://doi.org/10.1016/j.asr.2010.07.003
5. Defraigne P, Aerts W, Pottiaux E (2015) Monitoring of UTC(k)'s using PPP and IGS real-time products. GPS Solut 19(1):165–172. https://doi.org/10.1007/s10291-014-0377-5
6. Dow J, Neilan R, Rizos C (2009) The international GNSS service in a changing landscape of global navigation satellite systems. J Geod 83(7):689–689. https://doi.org/10.1007/s00190-009-0315-4
7. Ge Y, Zhou F, Liu T, Qin W, Wang S, Yang X (2019) Enhancing real-time precise point positioning time and frequency transfer with receiver clock modeling. GPS Solut 23(1):1–14. https://doi.org/10.1007/s10291-018-0814-y

8. Ge Y, Ding S, Qin W, Zhou F, Yang X, Wang S (2020) Performance of ionospheric-free PPP time transfer models with BDS-3 quad-frequency observations. Measurement 160:107836. https://doi.org/10.1016/j.measurement.2020.107836
9. Geng J, Shi C, Ge M, Dodson A, Lou Y, Zhao Q, Liu J (2012) Improving the estimation of fractional-cycle biases for ambiguity resolution in precise point positioning. J Geod 86(8):579–589. https://doi.org/10.1007/s00190-011-0537-0
10. Geng J, Guo J, Meng X, Gao K (2020) Speeding up PPP ambiguity resolution using triple-frequency GPS/BeiDou/Galileo/QZSS data. J Geod 94(1):1–15. https://doi.org/10.1007/s00190-019-01330-1
11. Guyennon N, Cerretto G, Tavella P, Lahaye F (2009) Further characterization of the time transfer capabilities of precise point positioning (PPP): the sliding batch procedure. IEEE Trans Ultrason Ferroelectr Freq Control 56(8):1634–1641. https://doi.org/10.1109/Tuffc.2009.1228
12. He Y, Baldwin K, Orr B, Warrington R, Wouters M, Luiten A, Mirtschin P, Tzioumis T, Phillips C, Stevens J, Lennon B, Munting S, Aben G, Newlands T, Rayner T (2018) Long-distance telecom-fiber transfer of a radio-frequency reference for radio astronomy. Optica 5(2):138–146. https://doi.org/10.1364/Optica.5.000138
13. Johnston G, Riddell A, Hausler G (2017) The International GNSS Service. In: Teunissen P, Montenbruck O (eds) Springer handbook of global navigation satellite systems, 1st edn. Springer, Cham, pp 967–982. https://doi.org/10.1007/978-3-319-42928-1
14. Kanj A, Valat D, Delporte J (2014) Absolute calibration of GNSS time transfer systems at CNES. In: 2014 European frequency and time forum (EFTF). IEEE, pp 459–462. https://doi.org/10.1109/EFTF.2014.7331535
15. Khodabandeh A, Teunissen P (2016) PPP-RTK and inter-system biases: the ISB look-up table as a means to support multi-system PPP-RTK. J Geod 90(9):837–851. https://doi.org/10.1007/s00190-016-0914-9
16. Khodabandeh A, Teunissen P (2018) On the impact of GNSS ambiguity resolution: geometry, ionosphere, time and biases. J Geod 92(6):637–658. https://doi.org/10.1007/s00190-017-1084-0
17. Leandro R, Langley R, Santos M (2008) UNB3m_pack: a neutral atmosphere delay package for radiometric space techniques. GPS Solut 12(1):65–70. https://doi.org/10.1007/s10291-007-0077-5
18. Lee S, Schutz B, Lee C, Yang S (2008) A study on the Common-View and All-in-View GPS time transfer using carrier-phase measurements. Metrologia 45(2):156–167. https://doi.org/10.1088/0026-1394/45/2/005
19. Lewandowski W, Petit G, Thomas C (1993) Precision and accuracy of GPS time transfer. IEEE Trans Instrum Meas 42(2):474–479. https://doi.org/10.1109/19.278607
20. Lisdat C, Grosche G, Quintin N, Shi C, Raupach S, Grebing C, Nicolodi D, Stefani F, Al-Masoudi A, Dorscher S, Hafner S, Robyr J, Chiodo N, Bilicki S, Bookjans E, Koczwara A, Koke S, Kuhl A, Wiotte F, Meynadier F, Camisard E, Abgrall M, Lours M, Legero T, Schnatz H, Sterr U, Denker H, Chardonnet C, Le Coq Y, Santarelli G, Amy-Klein A, Le Targat R, Lodewyck J, Lopez O, Pottie P (2016) A clock network for geodesy and fundamental science. Nat Commun 7(1):1–7. https://doi.org/10.1038/ncomms12443
21. Liu T, Yuan Y, Zhang B, Wang N, Tan B, Chen Y (2017) Multi-GNSS precise point positioning (MGPPP) using raw observations. J Geod 91(3):253–268. https://doi.org/10.1007/s00190-016-0960-3
22. Lopez O, Kanj A, Pottie P, Rovera D, Achkar J, Chardonnet C, Amy-Klein A, Santarelli G (2013) Simultaneous remote transfer of accurate timing and optical frequency over a public fiber network. Appl Phys B Lasers Opt 110(1):3–6. https://doi.org/10.1007/s00340-012-5241-0
23. Luna D, Perez D, Cifuentes A, Gomez D (2017) Three-cornered hat method via GPS common-view comparisons. IEEE Trans Instrum Meas 66(8):2143–2147. https://doi.org/10.1109/Tim.2017.2684918
24. Mi X, Zhang B, Yuan Y (2019a) Multi-GNSS inter-system biases: estimability analysis and impact on RTK positioning. GPS Solut 23(3):1–13. https://doi.org/10.1007/s10291-019-0873-8
25. Mi X, Zhang B, Yuan Y (2019b) Stochastic modeling of between-receiver single-differenced ionospheric delays and its application to medium baseline RTK positioning. Meas Sci Technol 30(9):095008. https://doi.org/10.1088/1361-6501/ab11b5
26. Mi X, Zhang B, Odolinski R, Yuan Y (2020) On the temperature sensitivity of multi-GNSS intra- and inter-system biases and the impact on RTK positioning. GPS Solut 24(4):1–14. https://doi.org/10.1007/s10291-020-01027-5
27. Mi X, Sheng C, El-Mowafy A, Zhang B (2021) Characteristics of receiver-related biases between BDS-3 and BDS-2 for five frequencies including inter-system biases, differential code biases, and differential phase biases. GPS Solut 25(3):1–11. https://doi.org/10.1007/s10291-021-01151-w
28. Milner W, Robinson J, Kennedy C, Bothwell T, Kedar D, Matei D, Legero T, Sterr U, Riehle F, Leopardi H, Fortier T, Sherman J, Levine J, Yao J, Ye J, Oelker E (2019) Demonstration of a timescale based on a stable optical carrier. Phys Rev Lett 123(17):173201. https://doi.org/10.1103/PhysRevLett.123.173201
29. Odijk D, Teunissen P (2008) ADOP in closed form for a hierarchy of multi-frequency single-baseline GNSS models. J Geodesy 82(8):473–492. https://doi.org/10.1007/s00190-007-0197-2
30. Odijk D, Zhang B, Khodabandeh A, Odolinski R, Teunissen P (2016) On the estimability of parameters in undifferenced, uncombined GNSS network and PPP-RTK user models by means of *S*-system theory. J Geod 90(1):15–44. https://doi.org/10.1007/s00190-015-0854-9
31. Odijk D, Khodabandeh A, Nadarajah N, Choudhury M, Zhang B, Li W, Teunissen P (2017) PPP-RTK by means of *S*-system theory: Australian network and user demonstration. J Spat Sci 62(1):3–27. https://doi.org/10.1080/14498596.2016.1261373
32. Odolinski R, Teunissen P (2017) Low-cost, 4-system, precise GNSS positioning: a GPS, Galileo, BDS and QZSS ionosphere-weighted RTK analysis. Meas Sci Technol 28(12):125801. https://doi.org/10.1088/1361-6501/aa92eb
33. Odolinski R, Teunissen P, Odijk D (2015) Combined BDS, Galileo, QZSS and GPS single-frequency RTK. GPS Solut 19(1):151–163. https://doi.org/10.1007/s10291-014-0376-6
34. Petit G (2021) Sub-10–16 accuracy GNSS frequency transfer with IPPP. GPS Solut 25(1):1–9. https://doi.org/10.1007/s10291-020-01062-2
35. Petit G, Kanj A, Loyer S, Delporte J, Mercier F, Perosanz F (2015) 1 x 10(-16) frequency transfer by GPS PPP with integer ambiguity resolution. Metrologia 52(2):301–309. https://doi.org/10.1088/0026-1394/52/2/301
36. Ray J, Senior K (2005) Geodetic techniques for time and frequency comparisons using GPS phase and code measurements. Metrologia 42(4):215–232. https://doi.org/10.1088/0026-1394/42/4/005
37. Roberts B, Blewitt G, Dailey C, Murphy M, Pospelov M, Rollings A, Sherman J, Williams W, Derevianko A (2017) Search for domain wall dark matter with atomic clocks on board global positioning system satellites. Nat Commun 8(1):1–9. https://doi.org/10.1038/s41467-017-01440-4
38. Shen Y, Li B, Xu G (2009) Simplified equivalent multiple baseline solutions with elevation-dependent weights. GPS Solut 13(3):165–171. https://doi.org/10.1007/s10291-008-0109-9
39. Su K, Jin S (2019) Triple-frequency carrier phase precise time and frequency transfer models for BDS-3. GPS Solut 23(3):1–12. https://doi.org/10.1007/s10291-019-0879-2
40. Teunissen P (1995) The least-squares ambiguity decorrelation adjustment: a method for fast GPS integer ambiguity estimation. J Geod 70(1–2):65–82. https://doi.org/10.1007/Bf00863419

41. Teunissen P (1998) The ionosphere-weighted GPS baseline precision in canonical form. J Geod 72(2):107–117. https://doi.org/10.1007/s001900050152
42. Teunissen P (1999) The probability distribution of the GPS baseline for a class of integer ambiguity estimators. J Geod 73(5):275–284. https://doi.org/10.1007/s001900050244
43. Teunissen P (2018) Distributional theory for the DIA method. J Geod 92(1):59–80. https://doi.org/10.1007/s00190-017-1045-7
44. Teunissen P, Khodabandeh A (2015) Review and principles of PPP-RTK methods. J Geod 89(3):217–240. https://doi.org/10.1007/s00190-014-0771-3
45. Teunissen P, Verhagen S (2009) The GNSS ambiguity ratio-test revisited: a better way of using it. Surv Rev 41(312):138–151. https://doi.org/10.1179/003962609x390058
46. Teunissen P (2020) GNSS precise point positioning. In: Position, navigation, and timing technologies in the 21st century: integrated satellite navigation, sensor systems, and civil applications, vol 1, pp 503–528. https://doi.org/10.1002/9781119458449.ch20
47. Tu R, Zhang P, Zhang R, Liu J, Lu X (2019) Modeling and performance analysis of precise time transfer based on BDS triple-frequency un-combined observations. J Geod 93(6):837–847. https://doi.org/10.1007/s00190-018-1206-3
48. Weinbach U, Schön S (2013) Improved GRACE kinematic orbit determination using GPS receiver clock modeling. GPS Solut 17(4):511–520. https://doi.org/10.1007/s10291-012-0297-1
49. Zha J, Zhang B, Liu T, Hou P (2021) Ionosphere-weighted undifferenced and uncombined PPP-RTK: theoretical models and experimental results. GPS Solut 25(4):1–12. https://doi.org/10.1007/s10291-021-01169-0
50. Zhang B, Chen Y, Yuan Y (2019) PPP-RTK based on undifferenced and uncombined observations: theoretical and practical aspects. J Geod 93(7):1011–1024. https://doi.org/10.1007/s00190-018-1220-5
51. Zhang P, Tu R, Gao Y, Zhang R, Han J (2020) Performance of Galileo precise time and frequency transfer models using quad-frequency carrier phase observations. GPS Solut 24(2):1–18. https://doi.org/10.1007/s10291-020-0955-7
52. Zhang B, Hou P, Zha J, Liu T (2021) Integer-estimable FDMA model as an enabler of GLONASS PPP-RTK. J Geod 95(8):1–21. https://doi.org/10.1007/s00190-021-01546-0

3 UDUC GNSS Time Transfer with Satellite Clocks Estimated

The accuracy and effectiveness of GNSS time transfer are inherently linked to the precision of satellite clock products. However, current research in GNSS has yet to thoroughly investigate the influence of these clock products on the overall performance of time transfer. As such, a GNSS time transfer model with integer ambiguity resolution (IAR) and satellite clocks estimated, not provided externally, has been proposed in this chapter, to explore the potential of GNSS time transfer. The research work and findings of this chapter are presented in the following publication:

Mi, X., Zhang, B., El-Mowafy, A., Wang, K., & Yuan, Y. (2023). On the potential of undifferenced and uncombined GNSS time and frequency transfer with integer ambiguity resolution and satellite clocks estimated. GPS Solutions, 27(1), 25. https://doi.org/10.1007/s10291-022-01363-8

GPS Solutions (2023) 27:25
https://doi.org/10.1007/s10291-022-01363-8

ORIGINAL ARTICLE

On the potential of undifferenced and uncombined GNSS time and frequency transfer with integer ambiguity resolution and satellite clocks estimated

Xiaolong Mi[1] · Baocheng Zhang[2,5] · Ahmed El-Mowafy[1] · Kan Wang[3,4] · Yunbin Yuan[2]

Received: 9 June 2022 / Accepted: 2 November 2022 / Published online: 23 November 2022

Abstract

The use of global navigation satellite systems (GNSS) has been a competitive way to provide high-precision and low-cost time and frequency transfer results. However, the traditional GNSS method, the precise point positioning (PPP), is usually based on the ionosphere-free (IF) combination, which is not flexible when applying multi-frequency scenarios. In addition, PPP relies on precise satellite clock products with an accuracy of tens of picoseconds, limiting the time and frequency transfer performance. More importantly, achieving integer ambiguity resolution (IAR) is challenging, which makes high-precision phase observations underutilized. To achieve a better time transfer performance, we must consider all those factors from the GNSS end. In this contribution, a new GNSS time and frequency model at the undifferenced and uncombined (UDUC) level is first derived. In the UDUC model, the satellite clocks are estimated together with other parameters, and the integer ambiguities are resolved in the double-differenced (DD) form for their reliable estimation. Our numerical tests suggest three major findings. First, with integer ambiguities resolved, the UDUC model with satellite clocks fixed showed a 20% to 50% improvement compared with the UDUC PPP model. Second, with IAR and satellite clocks estimated, the proposed UDUC model shows a 10%–40% improvement over the model with satellite clocks fixed. Third, with integer ambiguities resolved and satellite clocks estimated, GPS, Galileo, and BDS-3 all have the potential to achieve frequency transfer in the low-mid 10^{-17} range for averaging times within one day.

Keywords Time and frequency transfer · Global navigation satellite system (GNSS) · Integer ambiguity resolution (IAR) · Undifferenced and uncombined · Common-clock · BDS-3

Introduction

The Optical fiber, Two-Way Satellite Time and Frequency Transfer (TWSTFT), and Global Navigation Satellite System (GNSS) are three technical means of time and frequency transfer (Matsakis et al. 2014). Optical fiber has high accuracy but is expensive and its operating range is limited (Huang et al. 2016). The advantage of TWSTFT is that it utilizes the symmetry of a two-way signal propagation to achieve high precision (Fujieda et al. 2014). GNSS is currently the most widely used time transfer technology due to its simplicity and low cost (Defraigne et al. 2015; Guyennon et al. 2009). Compared with the common-view (CV) and all-in-view (AV) approaches, precise point positioning (PPP) uses phase observations and is not limited by distance, so it is widely used in the comparison of International Atomic Time (TAI) and Coordinated Universal Time (UTC) (Defraigne et al. 2013; Rose et al. 2014; Yao et al. 2015).

✉ Baocheng Zhang
b.zhang@whigg.ac.cn

[1] School of Earth and Planetary Sciences, Curtin University, Perth, Australia

[2] State Key Laboratory of Geodesy and Earth's Dynamics, Innovation Academy for Precision Measurement Science and Technology, Chinese Academy of Sciences, Wuhan, China

[3] National Time Service Center, Chinese Academy of Sciences, Xi'an, China

[4] University of Chinese Academy of Sciences, Beijing, China

[5] State Key Laboratory of Satellite Navigation System and Equipment Technology, The 54th Research Institute of China Electronics Technology Group Corporation, Shijiazhuang 050081, China

Classical PPP is usually based on an ionosphere-free (IF) combination and is usually applied to dual-frequency observations (Khodabandeh and Teunissen 2016). IF PPP is favored because the ionospheric delays, which are of no interest in time and frequency transfer, are eliminated. However, only one independent parameter, the ionospheric delay, gets eliminated, while more than one observable is sacrificed (Teunissen 2020). Compared with the IF combination, one can turn to the undifferenced and uncombined (UDUC) method, which is applied using original and uncorrelated observations and thus is flexible in multi-frequency scenarios (Odijk et al. 2016; Tu et al. 2019). The UDUC method has the added advantage of flexibly imposing dynamic constraints on all parameters to strengthen the model to the best extent possible (Zhang et al. 2019).

PPP can provide the synchronization error between the receiver time and the precise satellite clock products. These products are estimated by a global network comprising hundreds of GNSS receivers (Shi et al. 2019; Zhang et al. 2011). The International GNSS Service (IGS) final satellite clock products can achieve tens of picoseconds of precision (Guo and Geng 2018), while real-time satellite clocks can only achieve sub-nanosecond (Chen et al. 2018; Huang et al. 2014). The precision of the PPP-based time and frequency transfer thus relies on the precision of the satellite clock products used. Therefore, it is difficult for PPP to achieve a time transfer of precision of higher than a few dozen picoseconds, even with the final products.

The fixed integer carrier phase ambiguity is normally not targeted in the traditional PPP (Delporte et al. 2007; Petit et al. 2014). However, to retrieve information of high precision from GNSS, the integer characteristics of phase ambiguity should be recovered. Khodabandeh and Teunissen (2018) have theoretically proved the benefit of integer ambiguity resolution (IAR) on time and frequency transfer. Petit et al. (2015) have proposed the concept of integer PPP (IPPP) and achieved IAR in time and frequency transfer by considering the fractional cycle biases (FCB) (Geng et al. 2012). However, IPPP is also dependent on external precise satellite clock products (Petit 2021), just like the PPP. In addition, IPPP is still based on the IF combination, so it is not flexible in multi-frequency scenarios.

The precision and stability of optical clocks are about two orders of magnitude higher than the best cesium atomic clocks (Nicholson et al. 2015; Schuldt et al. 2021). Such unprecedented accuracy of optical clocks increases the requirements for time and frequency transfer techniques. However, the current PPP-based time and frequency transfer techniques cannot meet the standard of optical clocks. To better understand the potential of GNSS in time and frequency, it is necessary to study the impacts of the GNSS algorithm and equipment (Yao and Levine 2016), as this will determine whether GNSS can serve the optical clocks in the future.

We propose a new time and frequency transfer model in which satellite clocks are estimated together with other parameters. The model is based on UDUC GNSS observations as they have several advantages (Odijk et al. 2017; Zhang et al. 2019). After removing the rank deficiencies, the ambiguities are presented in a double-differenced (DD) form and then fixed using IAR strategies, ensuring that high-precision carrier phase observations are efficiently utilized. The paper aims to study the impacts of IAR and the precise satellite clock product and further explores the potential of GNSS time and frequency transfer using the proposed model. To explore the time transfer potential of GNSS itself, the common-clock time links are established to free the impact of external clocks. A common-clock time link refers to a time link connected to the same external atomic clock.

The next section presents a developed time and frequency model with IAR and satellite clocks estimated (from now on referred to as SCE model). In addition, the UDUC PPP model and the UDUC model with IAR and satellite clocks fixed (SCF model in what follows) are also derived to demonstrate the advantages of IAR and satellite clocks estimation. The following section presents the time and frequency transfer results for GPS, Galileo, and BDS-3 based on time links with zero and short baselines. Finally, in the last section, we summarize our findings and give our conclusions.

Methodology

In this section, we present three variants of the GNSS time and frequency transfer model: the UDUC PPP model, the SCF model, and the SCE model. We will show the process of constructing a full-rank GNSS time and transfer model with the help of the *S*-system theory (Odijk et al. 2016).

UDUC GNSS observation equations

AS the starting point of developing the GNSS time and frequency transfer model, we first give the equations for UDUC GNSS code and phase observations, which reads

$$
\begin{aligned}
p^s_{r,j} &= \rho^s_r + \tau^s_r + dt_r - dt^s + \mu_j I^s_r + d_{r,j} - d^s_{,j} + \varepsilon^s_{p,j} \\
\phi^s_{r,j} &= \rho^s_r + \tau^s_r + dt_r - dt^s - \mu_j I^s_r + \lambda_j N^s_{r,j} + \delta_{r,j} - \delta^s_{,j} + \varepsilon^s_{\phi,j}
\end{aligned}
\tag{1}
$$

where s, r, j represent the satellite, receiver, and frequency, respectively; $p^s_{r,j}$ and $\phi^s_{r,j}$ are the UDUC code and phase observables, respectively; ρ^s_r is the satellite-receiver range, τ^s_r is the tropospheric delay; dt_r and dt^s are the receiver and satellite clock offsets, respectively; I^s_r is the ionospheric delay on the first frequency and $\mu_j = \lambda_j^2 \big/ \lambda_1^2$ is the coefficient where λ_j is the wavelength on frequency j;$N_{r,j}^s$ is the undifferenced integer phase ambiguity. $d_{r,j}$ and $d_{,j}^s$ are the receiver and satellite code biases, respectively, and their counterpart $\delta_{r,j}$ and $\delta_{,j}^s$ are the receiver and satellite phase biases; $\varepsilon_{p,j}^s$ and $\varepsilon_{\phi,j}^s$ are the code and phase observation noise and miss-modeled random effects.

Model A: UDUC PPP model

Equation (1) represents a rank-deficient system, which means not all the unknowns can be solved separately, but only their linear combinations. Therefore, as the first step in constructing the full-rank model, it is necessary to identify and eliminate these rank deficiencies, which can be done using the S-system theory. For instance, assuming that m satellites with f frequencies are tracked, then several rank deficiencies need to be eliminated in (1) (Table 1).

As known, precise satellite clock products $d\tilde{t}^s = dt^s + d_{,IF}^s$ based on IF combination are essential for the PPP, where $d_{,IF}^s = \frac{\mu_2}{\mu_2-\mu_1} d_{,1}^s - \frac{\mu_1}{\mu_2-\mu_1} d_{,2}^s$. As such, the rank deficiencies between the receiver and satellite clocks and that between the satellite clocks, code biases, and phase biases no longer exist. Applying the S-system theory can solve the remaining six rank deficiencies, with the original parameters lumped to form the new estimable parameters (Mi et al. 2019; Odijk et al. 2016). Table 2 gives these estimable parameters and their interpretations in the UDUC PPP model. The tropospheric delay is solved in its original form, which is expressed as the sum of the dry and wet delays $\tau_r^s = (\tau_d)_r^s + m_r^s \tau_r$ (Boehm et al. 2006; Zhang et al. 2021). $(\tau_d)_r^s$ is the dry part, which can be corrected a priori using empirical models (Tuka and El-Mowafy, 2013). $m_r^s \tau_r$ is the wet part, which is modeled as the product of a pre-defined mapping function m_r^s and the unknown wet part of the unknown tropospheric wet zenith delay (ZWD) τ_r.

With the rank deficiencies solved, the full-rank UDUC PPP model for time and frequency transfer is expressed as

$$\begin{aligned} \tilde{p}_{r,j}^s &= \rho_r^s + m_r^s \tau_r + d\tilde{t}_r + \mu_j \tilde{I}_r^s - \tilde{d}_{r,j}^s + \varepsilon_{p,j}^s \\ \tilde{\phi}_{r,j}^s &= \rho_r^s + m_r^s \tau_r + d\tilde{t}_r - \mu_j \tilde{I}_r^s - \tilde{\delta}_{r,j}^s + \varepsilon_{\phi,j}^s \end{aligned} \tag{2}$$

where $\tilde{p}_{r,j}^s = p_{r,j}^s + d\tilde{t}^s - (\tau_d)_r^s$ and $\tilde{\phi}_{r,j}^s = \phi_{r,j}^s + d\tilde{t}^s - (\tau_d)_r^s$.

Model B: SCF model

The disadvantage of the classical PPP model with float ambiguities is that it does not take full advantage of the integer nature of phase ambiguities, which can be solved by considering common-view satellites between two receivers. Assuming the time and frequency transfer is implemented between two receivers A and B, then the satellite code and phase biases $d_{,j}^s - d_{,IF}^s - \mu_j d_{,GF}^s$ and $\delta_{,j}^s - d_{,IF}^s + \mu_j d_{,GF}^s$ are the same for the receivers A and B with the same satellites tracked. Taking some common parameters as the S-basis, the number of estimated parameters can be reduced, and the phase ambiguities can be

Table 2 Estimable unknown parameters and their interpretation formed by a commonly used S-basis in PPP (Liu et al. 2017), where $d_{r,GF} = \frac{1}{\mu_2-\mu_1}(d_{r,2} - d_{r,1})$, $d_{,GF}^s = \frac{1}{\mu_2-\mu_1}(d_{,2}^s - d_{,1}^s)$ and $d_{r,IF} = \frac{\mu_2}{\mu_2-\mu_1} d_{r,1} - \frac{\mu_1}{\mu_2-\mu_1} d_{r,2}$ (GF: geometry-free)

Estimable parameter	Notation and interpretation
Receiver clock	$d\tilde{t}_r = dt_r + d_{r,IF}$
Satellite code bias	$\tilde{d}_{r,j}^s = d_{,j}^s - d_{,IF}^s - \mu_j d_{,GF}^s - d_{r,j} + d_{r,IF} + \mu_j d_{r,GF}$; $j \geq 3$
Satellite phase bias	$\tilde{\delta}_{r,j}^s = \delta_{,j}^s - d_{,IF}^s + \mu_j d_{,GF}^s - \lambda_j N_{r,j}^s - \delta_{r,j} + d_{r,IF} - \mu_j d_{r,GF}$; $j \geq 1$
Ionospheric delay	$\tilde{I}_r^s = I_r^s + d_{r,GF} - d_{,GF}^s$
S-basis parameters	$d_{r,j}$, $\delta_{r,j}$, $d_{r,IF}$,$N_{r,j}^s$, $d_{r,GF}$, $d_{,GF}^s$

Table 1 Rank deficiencies in the UDUC GNSS observation equations, together with the sources and sizes of those rank deficiencies as presented in (1) (Odijk et al. 2016)

Type	Source of those rank deficiencies	Size
1	Between the receiver and satellite clocks	1
2	Between the receiver and satellite code biases	f
3	Between the receiver and satellite phase biases	f
4	Between the receiver clocks, code biases, and phase biases	1
5	Between the satellite clocks, code biases, and phase biases	m
6	Between the satellite phase biases and ambiguities	$f \times m$
7	Between the ionospheric delays and receiver code/phase biases	1
8	Between the ionospheric delays and satellite code/phase biases	m

constructed in the DD form, which is the most reliable form for IAR. In this situation, IAR can be realized through DD integer ambiguities, while precise external products provide satellite clocks, so this model can be called the SCF model. With IAR and satellite clocks introduced from external sources, the SCF model can be expressed as follows:

$$
\begin{aligned}
\tilde{p}^s_{A,j} &= \rho^s_A + m^s_A\tau_A + d\tilde{t}_A + \mu_j\tilde{I}^s_A - \tilde{d}^s_{A,j} + \varepsilon^s_{p,j}\\
\tilde{\phi}^s_{A,j} &= \rho^s_A + m^s_A\tau_A + d\tilde{t}_A - \mu_j\tilde{I}^s_A - \tilde{\delta}^s_{A,j} + \varepsilon^s_{\phi,j}\\
\tilde{p}^s_{B,j} &= \rho^s_B + m^s_B\tau_B + d\tilde{t}_B + \mu_j\tilde{I}^s_B - \tilde{d}^s_{A,j} + \tilde{d}_{AB,j} + \varepsilon^s_{p,j}\\
\tilde{\phi}^s_{B,j} &= \rho^s_B + m^s_B\tau_B + d\tilde{t}_B - \mu_j\tilde{I}^s_B - \tilde{\delta}^s_{A,j} + \tilde{\delta}_{AB,j} + \lambda_j N^{1s}_{AB,j} + \varepsilon^s_{\phi,j}
\end{aligned}
\tag{3}
$$

where $\tilde{p}^s_{r,j}$ and $\tilde{\phi}^s_{r,j}$ have the same definition as given in Equation (2). The interpretation of $\tilde{d}_{AB,j}$,$\tilde{\delta}_{AB,j}$ and $N^{1s}_{AB,j}$ are given in Table 3.

Equation (3) can be defined as the ionosphere-float SCF model as no relationship is assumed between I^s_A and I^s_B in this situation. However, for baselines with less than 10 km, I^s_A and I^s_B are sufficiently correlated such that they can be considered approximately equal. In this situation, we can enhance the model strength and achieve fast IAR by considering the regional ionospheric correlation between different receivers. Note in Equation (3) that $\tilde{I}^s_r = I^s_r + d_{r,GF} - d^s_{,GF}$, which includes $d_{r,GF}$ and $d^s_{,GF}$. However, if we choose $\tilde{I}^s_A$ as S-basis, then the between-receiver ionospheric delay can be written as $\tilde{I}^s_{AB} = I^s_{AB} + d_{AB,GF}$. For short baselines less than 10 km, it is safe to assume $I^s_{AB} = 0$ (Odolinski et al. 2015; Teunissen 1997) that the between-receiver differential code bias (DCB) $d_{AB,GF}$ can be separated. This model can be defined as the ionosphere-fixed SCF model, which reads

$$
\begin{aligned}
\tilde{p}^s_{A,j} &= \rho^s_A + m^s_A\tau_A + d\tilde{t}_A + \mu_j\tilde{I}^s_A - \tilde{d}^s_{A,j} + \varepsilon^s_{p,j}\\
\tilde{\phi}^s_{A,j} &= \rho^s_A + m^s_A\tau_A + d\tilde{t}_A - \mu_j\tilde{I}^s_A - \tilde{\delta}^s_{A,j} + \varepsilon^s_{\phi,j}\\
\tilde{p}^s_{B,j} &= \rho^s_B + m^s_B\tau_B + d\tilde{t}_B + \mu_j\tilde{I}^s_A + \mu_j d_{AB,GF} - \tilde{d}^s_{A,j} + \tilde{d}_{AB,j} + \varepsilon^s_{p,j}\\
\tilde{\phi}^s_{B,j} &= \rho^s_B + m^s_B\tau_B + d\tilde{t}_B - \mu_j\tilde{I}^s_A - \mu_j d_{AB,GF} - \tilde{\delta}^s_{A,j} + \tilde{\delta}_{AB,j} + \lambda_j N^{1s}_{AB,j} + \varepsilon^s_{\phi,j}
\end{aligned}
\tag{4}
$$

where the interpretation of the estimated parameters is given in Tables 2 and 3.

Model C: SCE model

The above two variants are free of the first and fifth types of rank deficiencies (in Table 1) with external satellite clocks fixed. However, high-precision time and frequency transfer are significantly impacted by the satellite clock products used. In this section, a time and frequency transfer model is constructed without using precise satellite clocks. For the rank deficiencies shown in Table 1 (except for the first and fifth ones), we would like to use the same S-basis with Model A and Model B. In addition, to construct DD phase ambiguities, the same S-basis are defined as Equation (3). For the new rank deficiency between the receiver and satellite clocks, the clock of receiver A is set as the S-basis. In addition, the new rank deficiencies between satellite clocks, code biases, and phase biases are eliminated by fixing the satellite IF code biases $d^s_{,IF}$ for each satellite. In this case, the satellite clocks are estimated rather than corrected by external sources, so this model can be called the SCE model. In this way, we can access the full-rank SCE model, which reads

$$
\begin{aligned}
\tilde{\tilde{p}}^s_{A,j} &= \rho^s_A - d\tilde{\tilde{t}}^s + \mu_j\tilde{I}^s_A - \tilde{d}^s_{A,j} + \varepsilon^s_{p,j}\\
\tilde{\tilde{\phi}}^s_{A,j} &= \rho^s_A - d\tilde{\tilde{t}}^s - \mu_j\tilde{I}^s_A - \tilde{\delta}^s_{A,j} + \varepsilon^s_{\phi,j}\\
\tilde{\tilde{p}}^s_{B,j} &= \rho^s_B + m^s_B\tau_{AB} + d\tilde{t}_{AB} - d\tilde{\tilde{t}}^s + \mu_j\tilde{I}^s_B - \tilde{d}^s_{A,j} + \tilde{d}_{AB,j} + \varepsilon^s_{p,j}\\
\tilde{\tilde{\phi}}^s_{B,j} &= \rho^s_B + m^s_B\tau_{AB} + d\tilde{t}_{AB} - d\tilde{\tilde{t}}^s - \mu_j\tilde{I}^s_B - \tilde{\delta}^s_{A,j} + \tilde{\delta}_{AB,j} + \lambda_j N^{1s}_{AB,j} + \varepsilon^s_{\phi,j}
\end{aligned}
\tag{5}
$$

where $\tilde{\tilde{p}}^s_{r,j} = p^s_{r,j} - (\tau_d)^s_r$ and $\tilde{\tilde{\phi}}^s_{r,j} = \phi^s_{r,j} - (\tau_d)^s_r$. $d\tilde{\tilde{t}}^s = dt^s - dt_A + d^s_{,IF} - d_{A,IF} - m^s_A\tau_A$ is the estimable satellite clock, and the between-receiver estimable clock is formulated as $d\tilde{t}_{AB} = dt_{AB} + d_{AB,IF}$. As can be seen, without precise satellite clocks, one cannot access the receiver clock of each station, but only the between-receiver clocks. As the ionospheric delay between different receivers is not considered in such a case, this model can be defined as the ionosphere-float SCE model.

For short baselines less than 10 km, if $I^s_{AB} = 0$ is assumed, and then, we choose $\tilde{I}^s_A$ as a S-basis as in (4), the ionosphere-fixed SCE model can be constructed similar to (4) as follows,

Table 3 Estimable unknown parameters and their interpretation as well as the used S-basis in the SCF model

Estimable parameter	Notation and interpretation
Between-receiver code bias	$\tilde{d}_{AB,j}{=}d_{B,j} - d_{A,j} - d_{AB,IF} - \mu_j d_{AB,GF};j \geq 3$
Between-receiver phase bias	$\tilde{\delta}_{AB,j}{=}\delta_{B,j} - \delta_{A,j} - d_{AB,IF} + \mu_j d_{AB,GF} + \lambda_j N^1_{AB,j};j \geq 1$
DD phase ambiguity	$N^{1s}_{AB,j}{=}N^s_{AB,j} - N^1_{AB,j}$
S-basis	$\tilde{d}_{A,j}, \tilde{\delta}_{A,j}, N^1_{AB,j}$

$$
\begin{aligned}
\tilde{\tilde{p}}_{A,j}^{s} &= \rho_A^s - d\tilde{\tilde{t}}^s + \mu_j \tilde{I}_A^s - \tilde{d}_{A,j}^s + \varepsilon_{p,j}^s \\
\tilde{\tilde{\phi}}_{A,j}^{s} &= \rho_A^s - d\tilde{\tilde{t}}^s - \mu_j \tilde{I}_A^s - \tilde{\delta}_{A,j}^s + \varepsilon_{\phi,j}^s \\
\tilde{\tilde{p}}_{B,j}^{s} &= \rho_B^s + m_B^s \tau_{AB} + d\tilde{t}_{AB} - d\tilde{\tilde{t}}^s + \mu_j \tilde{I}_A^s + \mu_j d_{AB,GF} - \tilde{d}_{A,j}^s + \tilde{d}_{AB,j} + \varepsilon_{p,j}^s \\
\tilde{\tilde{\phi}}_{B,j}^{s} &= \rho_B^s + m_B^s \tau_{AB} + d\tilde{t}_{AB} - d\tilde{\tilde{t}}^s - \mu_j \tilde{I}_A^s - \mu_j d_{AB,GF} - \tilde{\delta}_{A,j}^s + \tilde{\delta}_{AB,j} + \lambda_j N_{AB,j}^{1s} + \varepsilon_{\phi,j}^s
\end{aligned}
\tag{6}
$$

where the estimated unknowns and their interpretation are the same as in (5).

Table 4 gives a comparison of the UDUC PPP model (Model A), the SCF model (Model B), and the SCE model (Model C), for a better understanding of them.

Experimental results

This section starts with an outline of the experimental setup, including the characteristics of the experimental data sets considered for this study and our data processing strategies. Following that is an evaluation of the time and frequency transfer performance with the three models using GPS-only at two laboratories. This evaluation aims to illustrate the benefits of IAR and satellite clocks estimation by comparing the three models. Then, the potential of time and frequency performance of the SCE model using GPS, Galileo and BDS-3 is evaluated.

Experimental setup

We collected GNSS data from three laboratories, including the United States Naval Observatory (USNO), USA, the Physikalisch-Technische Bundesanstalt (PTB), Germany, and the Innovation Academy for Precision Measurement Science and Technology (APM), Chinese Academy of Sciences, China. The relevant characteristics of these experimental data sets considered for this study are shown in Table 5, including the station name, institute, reference clock, receiver and antenna type, and location of the receivers.

The first set of receivers, operated by the USNO with the same H-maser clock, create one zero baseline (USN7-USN8). We collect GPS observations at both L1 and L2 of those receivers at the USNO from August 7 to 13, 2021. At the PTB, the receivers of PTBB and PT10 are connected to the same H-maser clock, forming a short baseline, with data collection from February 4 to 10, 2022. In addition, one zero baseline (APM3-APM5) and one short baseline (APM4-APM5) are formed, which are connected to the same H-maser clock at the APM. The code and phase observations of GPS L1 + L2, Galileo E1 + E5a, and BDS-3 BIC + B2a are tracked for the three receivers at the APM. This set of experimental data corresponds to the period January 3–9, 2022.

The between-receiver single-differenced (SD) ionospheric and tropospheric delays are eliminated for the zero and short baselines; thus, the ionospheric-fixed variants of the SCF and SCE models are used. The common-clock configuration can eliminate the influence of any imprecision of the receiver clocks, making it possible to evaluate the potential of GNSS time and frequency transfer under almost ideal conditions. A bidirectional Kalman filter was used to avoid the convergence process (Liu and Zhang 2021). The precise

Table 4 The comparison of the three models developed above

Item	Model A	Model B	Model C
Observation	UDUC	UDUC	UDUC
Satellite clocks	Corrected by precise satellite clock products	Corrected by precise satellite clock products	Estimated as unknowns
Phase ambiguity	Coupled with other parameters	Integrated into a DD form, enabling IAR	Integrated into a DD form, enabling IAR
Ionospheric constraints	Not considered	Considered	Considered

Table 5 A general overview of GNSS data sets used in our analysis

Station name	Institute	Reference clock	Receiver type	Antenna type	Location
USN7	USNO	H-maser	SEPT POLARX5TR	TPSCR.G5	38.92°N, 77.7°W
USN8			SEPT POLARX5TR		
PTBB	PTB	H-maser	SEPT POLARX5TR	LEIAR25.R4	52.30°N, 110.46°E
PT10			JAVAD TRE_G3T	NAX3G+C	
APM3	APM	H-maser	SEPT POLARX5	TRM159800.00	30.53°N, 114.36°E
APM5			SEPT POLARX5		
APM4			TRIMBLE ALLOY	TRM5791.00	

Table 6 Main data processing strategies in this study for the three models

Item	Model A	Model B	Model C
Receiver clock	Estimated as white noise		
Ionospheric delays	Estimated as white noise		
Tropospheric delays	Dry delay: corrected by the UNB3m model (Leandro et al. 2008) Wet delay: estimated as a random-walk process (Hadas et al. 2017)		
Stochastic model	Elevation-dependent weighting (Shen et al. 2009) Phase and code standard deviation (STD): 0.003 m and 0.3 m		
Orbits	Precise orbits	Precise orbits	Broadcast orbits
Satellite clocks	Precise satellite clocks	Precise satellite clocks	Estimated as white noise
Satellite phase biases	Estimated as a time-constant		
Between-receiver DCB		Estimated as white noise	Estimated as white noise
Between-receiver phase biases		Estimated as a time-constant	Estimated as a time-constant
IAR		LAMBDA (Teunissen 1995) with a ratio test of a threshold of 3 (Teunissen and Verhagen 2009)	
Outlier detection and elimination	DIA (Teunissen 2018)		

satellite orbits and clocks were fixed using the IGS final products for both Models A and B, and the monthly DCBs published by the Center for Orbit Determination in Europe (CODE) were used. The main processing strategies for the three models are shown in Table 6. It should be mentioned that all models are based on in-house software, which can avoid the impact of differences in data processing strategies (such as tropospheric delay) of different software.

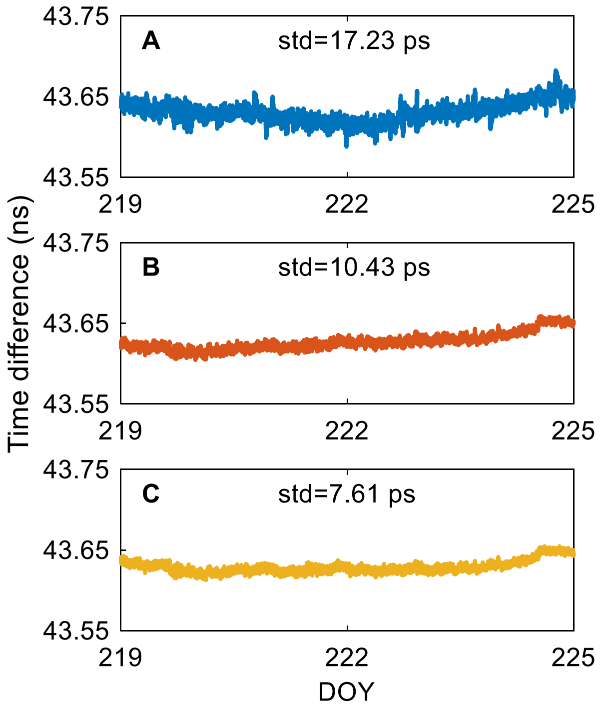

Fig. 1 Time difference between the receivers USN7 and USN8 with three different models using GPS L1/L2 observations on days of year (DOYs) 219–224, 2021

Experiments at USNO

Figure 1 shows the time difference obtained for the zero baseline USN7-USN8 using the three models discussed before. USN7 and USN8 are connected to the same H-maser clock and the same antenna; thus, the time difference is expected to be constant. Therefore, a comparison of the results can easily show which model has the best performance. We find that the STD of the time difference of the UDUC PPP model and the SCF model are 17.23 and 10.43 ps, respectively, showing an improvement of 39.5%. The benefits of the SCF model over the UDUC PPP model lie in two aspects. First, the common-view satellites are used to form the DD ambiguities to achieve IAR. Second, the ionospheric constraint is considered in the SCF model for easier IAR. The yellow curve shows that compared with the UDUC PPP model and the SCF model, the SCE model shows the smallest noise with 7.61 ps, showing 55.8 and 27.0% improvement, respectively. This shows that the use of satellite clock products does have an impact on time transfer. The advantage of the SCE model lies in that the satellite clocks are estimated synchronously with other parameters, making the model more rigorous.

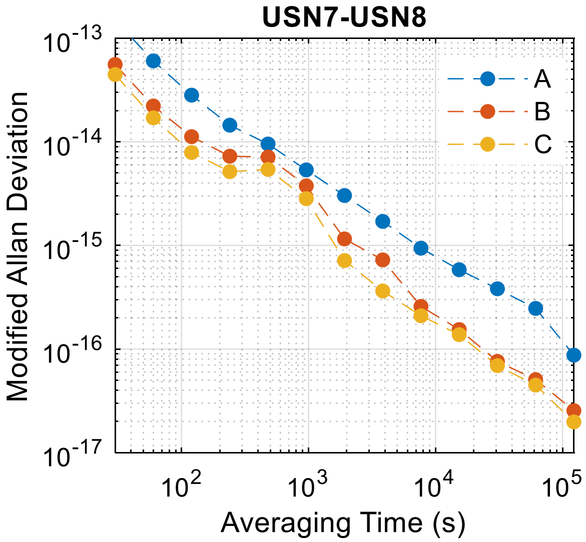

Fig. 2 MDEV of the USN7-USN8 with the PPP model (Model A), the SCF model (Model B) and the SCE model (Model C)

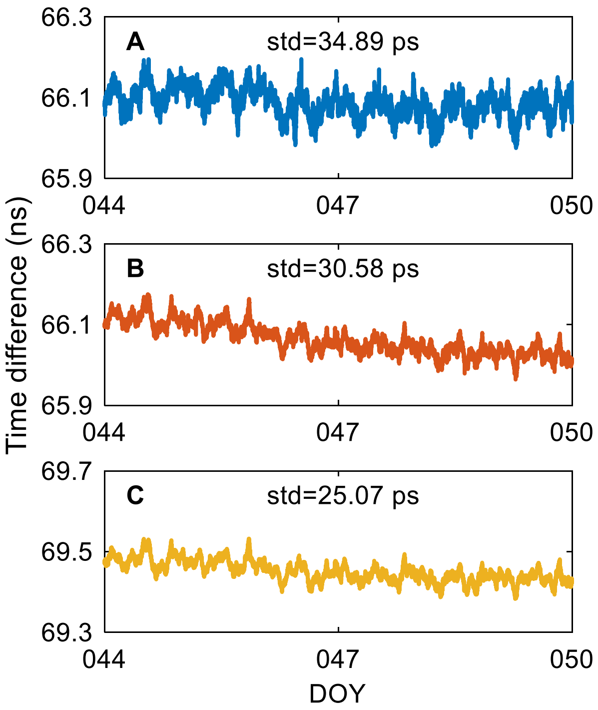

Fig. 3 Time difference between the receivers PTBB and PT10 with the three different models and GPS L1/L2 observations on DOYs 044–049, 2022

Figure 2 illustrates the modified Allan deviation (MDEV) of the time differences of the USN7-USN8. With the successful IAR, the frequency stability of the SCF model and SCE model reaches 5.6×10^{-14} and 4.5×10^{-14} for an averaging time at 30 s, respectively, while that of the UDUC PPP model can only reach 1.5×10^{-13}. The frequency stability for an averaging time at 15,360 s with the three models is 5.82×10^{-16}, 1.54×10^{-16} and 1.37×10^{-16}, respectively. Compared with the UDUC PPP model and the SCF model, the MDEV of the SCE model has improved by 76.4 and 11.0%, which shows the benefits of the IAR and satellite clocks estimation.

Experiments at PTB

The second experiment is based on the data collected at the PTB, Germany. The receivers PTBB and PT10 are connected to the same H-maser clock but with different antennas. From Fig. 3, we can see that the results from PTBB-PT10 are not as good as from USN7-USN8. This is reasonable since the antenna and receiver effects inevitably affect the time transfer performance. The corresponding STD of the time difference for the three models is 34.89, 30.58 and 25.07 ps, respectively. The STD of the SCF model improves 12.4% over the UDUC PPP model, due to the benefits of the IAR. In addition, the SCE model has gains of 28.1 and 18.0%, respectively, over the UDUC PPP model and the SCF model, showing the advantages of both IAR and satellite clocks estimation. It should be mentioned that the time difference of the UDUC PPP model and the SCF model is at the same level because the same precise satellite clock products are used. However, the situation is different for the SCE model, as only the broadcast ephemeris is used.

The MDEV of the three models for the PTBB-PT10 is shown in Fig. 4, from which we can confirm and extend

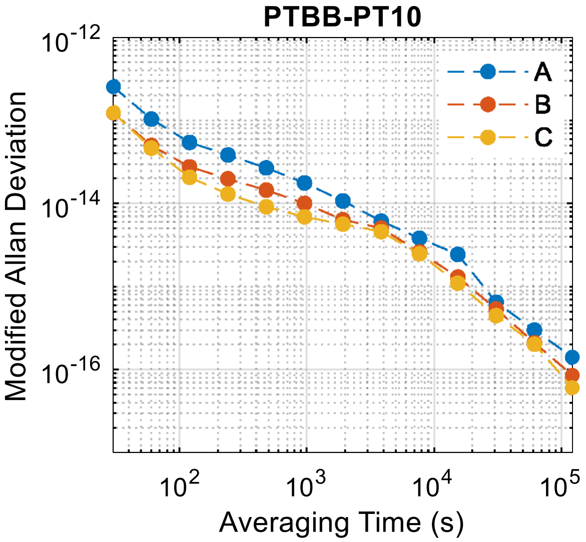

Fig. 4 MDEV of the PTBB-PT10 with the PPP model (Model A), the SCF model (Model B) and the SCE model (Model C)

our above findings. First, the SCF and the SCE models have improvements over the PPP model, as shown by its MDEV. The SCF model has an 18–52% improvement over the UDUC PPP model for averaging times at one day and below. Second, compared with the SCF model, with satellite clocks estimated together with other parameters, the SCE model can achieve better performance. For example, the frequency stability for an averaging time at one day for the two models is 6.03×10^{-17} and 8.51×10^{-17}. Compared with the SCF model, the SCE model shows an improvement of 29.0% for frequency stability, indicating the advantage of synchronously estimating satellite clocks.

Experiments at APM

From the previous experiments at USNO and PTB, the benefits of the SCE model were demonstrated using only GPS observations. In this test, using multi-GNSS data collected at the APM, the potential of time and frequency transfer performance of the proposed SCE model is evaluated using multi-GNSS.

Figure 5 depicts the time difference of the APM3-APM5 of the SCE model for GPS, Galileo, and BDS-3, from which two conclusions can be drawn. First, the time difference of APM3-APM5 for each constellation shows a trend. This is not surprising since the common-clock configuration makes the time transfer largely dependent on the between-receiver IF code bias ($d_{AB,IF}$). Although usually, in time transfer, it is assumed to be time invariant, this is not the case (Defraigne et al. 2021; Mi et al. 2021). The studies have shown that the receiver code bias can vary significantly, and an essential driving factor is the ambient temperature (Mi et al. 2020; Rieck et al. 2003; Zhang et al. 2020). Second, we can achieve picosecond time transfer with IAR and satellite clocks estimated for each constellation. The STD of the time difference for GPS, Galileo, and BDS-3 is 4.34, 4.56, 5.24 ps, respectively. It is worth noting that at APM3 and APM5, the same type of receiver is used and they are connected to the same H-maser clock and antenna. Thus, theoretically, this could be the limit for GNSS time transfer as the common error from receiver-end cable also be canceled. However, it can be seen from the results that the time transfer is not completely white noise because it is difficult to make the variation in the receiver bias completely consistent even with the same type of receiver (Mi et al. 2020).

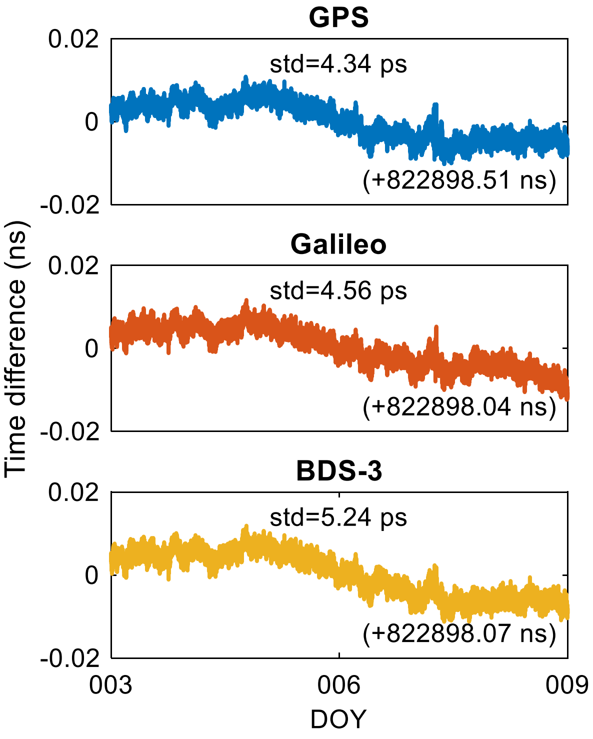

Fig. 5 Time difference between the receivers APM3 and APM5 of the SCE model for GPS, Galileo, and BDS-3 from DOYs 003–008, 2022

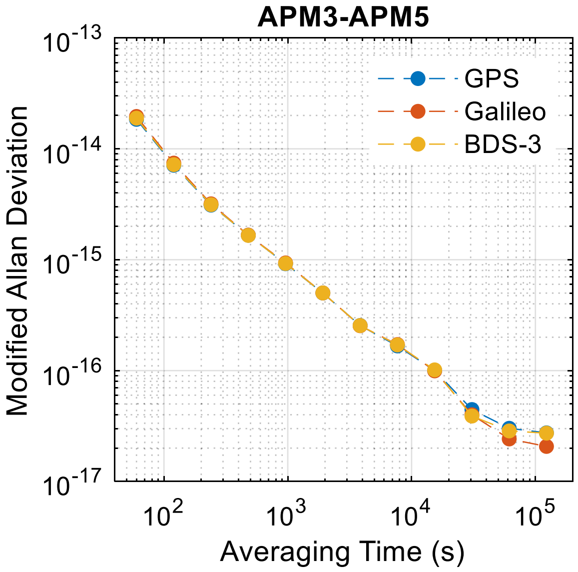

Fig. 6 MDEV of the APM3-APM5 of the SCE model for GPS, Galileo, and BDS-3 calculated from DOYs 003–008, 2022

Figure 6 depicts the MDEV of the APM3-APM5 time link with GPS, Galileo, and BDS-3, from which several conclusions can be drawn. First, GPS, Galileo, and BDS-3 show similar levels in terms of frequency stability. For example, the frequency stability of the APM3-APM5 with GPS, Galileo and BDS-3 is 5.01×10^{-16}, 5.01×10^{-16} and 4.81×10^{-16} for an averaging time at 1920 s. In the experiments in USNO and PTB, we demonstrate the superiority of the SCE model using GPS-only observations. Using the APM3-APM5, we find that with satellite clocks estimated and integer ambiguities resolved, Galileo and BDS-3 also have the potential to achieve 5×10^{-16} frequency transfer for averaging times

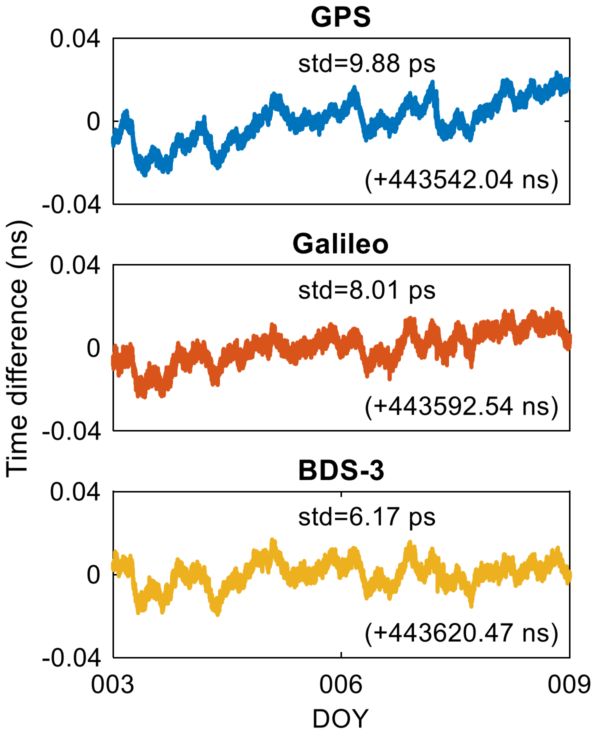

Fig. 7 Time difference between the receivers APM4 and APM5 of the SCE model for GPS, Galileo, and BDS-3 from DOYs 003–008, 2022

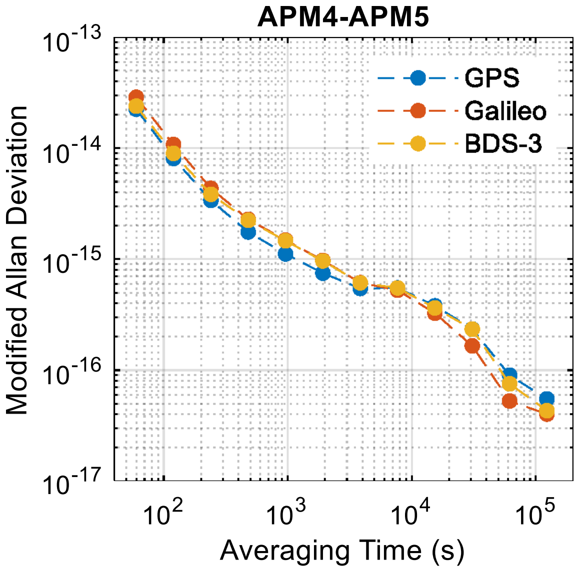

Fig. 8 MDEV of the APM4-APM5 using the SCE model for GPS, Galileo, and BDS-3 calculated from DOYs 003–008, 2022

within 30 min. The SCE model achieves such high frequency stability without reliance on precise satellite products, showing the significant benefit of the satellite clocks estimation. Second, GNSS has the potential to achieve sub-10^{-16} frequency transfer for averaging times at eight hours and above. As we can see from Fig. 6, although the performance of the three constellations is different, they can all achieve frequency transfer in the low-mid 10^{-17} range. For example, for an averaging time of one day, the frequency stability of APM3-APM5 with GPS, Galileo and BDS-3 is better than 3.01×10^{-17}, 2.41×10^{-17} and 2.85×10^{-17}, respectively.

Figures 7 and 8 show the time difference and corresponding MDEV for another baseline, APM4-APM5, with different types of receivers and antennas. The result of this time link is not as good as the APM3-APM5 with the same type of receiver and antenna, which shows the effect of receiver and antenna that must be considered. However, even in this case, GPS, Galileo, and BDS-3 can still achieve time transfer on the order of picoseconds. The STD of the time difference for GPS, Galileo, and BDS-3 are 9.88, 8.01, 6.17 ps, respectively. The time transfer results of the three constellations have different trends, which are believed to be caused by the antenna, the receiver, and the cable. Concerning the frequency stability, all three constellations can reach sub-10^{-16} for averaging times at half the day and above.

It is, however, still challenging to achieve picosecond time transfer and low-mid 10^{-17} range frequency transfer based on current atomic clocks and methods for the following reasons. First, the best H-masers are only of sub-nanosecond accuracy with $1-2 \times 10^{-16}$ frequency stability. Existing equipment can thus hardly reach the expected accuracy and stability. Second, the distance over which time and frequency transfer is needed is usually hundreds or even thousands of kilometers, so it is challenging to realize IAR without accurate atmospheric information. With the popularization of optical clocks and precise modeling of the atmospheric delays, it can be expected that picosecond time transfer results and sub-10^{-16} frequency transfer with GNSS will be demonstrated.

Conclusion

The development of high-precision optical clocks has put forward a higher demand for time and frequency transfer, which is challenging to be met by the existing GNSS techniques. In this contribution, we presented a new model based on UDUC observations, where the satellite clocks are estimated in the model to avoid the impact of external satellite clock products. In addition, DD ambiguities are formed in the model, which enables high-precision carrier-phase observations to be fully utilized through IAR.

Based on GNSS data from three laboratories, the proposed SCE model was used to evaluate the potential of GNSS time and frequency transfer. In addition, the UDUC

PPP and the SCF models were compared to demonstrate the benefits of IAR and satellite clocks estimation, respectively. According to the experimental results, we found that with IAR, the method using the SCF model improved the precision of time transfer and frequency stability by 20%–50%, showing the benefits of IAR. Furthermore, the SCE model showed a 10%–40% improvement over the SCF model. More importantly, we demonstrated that for averaging times within one day, low-mid 10^{-17} range frequency transfer could be potentially achieved by GPS, Galileo, and BDS-3 once ultra-precise clocks are available.

This study preliminarily proves that GNSS has the potential of reaching picosecond time transfer and sub-10^{-16} frequency transfer, which is expected to be realized with optical clocks. It facilitates our understanding of the advantages of satellite clocks estimation and IAR. However, some theoretical and technical problems, such as expanding the non-common-view model and high-precision atmospheric delay corrections, need to be solved in practice. Our future work will focus on those theoretical and technical problems and continue to explore the improvements and advantages of GNSS for time and frequency transfer.

Acknowledgements This work was partially funded by the Australian Research Council Discovery Project (Grant No. DP 190102444), the National Natural Science Foundation of China (Grant No. 42022025), the Open Fund of Hubei Luojia Laboratory (Grant No. 220100061), and the National Time Service Center, Chinese Academy of Sciences (No. E167SC14). Baocheng Zhang is supported by the CAS Pioneer Hundred Talents Program. We thank PTB and USNO for providing GNSS data. We also thank the IGS for providing precise orbit, clock products and data.

Data availability The datasets generated during the current study are available based on a reasonable request.

Declarations

Conflict of interest All authors declare that they have no conflicts of interest.

References

Boehm J, Werl B, Schuh H (2006) Troposphere mapping functions for GPS and very long baseline interferometry from European Centre for Medium-Range Weather Forecasts operational analysis data. J Geophys Res: Solid Earth 111:2406. https://doi.org/10.1029/2005JB003629

Chen Y, Yuan Y, Zhang B, Liu T, Ding W, Ai Q (2018) A modified mix-differenced approach for estimating multi-GNSS realtime satellite clock offsets. GPS Solut 22:1–10. https://doi.org/10.1007/s10291-018-0739-5

Defraigne P, Aerts W, Harmegnies A, Petit G, Rovera D, Uhrich P (2013) Advances in multi-GNSS time transfer Joint European Frequency and Time Forum & International Frequency Control Symposium. https://doi.org/10.1109/EFTF-IFC.2013.6702126

Defraigne P, Aerts W, Pottiaux E (2015) Monitoring of UTC(k)'s using PPP and IGS realtime products. GPS Solut 19:165–172. https://doi.org/10.1007/s10291-014-0377-5

Defraigne P, Pinat E, Bertrand B, Uhrich P, Chupin B, Riedel F (2021) Stability of hardware delays of GNSS signals. 2021 joint conference of the European frequency and time forum and IEEE international frequency control symposium (EFTF/IFCS). https://doi.org/10.1109/EFTF/IFCS52194.2021.9604324

Delporte J, Mercier F, Laurichesse D, Galy O (2007) Fixing integer ambiguities for GPS carrier phase time transfer. Proceedings of the 2007 IEEE international frequency control symposium-jointly with the 21st European frequency and time forum 1–4:927–932 doi: https://doi.org/10.1109/Freq.2007.4319215

Fujieda M, Piester D, Gotoh T, Becker J, Aida M, Bauch A (2014) Carrier-phase two-way satellite frequency transfer over a very long baseline. Metrologia 51:253. https://doi.org/10.1088/0026-1394/51/3/253

Geng J, Shi C, Ge M, Dodson A, Lou Y, Zhao Q, Liu J (2012) Improving the estimation of fractional-cycle biases for ambiguity resolution in precise point positioning. J Geod 86:579–589. https://doi.org/10.1007/s00190-011-0537-0

Guo J, Geng J (2018) GPS satellite clock determination in case of inter-frequency clock biases for triple-frequency precise point positioning. J Geod 92:1133–1142. https://doi.org/10.1007/s00190-017-1106-y

Guyennon N, Cerretto G, Tavella P, Lahaye F (2009) Further characterization of the time transfer capabilities of precise point positioning (PPP): the sliding batch procedure. IEEE Trans Ultrason Ferroelectr Freq Control 56:1634–1641. https://doi.org/10.1109/Tuffc.2009.1228

Hadas T, Teferle F, Kazmierski K, Hordyniec P, Bosy J (2017) Optimum stochastic modeling for GNSS tropospheric delay estimation in realtime. GPS Solut 21:1069–1081. https://doi.org/10.1007/s10291-016-0595-0

Huang Y, Fujieda M, Takiguchi H, Tseng W, Tsao H (2016) Stability improvement of an operational two-way satellite time and frequency transfer system. Metrologia 53(2):881. https://doi.org/10.1088/0026-1394/53/2/881

Huang G, Zhang Q, Xu G (2014) Realtime clock offset prediction with an improved model. GPS Solut 18:95–104. https://doi.org/10.1007/s10291-013-0313-0

Khodabandeh A, Teunissen P (2016) PPP-RTK and inter-system biases: the ISB look-up table as a means to support multi-system PPP-RTK. J Geod 90:837–851. https://doi.org/10.1007/s00190-016-0914-9

Khodabandeh A, Teunissen P (2018) On the impact of GNSS ambiguity resolution: geometry, ionosphere, time and biases. J Geod 92:637–658. https://doi.org/10.1007/s00190-017-1084-0

Leandro R, Langley R, Santos M (2008) UNB3m_pack: a neutral atmosphere delay package for radiometric space techniques. GPS Solut 12:65–70. https://doi.org/10.1007/s10291-007-0077-5

Liu T, Zhang B (2021) Estimation of code observation-specific biases (OSBs) for the modernized multi-frequency and multi-GNSS signals: an undifferenced and uncombined approach. J Geod 95(8):1–20. https://doi.org/10.1007/s00190-021-01549-x

Liu T, Yuan Y, Zhang B, Wang N, Tan B, Chen Y (2017) Multi-GNSS precise point positioning (MGPPP) using raw observations. J Geod 91:253–268. https://doi.org/10.1007/s00190-016-0960-3

Matsakis D, Defraigne P, Banerjee P (2014) Precise time and frequency transfer. URSI Radio Sci Bull 351:29–44. https://doi.org/10.23919/URSIRSB.2014.7909843

Mi X, Sheng C, El-Mowafy A, Zhang B (2021) Characteristics of receiver-related biases between BDS-3 and BDS-2 for five frequencies including inter-system biases, differential code biases, and differential phase biases. GPS Solut 25:1–11. https://doi.org/10.1007/s10291-021-01151-w

Mi X, Zhang B, Odolinski R, Yuan Y (2020) On the temperature sensitivity of multi-GNSS intra- and inter-system biases and the impact on RTK positioning. GPS Solut 24:1–14. https://doi.org/10.1007/s10291-020-01027-5

Mi X, Zhang B, Yuan Y (2019) Multi-GNSS inter-system biases: estimability analysis and impact on RTK positioning. GPS Solut 23:1–13. https://doi.org/10.1007/s10291-019-0873-8

Nicholson T et al (2015) Systematic evaluation of an atomic clock at 2 x 10 (-18) total uncertainty. Nat Commun 6:1–8. https://doi.org/10.1038/ncomms7896

Odijk D, Khodabandeh A, Nadarajah N, Choudhury M, Zhang B, Li W, Teunissen P (2017) PPP-RTK by means of *S*-system theory: Australian network and user demonstration. J Spat Sci 62:3–27. https://doi.org/10.1080/14498596.2016.1261373

Odijk D, Zhang B, Khodabandeh A, Odolinski R, Teunissen P (2016) On the estimability of parameters in undifferenced, uncombined GN network and PPP-RTK user models by means of *S*-system theory. J Geod 90(1):15–44. https://doi.org/10.1007/s00190-015-0854-9

Odolinski R, Teunissen P, Odijk D (2015) Combined BDS, Galileo, QZSS and GPS single-frequency RTK. GPS Solut 19:151–163. https://doi.org/10.1007/s10291-014-0376-6

Petit G (2021) Sub-10(-16) accuracy GNSS frequency transfer with IPPP. GPS Solut 25:1–9. https://doi.org/10.1007/s10291-020-01062-2

Petit G, Kanj A, Harmegnies A, Loyer S, Delporte J, Mercier F, Perosanz F (2014) GPS frequency transfer with IPPP. 2014 European Frequency and Time Forum (EFTF):451–454. https://doi.org/10.1109/EFTF.2014.7331533

Petit G, Kanj A, Loyer S, Delporte J, Mercier F, Perosanz F (2015) 1 x 10(-16) frequency transfer by GPS PPP with integer ambiguity resolution. Metrologia 52:301–309. https://doi.org/10.1088/0026-1394/52/2/301

Rieck C, Jarlemark P, Jaldehag K, Johansson J (2003) Thermal influence on the receiver chain of GPS carrier phase equipment for time and frequency transfer. IEEE international frequency control symposium and PDA exhibition jointly with the 17th European frequency and time forum. https://doi.org/10.1109/FREQ.2003.1275110

Rose J, Watson R, Allain D, Mitchell C (2014) Ionospheric corrections for GPS time transfer. Radio Sci 49:196–206. https://doi.org/10.1002/2013rs005212

Schuldt T et al (2021) Optical clock technologies for global navigation satellite systems. GPS Solut 25:1–11. https://doi.org/10.1007/s10291-021-01113-2

Shen Y, Li B, Xu G (2009) Simplified equivalent multiple baseline solutions with elevation-dependent weights. GPS Solut 13:165–171. https://doi.org/10.1007/s10291-008-0109-9

Shi C, Guo S, Gu S, Yang X, Gong X, Deng Z, Ge M, Schuh H (2019) Multi-GNSS satellite clock estimation constrained with oscillator noise model in the existence of data discontinuity. J Geod 93:515–528. https://doi.org/10.1007/s00190-018-1178-3

Teunissen P (1995) The least-squares ambiguity decorrelation adjustment: a method for fast GPS integer ambiguity estimation. J Geod 70:65–82. https://doi.org/10.1007/Bf00863419

Teunissen P (1997) On the sensitivity of the location, size and shape of the GPS ambiguity search space to certain changes in the stochastic model. J Geod 71:541–551. https://doi.org/10.1007/s001900050122

Teunissen P (2018) Distributional theory for the DIA method. J Geod 92:59–80. https://doi.org/10.1007/s00190-017-1045-7

Teunissen P (2020) GNSS precise point positioning. Position, navigation, and timing technologies in the 21st Century: integrated satellite navigation. Sensor Syst, Civ Appl 1:503–528. https://doi.org/10.1002/9781119458449.ch20

Teunissen P, Verhagen S (2009) The GNSS ambiguity ratio-test revisited: a better way of using it. Surv Rev 41:138–151. https://doi.org/10.1179/003962609x390058

Tuka A, El-Mowafy A (2013) Performance evaluation of different troposphere delay models and mapping functions. Measurement 46:928–937. https://doi.org/10.1016/j.measurement.2012.10.015

Tu R, Zhang P, Zhang R, Liu J, Lu X (2019) Modeling and performance analysis of precise time transfer based on BDS triple-frequency un-combined observations. J Geod 93:837–847. https://doi.org/10.1007/s00190-018-1206-3

Yao J, Skakun I, Jiang Z, Levine J (2015) A detailed comparison of two continuous GPS carrier-phase time transfer techniques. Metrologia 52:666–676. https://doi.org/10.1088/0026-1394/52/5/666

Yao J, Levine J (2016) A study of GPS carrier-phase time transfer noise based on NIST GPS receivers. J Res Nat Inst Stand Technol 121:372. https://doi.org/10.6028/jres.121.017

Zhang B, Chen Y, Yuan Y (2019) PPP-RTK based on undifferenced and uncombined observations: theoretical and practical aspects. J Geod 93:1011–1024. https://doi.org/10.1007/s00190-018-1220-5

Zhang H, Yuan Y, Li W (2021) An analysis of multisource tropospheric hydrostatic delays and their implications for GPS/GLONASS PPP-based zenith tropospheric delay and height estimations. J Geod 95:1–19. https://doi.org/10.1007/s00190-021-01535-3

Zhang X, Li X, Guo F (2011) Satellite clock estimation at 1 Hz for realtime kinematic PPP applications. GPS Solut 15:315–324. https://doi.org/10.1007/s10291-010-0191-7

Zhang X, Zhang B, Yuan Y, Zha J (2020) Extending multipath hemispherical model to account for time-varying receiver code biases. Adv Space Res 65:650–662. https://doi.org/10.1016/j.asr.2019.11.003

Xiaolong Mi is a Ph.D. candidate at Curtin University and the Innovation Academy for Precision Measurement Science and Technology, Chinese Academy of Sciences. His research focuses on high-precision GNSS positioning, GNSS time and frequency transfer with integer ambiguity resolution, multi-GNSS inter-operability and software development.

Baocheng Zhang is a Professor at the Innovation Academy for Precision Measurement Science and Technology, Chinese Academy of Sciences. His research focuses on modeling multiple global navigation satellite systems for integer ambiguity resolution enabled precise point positioning (PPP-RTK) applications.

Ahmed El-Mowafy is a Professor and Director of Graduate Research, School of Earth and Planetary Sciences, Curtin University, Australia. He obtained his Ph.D. from the University of Calgary, Canada, in 1995 and has more than 200 publications in precise positioning and navigation using GNSS, quality control, POD, integrity monitoring and estimation theory.

Kan Wang is a Professor at the National Time Service Center, Chinese Academy of Sciences. She received her Ph.D. in GNSS advanced modeling from ETH Zurich in 2016 and worked at Curtin University until 2021. Her research interests include high precision GNSS positioning, LEO precise orbit determination, SBAS and integrity monitoring.

Yunbin Yuan is a Professor and the GNSS Application and Research Group director at the Innovation Academy for Precision Measurement Science and Technology, Chinese Academy of Sciences. His current research interests are the following: (1) GNSS-based spatial environmental monitoring and analysis, (2) high-precision GNSS satellite navigation and positioning, and (3) GNSS applications to orbit determination for LEO satellites.

4 Characteristics of Multi-Frequency Multi-GNSS Receiver Biases

Calibrating receiver bias holds paramount importance in high-precision GNSS applications, including but not limited to positioning, time transfer, and ionospheric monitoring. In this chapter, an in-depth analysis of receiver bias characteristics in multi-frequency multi-GNSS scenarios is carried out. The outcomes of this research will pave the way for the next chapter, which aims to investigate and quantify the impact of GNSS receiver bias on time transfer. The research in this chapter is presented and included in the following publication:

Mi, X., Sheng, C., El-Mowafy, A., & Zhang, B. (2021). Characteristics of receiver-related biases between BDS-3 and BDS-2 for five frequencies including inter-system biases, differential code biases, and differential phase biases. GPS Solutions, 25(3), 113. https://doi.org/10.1007/s10291-021-01151-w

GPS Solutions (2021) 25:113
https://doi.org/10.1007/s10291-021-01151-w

ORIGINAL ARTICLE

Characteristics of receiver-related biases between BDS-3 and BDS-2 for five frequencies including inter-system biases, differential code biases, and differential phase biases

Xiaolong Mi[1,2,3,4] · **Chuanzhen Sheng**[1] · **Ahmed El-Mowafy**[2] · **Baocheng Zhang**[3]

Received: 4 January 2021 / Accepted: 4 June 2021 / Published online: 16 June 2021

Abstract

It is foreseeable that the BeiDou navigation satellite system with global coverage (BDS-3) and the BeiDou navigation satellite (regional) system (BDS-2) will coexist in the next decade. Care should be taken to minimize the adverse impact of the receiver-related biases, including inter-system biases (ISBs), differential code biases (DCB), and differential phase biases (DPB) on the positioning, navigation, and timing (PNT) provided by global navigation satellite systems (GNSS). Therefore, it is important to ascertain the intrinsic characteristics of receiver-related biases, especially in the context of the combination of BDS-3 and BDS-2, which have some differences in their signal level. We present a method that enables time-wise retrieval of between-receiver ISBs, DCB, and DPB from multi-frequency multi-GNSS observations. With this method, the time-wise estimates of the receiver-related biases between BDS-3 and BDS-2 are determined using all five frequencies available in different receiver pairs. Three major findings are suggested based on our test results. First, code ISBs are significant on the two overlapping frequencies B1II and B2b/B2I between BDS-3 and BDS-2 for a baseline with non-identical receiver pairs, which disrupts the compatibility of the two constellations. Second, epoch-wise DCB estimates of the same type in BDS-3 and BDS-2 can show noticeable differences. Thus, it is unreasonable to treat them as one constellation in PNT applications. Third, the DPB of BDS-3 and BDS-2 may have significant short-term variations, which can be attributed to, on the one hand, receivers composing baselines, and on the other hand, frequencies.

Keywords BeiDou navigation satellite system with global coverage (BDS-3) · BeiDou navigation satellite (regional) system (BDS-2) · Inter-system biases (ISBs) · Differential code biases (DCB) · Differential phase biases (DPB)

Introduction

The BeiDou navigation satellite system with global coverage (BDS-3) has been fully operational since July 2020 and has the potential to enable a wide range of applications for positioning, navigation, and timing (PNT) all over the world (Yang et al. 2020). Its constellation comprises 30 satellites, including three satellites in GEostationary Orbit (GEO), three in Inclined GeoSynchronous Orbit (IGSO), and 24 in Medium-altitude Earth Orbit (MEO) (Wang et al. 2019). To achieve compatibility and interoperability with other global navigation satellite systems (GNSS), and backward compatibility with the BeiDou navigation satellite (regional) system (BDS-2), BDS-3 transmits five navigational signals in space, namely B1I at 1561.098 MHz, B2b at 1207.140 MHz, B3I at 1268.520 MHz, B1C at 1575.42 MHz and B2a at 1176.450 MHz (Yang et al. 2018; Yuan et al. 2020). Meanwhile, attention should be paid to the fact that, although

✉ Baocheng Zhang
b.zhang@whigg.ac.cn

[1] State Key Laboratory of Satellite Navigation System and Equipment Technology, The 54th Research Institute of China Electronics Technology Group Corporation, Shijiazhuang 050081, China

[2] School of Earth and Planetary Sciences, Curtin University, Perth 6102, Australia

[3] State Key Laboratory of Geodesy and Earth's Dynamics, Innovation Academy for Precision Measurement Science and Technology, Chinese Academy of Sciences, Wuhan, China

[4] University of Chinese Academy of Sciences, Beijing, China

BDS-3 has already been operational, BDS-2 will still be in service for at least another decade (Yang et al. 2019; Mi et al. 2020b) and forms an important part of BDS globalization. As a regional system serving the Asia–Pacific, BDS-2 constellation comprises five GEO satellites, seven IGSO satellites, and three MEO satellites (CSNO 2019; Montenbruck et al. 2013). Signals at three frequencies are used in BDS-2, namely B1I at 1561.098 MHz, B2I at 1207.140 MHz, and B3I at 1268.520 MHz, ensuring the PNT service of BDS-2 (Odolinski et al. 2014b; Yang et al. 2014).

It has long been recognized that multiple constellations and multiple frequencies are becoming available that benefit PNT services in accuracy, integrity, and availability (Odijk and Teunissen 2012; Tian et al. 2017). In such cases, in addition to the unification of coordinate and time reference frames, differences in receiver hardware delays related to using signals from different systems should also be considered (Gioia and Borio 2016). These biases are called inter-system biases (ISBs) and are caused by the correlation process within the GNSS receiver (Gao et al. 2017a; Paziewski and Wielgosz 2014). In general, the effect of the receiver ISBs is considered a major source of error in the combined processing of data from different GNSS (Odijk et al. 2016). For example, ISBs have to be considered not only in real-time kinematic (RTK) positioning and precise point positioning (PPP) (Gao et al. 2019; Geng et al. 2019), but also in integer ambiguity resolution enabled PPP (PPP-RTK) (Khodabandeh and Teunissen 2016). In addition, applications based on multi-GNSS observations, such as time and frequency transfer (Tu et al. 2019; Verhasselt and Defraigne 2019), and atmospheric retrieval (Lu et al. 2020; Pan and Guo 2018), also need to pay attention to the impact of ISBs.

In addition to ISBs, the hardware delay differences experienced by different frequencies in a single GNSS constellation, namely differential code biases (DCB) and differential phase biases (DPB), are also important sources of errors limiting GNSS-based PNT applications (Odolinski and Teunissen 2017b; Sanz et al. 2017). For example, the lumped effect of satellite and receiver DCB and DPB is generally considered a major source of error in ionospheric retrieval from GNSS observables (Brunini and Azpilicueta 2010). Fortunately, the satellite DCB and DPB are fairly stable over a considerable time for each GNSS constellation (Sardon et al. 1994). The variability of receiver DCB and DPB may be evident over a relatively short period, e.g., two hours to one day, due to temperature perturbations around the receivers (Zha et al. 2019; Zhang and Teunissen, 2015; Zhang et al. 2016). Thus, the handling of receiver DCB and DPB is important to ensure GNSS-derived ionospheric retrieval accuracy and reliability. Furthermore, precision and reliability of positioning and time and frequency transfer are also constrained by receiver DCB and DPB (Dach et al. 2002; Odolinski et al. 2015). With high-precision and high-reliability DCB and DPB, PPP and RTK, as well as PPP-RTK can reach even higher levels (Gao et al. 2017b; Odolinski and Teunissen 2017a; Psychas et al. 2019). Moreover, accurate calibration of DCB and DPB is an important prerequisite for time and frequency transfer based on GNSS (Defraigne and Baire 2011; Huang and Defraigne 2016).

Therefore, it is important to ascertain the intrinsic characteristics of receiver-related biases between BDS-3 and BDS-2, since they are treated, quite naturally, as one system. For this purpose, we first present a method that allows DCB, DPB, and ISBs to be estimated simultaneously and continuously. With this method, the characteristics of code and phase ISBs between BDS-3 and BDS-2, and the DCB and DPB of BDS-3 and BDS-2 are determined.

Calibration of receiver-related biases using multi-GNSS observables

The system of code and phase observation equations based on single-differenced (SD), serving as a starting point of developing the algorithm, reads (Odolinski et al. 2015)

$$
\begin{aligned}
p_{ab,j}^{s_*}(i) &= g_{ab}^{s_*}(i)\cdot x_{ab}(i) + dt_{ab}(i) + d_{ab,j}^{*}(i) + \mu_j l_{ab}^{s_*} + T_{ab}^{s_*} + \varepsilon_{ab,j}^{s_*} \\
\phi_{ab,j}^{s_*}(i) &= g_{ab}^{s_*}(i)\cdot x_{ab}(i) + dt_{ab}(i) + \delta_{ab,j}^{*}(i) - \mu_j l_{ab}^{s_*} + T_{ab}^{s_*} + \lambda_j z_{ab,j}^{s_*} + e_{ab,j}^{s_*}
\end{aligned}
\tag{1}
$$

where $p_{ab,j}^{s_*}(i)$ and $\phi_{ab,j}^{s_*}(i)$ are the SD code and phase observations associated with two receivers a and b. GNSS constellation is $*$, which is distinguished by different letters ($*= A, B, \ldots$). The satellite identifier is s_*, the frequency is j, and i denotes the epoch. $x_{ab}(i)$ is the column vector of geometric unknowns and the corresponding coefficient $g_{ab}^{s_*}(i)$ is the receiver-to-satellite unit vector. $dt_{ab}(i)$ is the SD receiver clock between a and b. The symbols $d_{ab,j}^{*}(i)$ and $\delta_{ab,j}^{*}(i)$ denote, respectively, the SD receiver code biases and phase biases.$l_{ab}^{s_*}$ is the SD slant ionospheric delay, and $\mu_j = f_1^2 \big/ f_j^2$ is the frequency-dependent factor.$T_{ab}^{s_*}$ denotes the SD tropospheric delay. $z_{ab,j}^{s_*}$ denotes the SD ambiguity and λ_j denotes the wavelength, respectively. Note that all of the variables involved in (1) are in meters, except $z_{ab,j}^{s_*}$ is in cycles. $\varepsilon_{ab,j}^{s_*}$ and $e_{ab,j}^{s_*}$ denote the SD random observation noise and unmodeled effects such as multipath for the code and phase observations, respectively.

Consider a zero baseline or a short one of less than a few kilometers, we can assume no differential ionospheric and tropospheric effects. In this case, the model can also be referred to as an ionospheric-fixed and tropospheric-fixed model. Then, the SD code and phase observation is rewritten as (Odolinski et al. 2014a)

$$
\begin{aligned}
p^{s_*}_{ab,j}(i) &= g^{s_*}_{ab}(i) \cdot x_{ab}(i) + dt_{ab}(i) + d^*_{ab,j}(i) + \varepsilon^{s_*}_{ab,j} \\
\phi^{s_*}_{ab,j}(i) &= g^{s_*}_{ab}(i) \cdot x_{ab}(i) + dt_{ab}(i) + \delta^*_{ab,j}(i) + \lambda_j z^{s_*}_{ab,j} + e^{s_*}_{ab,j}
\end{aligned}
\tag{2}
$$

However, even though (2) does not depend on ionospheric and tropospheric delays, the model is still not of full rank. A rank deficit occurs in two ways. One is the linear dependency between the columns of the receiver clock and the code/phase biases, and the other is the column dependency between phase biases and the SD ambiguities (Mi et al. 2019a, b). By applying the S-system transformation, full rank can be achieved by constraining a minimum set of parameters, or S-basis (Zhang et al. 2018). It should be noted that the choice of S-basis is not unique, which dictates the estimability and the interpretation of parameters. For example, the rank deficiency of the first type can be solved by fixing the receiver code biases of one- or multi-constellation, which results in two different models: classical differencing and inter-system differencing. A detailed explanation and comparison of classical differencing and inter-system differencing can be found in Mi et al. (2020a), which will not be repeated here. In our study, inter-system differencing is adopted. Thus, the rank deficiency between the columns of the receiver clock and the code/ phase biases are solved by fixing the code biases on the first frequency of only one of the constellations. Also, we have the rank defects between phase biases and ambiguities, which are solved by fixing the SD ambiguities of one reference satellite per constellation. Once the rank defects have been solved, we have the following full-rank model

$$
\begin{aligned}
p^{s_A}_{ab,j}(i) &= g^{s_A}_{ab}(i) \cdot x_{ab}(i) + d\tilde{t}_{ab}(i) + \tilde{d}^A_{ab,j}(i) + \varepsilon^{s_A}_{ab,j} \\
\phi^{s_A}_{ab,j}(i) &= g^{s_A}_{ab}(i) \cdot x_{ab}(i) + d\tilde{t}_{ab}(i) + \tilde{\delta}^A_{ab,1}(i) + \tilde{\delta}^A_{ab,j}(i) + \lambda_j z^{1_A s_A}_{ab,j} + e^{s_A}_{ab,j} \\
p^{s_*}_{ab,j}(i) &= g^{s_*}_{ab}(i) \cdot x_{ab}(i) + d\tilde{t}_{ab}(i) + \tilde{d}^*_{ab,j}(i) + \varepsilon^{s_*}_{ab,j} \\
\phi^{s_*}_{ab,j}(i) &= g^{s_*}_{ab}(i) \cdot x_{ab}(i) + d\tilde{t}_{ab}(i) + \tilde{\delta}^A_{ab,1}(i) + \tilde{\delta}^*_{ab,j}(i) + \lambda_j z^{1_* s_*}_{ab,j} + e^{s_*}_{ab,j}
\end{aligned}
\tag{3}
$$

where $\tilde{d}^A_{ab,j}(i)$ and $\tilde{\delta}^A_{ab,j}(i)$ are the DCB and DPB, and their counterpart $\tilde{d}^*_{ab,j}(i)$ and $\tilde{\delta}^*_{ab,j}(i)$ are the code and phase ISBs, and their interpretations are given in Table 1.

Recall that in the estimable form of DPB $\tilde{\delta}^A_{ab,j}(i) = \delta^A_{ab,j}(i) - \delta^A_{ab,1}(i) + \lambda_j z^{1_A}_{ab,j} - \lambda_1 z^{1_A}_{ab,1}$ and phase ISBs $\tilde{\delta}^*_{ab,j}(i) = \delta^*_{ab,j}(i) - \delta^A_{ab,1}(i) + \lambda_j z^{1_*}_{ab,j} - \lambda_1 z^{1_A}_{ab,1}$, the datum ambiguities $\lambda_j z^{1_A}_{ab,j} - \lambda_1 z^{1_A}_{ab,1}$ and $\lambda_j z^{1_*}_{ab,j} - \lambda_1 z^{1_A}_{ab,1}$ correspond to the reference satellites $s_A = 1_A$ and $s_* = 1_*$. As is well known that one reference cannot be visible for a long time (usually less than a few hours). In general, when the observation period exceeds a few tens of hours, it is inevitable to change the reference satellite more than once. However, in this case, abrupt jumps will be introduced in the epoch-wise estimates of DPB and phase ISBs, which is not helpful in restoring their characteristics.

The datum ambiguities can be considered time-invariant as long as the reference satellites are tracked continuously without cycle slip. Thus, for multi-epochs, the number of rank defects between phase biases and the ambiguities remains unchanged and is independent of the epoch number. Hence, when the SD ambiguities of one satellite ($\lambda_j z^{1_*}_{ab,j}$) are selected as a datum at epoch i, the SD ambiguities of the remaining satellites ($\lambda_j z^{s_*}_{ab,j}, s = 2, 3, \cdots, m$) will absorb $\lambda_j z^{1_*}_{ab,j}$, and thus have the DD form ($\lambda_j z^{1_* s_*}_{ab,j}$). Then,$\lambda_j z^{1_* s_*}_{\mathrm{ab},j}$ can be transferred to epoch $i+1$, even though the reference satellite is no longer visible,$\lambda_j z^{1_*}_{ab,j}$ in $\lambda_j z^{1_* s_*}_{ab,j}$ can still serve as a datum. In this case, the SD code and phase observation equations at epoch $i+1$ read:

$$
\begin{aligned}
p^{s_A}_{ab,j}(i+1) &= g^{s_A}_{ab}(i+1) \cdot x_{ab}(i+1) + d\tilde{t}_{ab}(i+1) + \tilde{d}^A_{ab,j}(i+1) + \varepsilon^{s_A}_{ab,j} \\
\phi^{s_A}_{ab,j}(i+1) &= g^{s_A}_{ab}(i+1) \cdot x_{ab}(i+1) + d\tilde{t}_{ab}(i+1) + \tilde{\delta}^A_{ab,1}(i+1) + \tilde{\delta}^A_{ab,j}(i+1) + \lambda_j z^{1_A s_A}_{ab,j} + e^{s_A}_{ab,j} \\
p^{s_*}_{ab,j}(i+1) &= g^{s_*}_{ab}(i+1) \cdot x_{ab}(i+1) + d\tilde{t}_{ab}(i+1) + \tilde{d}^*_{ab,j}(i+1) + \varepsilon^{s_*}_{ab,j} \\
\phi^{s_*}_{ab,j}(i+1) &= g^{s_*}_{ab}(i+1) \cdot x_{ab}(i+1) + d\tilde{t}_{ab}(i+1) + \tilde{\delta}^A_{ab,1}(i+1) + \tilde{\delta}^*_{ab,j}(i+1) + \lambda_j z^{1_* s_*}_{ab,j} + e^{s_*}_{ab,j}
\end{aligned}
\tag{4}
$$

Table 1 Estimable unknown parameters and their interpretation for the SD ionospheric-fixed, tropospheric-fixed model

Notation and interpretation	Estimable parameter
$d\tilde{t}_{ab}(i) = dt_{ab}(i) + d^A_{ab,1}(i)$	Receiver clock with code biases for $j = 1$
$\tilde{d}^A_{ab,j}(i) = d^A_{ab,j}(i) - d^A_{ab,1}(i)$	Receiver DCB, where $j \geq 2$
$\tilde{\delta}^A_{ab,1}(i) = \delta^A_{ab,1}(i) - d^A_{ab,1}(i) + \lambda_1 z^{1_A}_{ab,1}$	Receiver phase bias of the first frequency
$\tilde{\delta}^A_{ab,j}(i) = \delta^A_{ab,j}(i) - \delta^A_{ab,1}(i) + \lambda_j z^{1_A}_{ab,j} - \lambda_1 z^{1_A}_{ab,1}$	Receiver DPB, where $j \geq 2$
$\tilde{d}^*_{ab,j}(i) = d^*_{ab,j}(i) - d^A_{ab,1}(i)$	Receiver code ISBs, where $j \geq 1$
$\tilde{\delta}^*_{ab,j}(i) = \delta^*_{ab,j}(i) - \delta^A_{ab,1}(i) + \lambda_j z^{1_*}_{ab,j} - \lambda_1 z^{1_A}_{ab,1}$	Receiver phase ISBs, where $j \geq 1$
$z^{1_* s_*}_{ab,j} = z^{s_*}_{ab,j} - z^{1_*}_{ab,j}$	Double-differenced (DD) integer ambiguities

where $\tilde{\delta}^{A}_{ab,j}(i+1) = \delta^{A}_{ab,j}(i+1) - \delta^{A}_{ab,1}(i+1) + \lambda_j z^{1_A}_{ab,j} - \lambda_1 z^{1_A}_{ab,1}$ and $\tilde{\delta}^{*}_{ab,j}(i+1) = \delta^{*}_{ab,j}(i+1) - \delta^{A}_{ab,1}(i+1) + \lambda_j z^{1_*}_{ab,j} - \lambda_1 z^{1_A}_{ab,1}$.

In this way, the DPB and phase ISBs are estimated continuously without changing the reference satellite.

To accurately calibrate these biases, the baseline and DD ambiguities are precisely estimated in advance using a strategy that does not change the reference satellite. Then, the baseline and DD ambiguities are subtracted from (3). In this case, the SD code and phase observation equations with fixed baseline and ambiguities are expressed as,

$$\begin{aligned}
\tilde{p}^{s_A}_{ab,j}(i) &= d\tilde{t}_{ab}(i) + \tilde{d}^{A}_{ab,j}(i) + \varepsilon^{s_A}_{ab,j} \\
\tilde{\phi}^{s_A}_{ab,j}(i) &= d\tilde{t}_{ab}(i) + \tilde{\delta}^{A}_{ab,1}(i) + \tilde{\delta}^{A}_{ab,j}(i) + e^{s_A}_{ab,j} \\
\tilde{p}^{s_*}_{ab,j}(i) &= d\tilde{t}_{ab}(i) + \tilde{d}^{*}_{ab,j}(i) + \varepsilon^{s_*}_{ab,j} \\
\tilde{\phi}^{s_*}_{ab,j}(i) &= d\tilde{t}_{ab}(i) + \tilde{\delta}^{A}_{ab,1}(i) + \tilde{\delta}^{*}_{ab,j}(i) + e^{s_*}_{ab,j}
\end{aligned} \tag{5}$$

where $\tilde{p}^{s_A}_{ab,j}(i) = p^{s_A}_{ab,j}(i) - g^{s_A}_{ab}(i) \cdot x_{ab}(i)$ and $\tilde{\phi}^{s_A}_{ab,j}(i) = \phi^{s_A}_{ab,j}(i) - g^{s_A}_{ab}(i) \cdot x_{ab}(i) - \lambda_j z^{1_A s_A}_{ab,j}$, with their counterparts $\tilde{p}^{s_*}_{ab,j}(i) = p^{s_*}_{ab,j}(i) - g^{s_*}_{ab}(i) \cdot x_{ab}(i)$ and $\tilde{\phi}^{s_*}_{ab,j}(i) = \phi^{s_*}_{ab,j}(i) - g^{s_*}_{ab}(i) \cdot x_{ab}(i) - \lambda_j z^{1_* s_*}_{ab,j}$. Since the datum in DD ambiguities has not changed, no discontinuity will be present in the estimates of DPB and phase ISBs.

Experimental setup

In our analysis, we selected two sets of GNSS data, measured by three and four collocated receivers, respectively, with five observation types (B1I, B1C, B2a, B2b, B3I) of BDS-3 and three types (B1I, B2I, B3I) of BDS-2. See Table 2 for detailed characteristics. Two points deserve noted from the table. First, the receivers with IDs APM1, APM2, APM3, and APM4, which comprise two Trimble and two Septentrio receivers, are connected to a common antenna, implying that they can create a total of six zero baselines. Second, the receivers IGG1, IGG2, and IGG3 are each equipped with a single antenna, creating three baselines, with lengths of 1.8 m, 5.6 m, and 6.7 m. The sampling interval of the first set of receivers (AMP1 to AMP4) was 30 s and that of the second set (IGG1 to IGG3) was 10 s.

The cutoff elevation angle was set to 10° to discard particularly noisy code and phase observations. The elevation-dependent weighting function used can be expressed as $\sigma^{s_*}_{\phi} = \sigma^{u}_{\phi}/\sin(E^{s_*})$ and $\sigma^{s_*}_{p} = \sigma^{u}_{p}/\sin(E^{s_*})$ (Euler and Goad 1991), where $\sigma^{s_*}_{\phi}$ and $\sigma^{s_*}_{p}$ donate the standard deviations of the phase and code observations of satellite s_*, $E^{s_*}_{r}$ is the elevation of satellite, σ^{u}_{ϕ} and σ^{u}_{p} are the undifferenced zenith-referenced a priori phase and code standard deviations, assumed here as 3 mm and 0.3 m, respectively. The satellite positions that are required for elevation angle determination are computed using the broadcast ephemeris. The Detection, Identification and Adaptation (DIA) procedure is used to detect and eliminate the effect of outliers (Teunissen 2018), and the LAMBDA method was used for integer ambiguity resolution (Teunissen 1995; Chang et al. 2005). For the sake of brevity, only partial baselines selected during some of the experimental days are reported here in the analysis of ISBs, DCB and DPB estimates. These results are representative of all the experimental results that we obtained. In addition, in order to reduce the impact of the multipath effect caused by the tall buildings around the receivers, sidereal filtering is implemented (Wang et al. 2018). In sidereal filtering, the multipath model needs to be shifted by a certain period, usually close to a sidereal day, thus, this method is only applicable to APM1 to APM4 with multiple days of observations available.

Characterization of BDS-3 and BDS-2 ISBs estimates

This section first describes the B1I and B3I code and phase ISBs estimates between BDS-3 and BDS-2, as those frequencies are identical in the two constellations. Then, the characterization of ISBs estimates between BDS-3 B2b and BDS-2 B2I, which are overlapping frequencies but with different signal modulations, is analyzed separately.

Figure 1 shows the estimates of B1I and B3I code ISBs between BDS-3 and BDS-2. When comparing the right-hand panels showing the B3I code ISBs, with the left-hand panels of B1I ISBs, we can see that the B3I code ISBs estimates fluctuate randomly around zero. In other words, for B3I signals, the code ISBs are not shown to be present for

Table 2 An overview of GNSS data used in this work

Receiver ID	Receiver type	Antenna type	Location	Observation period
APM1	Trimble ALLOY	Trimble Zephyr 3	114.37°E, 30.57°N	DOY 339–342 of 2020
APM2	Trimble ALLOY			
APM3	Septentrio POLARX5			
APM4	Septentrio POLARX5			
IGG1	Trimble ALLOY	South GR3-G3		DOY 265 of 2020
IGG2	Septentrio POLARX5	South GR3-G3		
IGG3	Trimble R10-2	Trimble R10-2		

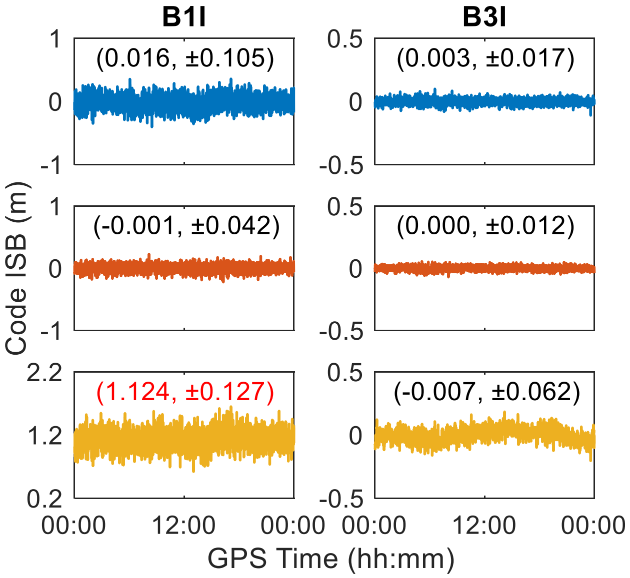

Fig. 1 Time series of B1I (left) and B3I (right) code ISBs estimates between BDS-3 and BDS-2 on DOY 340, 2020. Three zero baselines are used, including APM1-APM2 with two ALLOY receivers (top), APM3-APM4 with two POLARX5 receivers (middle), APM1-APM3 with ALLOY and POLARX5 receivers (bottom). The numbers in each panel represent the mean and standard deviation (STD) in meters

baselines consisting of both identical and different receiver types. Considering the two bottom panels, a key finding is shown. The code ISBs estimates of B3I fluctuate randomly around zero while those of B1I show significant values with a mean of 1.124 m, which means the presence of B1I code ISBs between BDS-3 and BDS-2 must be considered for baselines composed of different receivers.

Figure 2 depicts the B1I code ISBs estimated for each of the three baselines composed of different receivers connected to separate antennas. As might have been expected, the B1I code ISBs between BDS-3 and BDS-2 is not close to zero for any of the three baselines, indicating a significant bias. The trend in the ISBs estimates, particularly for IGG1-IGG3 and IGG2-IGG3, can be attributed to multipath effects. However, due to the short observation time, sidereal filtering cannot be used to weaken the influence of multipath. Even so, these results confirm the previous observation that the B1I code ISBs based on a mixed-receiver combination are nonzero, and this suggests that we should consider the difference between B1I code of BDS-3 and BDS-2 in practice.

Figure 3 is analogous to Fig. 1 but illustrating the results of B1I and B3I phase ISBs between BDS-3 and BDS-2. Unexpectedly, unlike the code ISBs, we find that, for each baseline considered, using both identical and mixed-receiver pairs, the B1I and B3I phase ISBs are always randomly distributed around a mean value almost zero. In other words, there is no reason to expect the presence of phase ISBs for B1I and B3I between BDS-3 and BDS-2.

Figure 4 shows the estimates of code and phase ISBs between BDS-3 B2b and BDS-2 B2I, from which two conclusions can be drawn. First, similar to the B1I and B3I

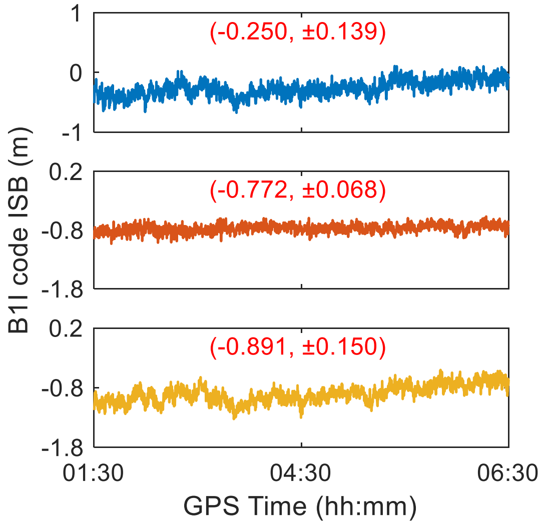

Fig. 2 Time series of B1I code ISBs estimates between BDS-3 and BDS-2 on DOY 265 of 2020. Three short baselines are used, including IGG1-IGG3 with ALLOY and TR12 receivers (top), IGG1-IGG2 with ALLOY and POLARX5 receivers (middle), IGG2-IGG3 with POLARX5 and TR12 receivers (bottom). The numbers in each panel represent the mean and STD in meters

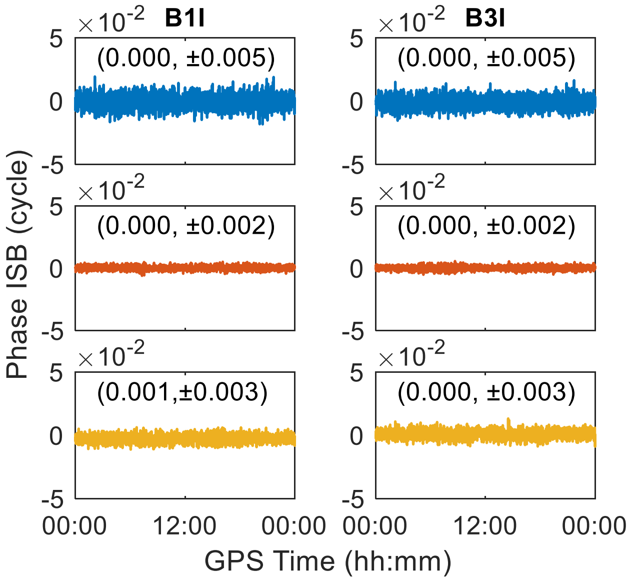

Fig. 3 Time series of BDS-3-BDS-2 B1I (left) and B3I (right) phase ISBs estimates on DOY 340 of 2020. Three zero baselines are used, including APM1-APM2 with two ALLOY receivers (top), APM3-APM4 with two POLARX5 receivers (middle), APM1-APM3 with ALLOY and POLARX5 receivers (bottom). The numbers in each panel represent the mean and STD in cycles

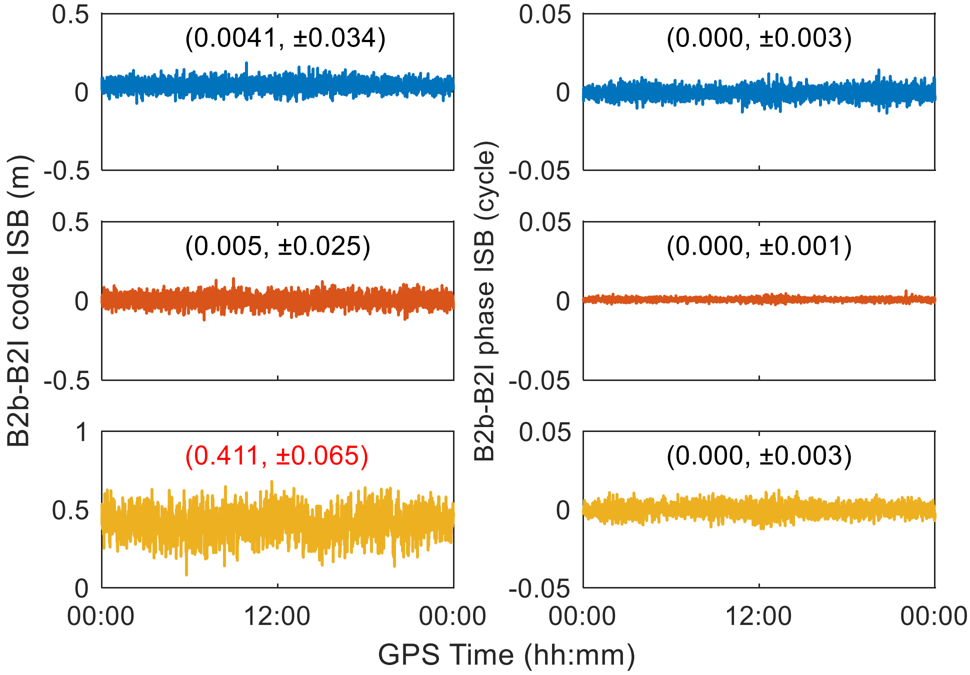

Fig. 4 Time series of code (left) and phase (right) ISBs estimates between BDS-3 B2b and BDS-2 B2I on DOY 340 of 2020. Three zero baselines are used, including APM1-APM2 with two ALLOY receivers (top), APM3-APM4 with two POLARX5 receivers (middle), APM1-APM3 with ALLOY and POLARX5 receivers (bottom). The numbers in each panel represent the mean and STD. The three panels on the left are in meters, while the units on the right are in cycles

phase ISBs between BDS-3 and BDS-2, interoperability can be achieved for the phase observations between BDS-3 B2b and BDS-2 B2I. Second, the mean of the code ISBs between BDS-3 B2b and BDS-2 B2I based on APM1-APM3, a mixed-receiver combination, are estimated as nonzero, thereby suggesting the code ISBs should be considered when mixing BDS-3 B2b and BDS-2 B2I for a baseline with non-identical receiver pairs.

Similar to Fig. 2, but for different signals, Fig. 5 shows the code ISBs between BDS-3 B2b and BDS-2 B2I for the short three baselines. Likewise, there is a certain trend in each panel, which we believe is also due to the multipath effect. Overall, it can be confirmed that there are nonzero mean code ISBs between BDS-3 B2b and BDS-2 B2I, which breaks the interoperability between BDS-3 and BDS-2.

To summarize, two conclusions can be drawn. First, there are no ISBs on the phase observations of the three overlapping frequencies of BDS-3 and BDS-2, so they can be treated as one constellation. Second, and more importantly, the code observations of BDS-3 and BDS-2 can be compatible on B3I but not on B1I and B2I/B2b, for a baseline with non-identical receiver pairs. Thus, the differences in code observations of B1I and B2I/B2b between the two constellations must be considered when mixing BDS-3 and BDS-2 observations.

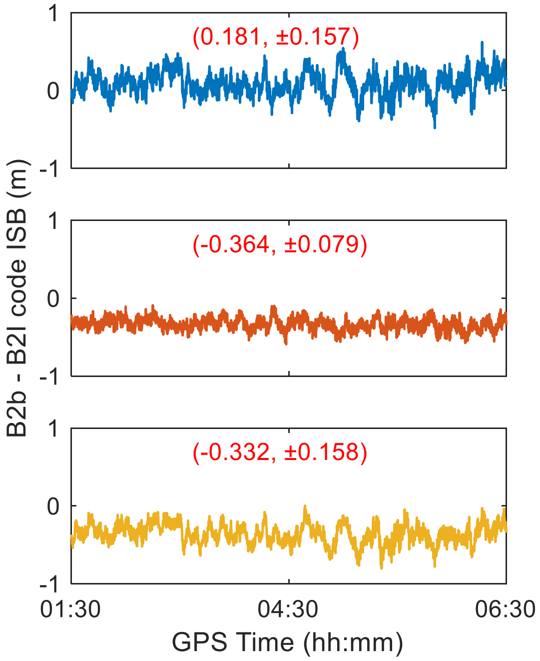

Fig. 5 Time series of code ISBs estimates between BDS-3 B2b and BDS-2 B2I on DOY 265 of 2020. Three short baselines are used, including IGG1-IGG3 with ALLOY and TR12 receivers (top), IGG1-IGG2 with ALLOY and POLARX5 receivers (middle), IGG2-IGG3 with POLARX5 and TR12 receivers (bottom). The numbers in each panel represent the mean and STD in meters

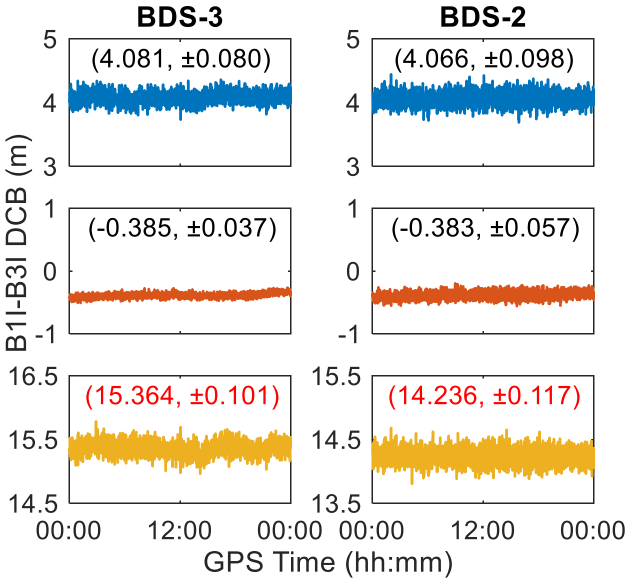

Fig. 6 Time series of BDS-3 (left) and BDS-2 (right) B1I-B3I DCB estimates on DOY 340 of 2020. Three zero baselines are used, including APM1-APM2 with two ALLOY receivers (top), APM3-APM4 with two POLARX5 receivers (middle), APM1-APM3 with a mix of ALLOY and POLARX5 receivers (bottom). The numbers in each panel represent the mean and STD in meters

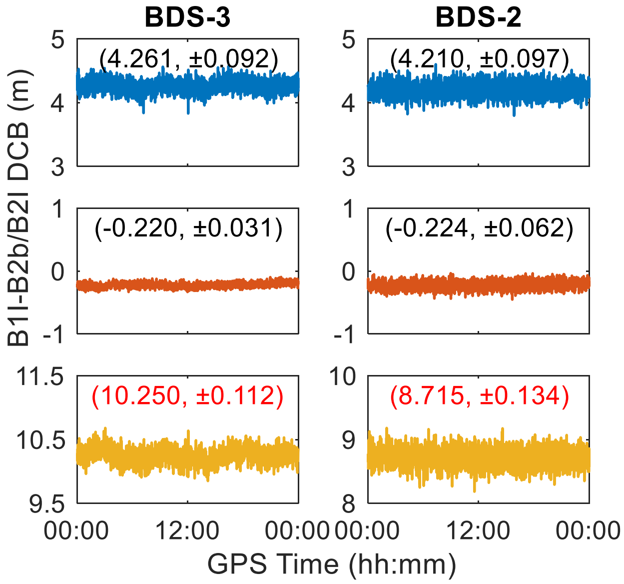

Fig. 7 Time series of BDS-3 B1I-B2b (left) and BDS-2 B1I-B2I (right) DCB on DOY 340 of 2020. Three zero baselines are used, including APM1-APM2 with two ALLOY receivers (top), APM3-APM4 with two POLARX5 receivers (middle), APM1-APM3 with ALLOY and POLARX5 receivers (bottom). The numbers in each panel represent the mean and STD in meters

Characterization of BDS-3 and BDS-2 DCB estimates

In this section, the DCB of the common frequencies (B1I-B3I, B1I-B2b/B2I) of BDS-3 and BDS-2 are first analyzed. Then, using B1I as a reference, DCB of the new frequencies of BDS-3 (B1I-B1C and B1I-B2a) will be reported.

Figure 6 shows the B1I-B3I DCB of BDS-3 (left) and BDS-2 (right), with each color representing a different baseline. Normally, one would expect DCB of the same frequency combination to be completely consistent for BDS-3 and BDS-2, as they are considered one constellation. The expected results can be seen in the baselines with identical receiver pairs (blue and red lines), where the DCB of B1I-B3I barely differs between BDS-3 and BDS-2. However, the situation becomes different when referring to a mixed-receiver combination. Here, we see there is a clear distinction of B1I-B3I DCB between BDS-3 and BDS-2, with a difference of 1.128 m. In this case, the difference of B1I-B3I DCB between BDS-3 and BDS-2 must be taken into account and ignoring it may adversely affect PNT applications. Moreover, focusing on each panel, we see that these estimates fluctuate randomly around their mean value, with no apparent trend over time, indicating that B1I-B3I DCB has no significant short-term change for each of the above three baselines.

Figure 7 is analogous to Fig. 6, except that it shows the DCB of BDS-3 B1I-B2b and BDS-2 B1I-B2I. These results confirm the previous observations that for a baseline

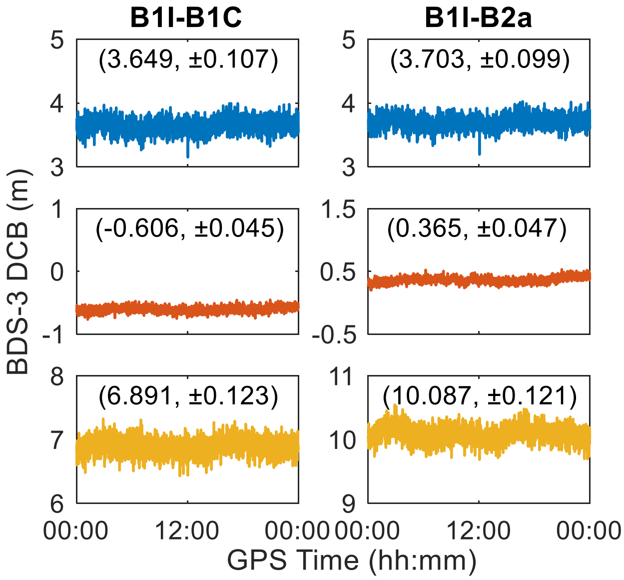

Fig. 8 Time series of BDS-3 B1I-B1C (left) and B1I-B2a (right) DCB estimates on DOY 340 of 2020. Three baselines are used, including APM1-APM2 with two ALLOY receivers (top), APM3-APM4 with two POLARX5 receivers (middle), APM1-APM3 with ALLOY and POLARX5 receivers (bottom). The numbers in each panel represent the mean and STD in meters

comprising the same receiver type, no difference will occur between the DCB of the overlapping frequency combination of BDS-3 and BDS-2. However, at the same time, the characteristics of DCB between BDS-3 and BDS-2 based on the mixed-receiver combination are interesting. The bottom two panels (yellow lines) show a difference between BDS-3 B1I-B2b and BDS-2 B1I-B2I of 1.535 m, which indicates the DCB difference between BDS-3 B1I-B2b and BDS-2 B1I-B2I should be carefully considered.

Figure 8 shows the BDS-3 B1I-B1C and B1I-B2a DCB estimates, from which we can see that the values of DCB are significant, but the intra-day stability is also noticeable. After sidereal filtering, although the multipath effect is obviously weakened, we can still see that the DCB estimation has a certain trend, e.g., see bottom right. This phenomenon can be attributed to the combination of residual multipath effects and other unmodeled errors.

An important conclusion can be drawn that inconsistencies in the characterization of B1I-B3I and B1I-B2b/B2I DCB in BDS-2 and BDS-3 must be fully considered in PNT applications.

Characterization of BDS-3 and BDS-2 DPB estimates

Concerning the DPB, Fig. 9 shows the estimates of B1I-B3I DPB of BDS-3 (left) and BDS-2 (right) for three pairs of receivers APM1-APM2 (blue line), APM3-APM4 (red line), and APM1-APM3 (yellow line) on day 340 of 2020. Recall that the estimable of DPB is $\tilde{\delta}^A_{ab,j}(i) = \delta^A_{ab,j}(i) - \delta^A_{ab,1}(i) + \lambda_j z^{1_A}_{ab,j} - \lambda_1 z^{1_A}_{ab,1}$, where the datum ambiguities $\lambda_j z^{1_A}_{ab,j} - \lambda_1 z^{1_A}_{ab,1}$ are included. Thus, we can only analyze the fractional part of DPB without obtaining its absolute value. However, from the compatibility of BDS-3 and BDS-2 in phase ISBs, DPB should also be compatible for the two constellations since DPB and phase ISBs have a linear relationship that can be inferred from each other.

We pay attention here to the three cases depicted in Fig. 9, from which two conclusions can be drawn. First, it is found that the B1I-B3I DPB of BDS-3 and BDS-2 are slightly different in magnitude due to the datum ambiguities, but remarkably similar in the trend (compare left and right). This also illustrates the compatibility of DPB between BDS-3 and BDS-2. Second, the short-term temporal variations of B1I-B3I DPB are significant in BDS-3 and BDS-2. See the second case (red lines), except for the obvious intra-day variation, there is an obvious jump around 12:00 (see green ellipse). We think this is probably due to a sudden change in the ambient temperature (Zhang et al. 2016; Mi et al. 2020b). The same phenomenon occurs in the third case (yellow lines). From the comparison of the three baselines, it can be concluded that the response of different receivers to ambient temperature is inconsistent.

Similar to Fig. 9, Fig. 10 shows the DPB but for the BDS-3 B1I-B2b and BDS-2 B1I-B2I. These results confirm the previous conclusions that the short-term temporal

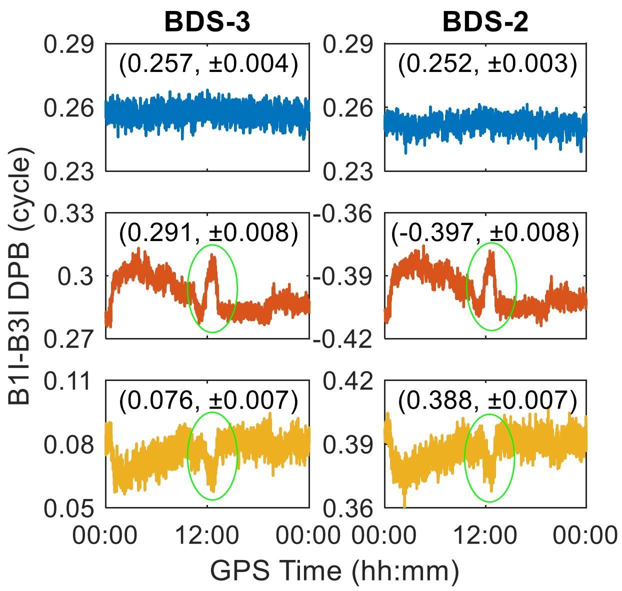

Fig. 9 Time series of BDS-3 (left) and BDS-2 (right) B1I-B3I DPB estimates on DOY 340 of 2020. Three zero baselines are used, including APM1-APM2 with two ALLOY receivers (top), APM3-APM4 with two POLARX5 receivers (middle), APM1-APM3 with ALLOY and POLARX5 receivers (bottom). The numbers in each panel represent the mean and STD in cycles

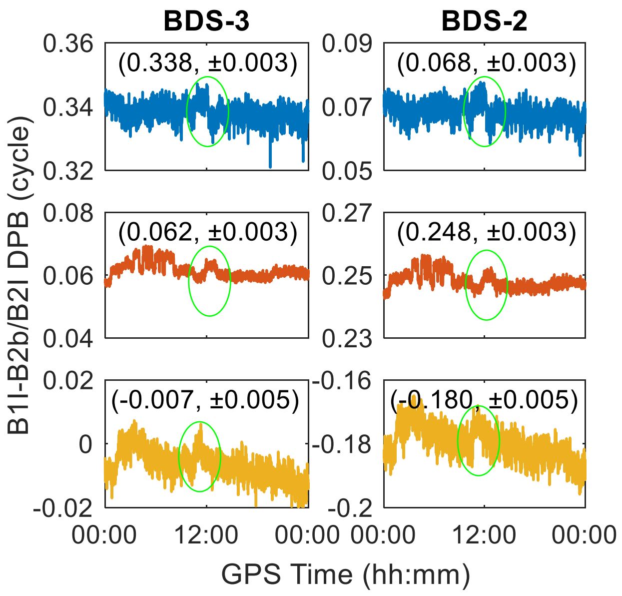

Fig. 10 Time series of BDS-3 B1I-B2b (left) and BDS-2 B1I-B2I (right) DPB estimates on DOY 340 of 2020. Three zero baselines are used, including APM1-APM2 with two ALLOY receivers (top), APM3-APM4 with two POLARX5 receivers (middle), APM1-APM3 with ALLOY and POLARX5 receivers (bottom). The numbers in each panel represent the mean and STD in cycles

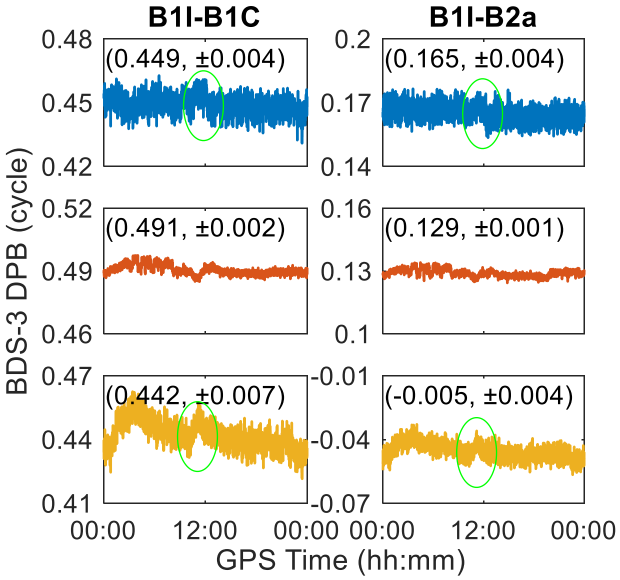

Fig. 11 Time series of BDS-3 B1I-B1C (left) and B2I-B2a (right) DPB estimates on DOY 340 of 2020. Three zero baselines are used, including APM1-APM2 with two ALLOY receivers (top), APM3-APM4 with two POLARX5 receivers (middle), APM1-APM3 with ALLOY and POLARX5 receivers (bottom). The numbers in each panel represent the mean and STD in cycles

variations of DPB must be considered in BDS-3, BDS-2, and their combination. In addition, interestingly, the short-term variations are present in all three cases, especially the jump at around 12:00. Combined with the DPB characteristics of B1I-B3I, this can be attributed to the fact that the B2I and B2b signals of the receivers involved in the experiment are more sensitive to the environment. Thus, it can be concluded that different frequencies have different response mechanisms to ambient temperature.

Figure 11 is analogous to Fig. 8, except it shows the DPB estimates for three baselines. Pay attention to the differences between the receivers used; we can see that the DPB estimates of B1I-B1C and that of B1I-B2a are slightly different in their magnitude and mean values, but noticeably similar in their trend. This also indicates that the receiver-related biases of B1C and B2a of the used receivers have similar mechanisms in response to the environment. Back to Fig. 9, a similar phenomenon also exists in the DPB estimates of B1I-B2b, which means B2b has an environment response similar to that of B1C and B2a.

One important conclusion can be drawn from this analysis. The receiver-related DPB of BDS-3 and BDS-2 may have short-term variations, which can be estimated by analyzing the performance of different receivers and frequencies.

Conclusions

We have presented a method for simultaneously estimating the receiver-related biases, including inter-system biases (ISBs), differential code biases (DCB), and differential phase biases (DPB). This method has the following characteristics, which make it well suited for use in retrieving receiver-related biases. First, an advantage has been taken of not changing reference satellites, thereby enabling the continuity of DPB and phase ISBs estimates. Second, use has been made of a single-differenced (SD) full-rank model. This ensures compatibility of all kinds of cases from single-frequency single-constellation to multi-frequency multi-constellation data, and more importantly, the reasonable simultaneously estimation of DCB, DPB, and ISBs.

Special care should be taken when using BeiDou navigation satellite system with global coverage (BDS-3) and the BeiDou navigation satellite (regional) system (BDS-2), as they are considered compatible and thus treated as one constellation. With this in mind, we applied the method detailed above to several sets of GNSS data with all five frequencies of BDS-3 and three frequencies of BDS-2, covering a range of receiver types and observation periods. The time-wise estimates of the DCB, DPB, and ISBs between BDS-3 and BDS-2, using all five frequencies available, were presented.

It was experimentally shown that the phase observations of the three overlapping frequencies between BDS-3 and BDS-2 are indeed compatible. In other words, the phase observations of the three overlapping frequencies can be processed as one constellation when mixing BDS-3 and BDS-2. However, when we referred to code observations, the situation got complicated. The code ISBs of B1I and B2b/B2I between BDS-3 and BDS-2 are estimated as nonzero but of B3I are not. That is to say, for code observations, only B3I can achieve full compatibility between BDS-3 and BDS-2, and the differences of B1I and B2b/B2I between BDS-3 and BDS-2 must be taken into account. In addition, care should be taken to the difference of DCB involving B1I and B2I/B2b between BDS-3 and BDS-2, as they were found to be significant in our experiment. Moreover, interestingly, we found that DPB of BDS-3 and BDS-2 may have significant short-term variations, which are closely related to receiver and frequency.

Acknowledgements This work was partially funded by the National Natural Science Foundation of China (Grant Nos. 42022025, 41774042) and the Scientific Instrument Developing Project of the Chinese Academy of Sciences (Grant No. YJKYYQ20190063). The corresponding author is supported by the CAS Pioneer Hundred Talents Program.

Data availability The raw data were provided by the Innovation Academy for Precision Measurement Science and Technology, Chinese Academy of Sciences, Wuhan, China. The raw data used during the study are available from the corresponding author upon reasonable request.

References

Brunini C, Azpilicueta F (2010) GPS slant total electron content accuracy using the single layer model under different geomagnetic regions and ionospheric conditions. J Geodesy 84(5):293–304. https://doi.org/10.1007/s00190-010-0367-5

Chang X, Yang X, Zhou T (2005) MLAMBDA: a modified LAMBDA method for integer least-squares estimation. J Geodesy 79(9):552–565

CSNO (2019) Development of the BeiDou navigation satellite system (version 4.0). http://en.beidou.gov.cn/SYSTEMS/Officialdocument/202001/P020200116329195978690.pdf

Dach R, Schildknecht T, Springer T, Dudle G, Prost L (2002) Continuous time transfer using GPS carrier phase. IEEE Trans Ultrason Ferroelectr Freq Control 49(11):1480–1490. https://doi.org/10.1109/Tuffc.2002.1049729

Defraigne P, Baire Q (2011) Combining GPS and GLONASS for time and frequency transfer. Adv Space Res 47(2):265–275. https://doi.org/10.1016/j.asr.2010.07.003

Euler HJ, Goad CC (1991) On optimal filtering of GPS dual frequency observations without using orbit information. Bull Géod 65(2):130–143

Gao W, Meng X, Gao C, Pan S, Wang D (2017a) Combined GPS and BDS for single-frequency continuous RTK positioning through real-time estimation of differential inter-system biases. GPS Solut 22(1):20. https://doi.org/10.1007/s10291-017-0687-5

Gao Z, Ge M, Shen W, Zhang H, Niu X (2017b) Ionospheric and receiver DCB-constrained multi-GNSS single-frequency PPP integrated with MEMS inertial measurements. J Geodesy 91(11):1351–1366. https://doi.org/10.1007/s00190-017-1029-7

Gao W, Pan S, Gao C, Wang Q, Shang R (2019) Tightly combined GPS and GLONASS for RTK positioning with consideration of differential inter-system phase bias. Meas Sci Technol 30(5):054001. https://doi.org/10.1088/1361-6501/ab03bc

Geng J, Li X, Zhao Q, Li G (2019) Inter-system PPP ambiguity resolution between GPS and BeiDou for rapid initialization. J Geodesy 93(3):383–398. https://doi.org/10.1007/s00190-018-1167-6

Gioia C, Borio D (2016) A statistical characterization of the Galileo-to-GPS inter-system bias. J Geodesy 90(11):1279–1291. https://doi.org/10.1007/s00190-016-0925-6

Huang W, Defraigne P (2016) BeiDou time transfer with the standard CGGTTS. IEEE Trans Ultrason Ferroelectr Freq Control 63(7):1005–1012. https://doi.org/10.1109/Tuffc.2016.2517818

Khodabandeh A, Teunissen PJG (2016) PPP-RTK and inter-system biases: the ISB look-up table as a means to support multi-system PPP-RTK. J Geodesy 90(9):837–851. https://doi.org/10.1007/s00190-016-0914-9

Lu C, Feng Gu, Zheng Y, Zhang K, Tan H, Dick G, Wickert J (2020) Real-time retrieval of precipitable water vapor from Galileo observations by using the MGEX network. IEEE Trans Geosci Remote Sens 58(7):4743–4753. https://doi.org/10.1109/Tgrs.2020.2966774

Mi X, Zhang B, Yuan Y (2019a) Multi-GNSS inter-system biases: estimability analysis and impact on RTK positioning. GPS Solut 23(3):81. https://doi.org/10.1007/s10291-019-0873-8

Mi X, Zhang B, Yuan Y (2019b) Stochastic modeling of between-receiver single-differenced ionospheric delays and its application to medium baseline RTK positioning. Meas Sci Technol 30(9):095008. https://doi.org/10.1088/1361-6501/ab11b5

Mi X, Zhang B, Odolinski R, Yuan Y (2020a) On the temperature sensitivity of multi-GNSS intra- and inter-system biases and the impact on RTK positioning. GPS Solut 24(4):112. https://doi.org/10.1007/s10291-020-01027-5

Mi X, Zhang B, Yuan Y, Luo X (2020b) Characteristics of GPS, BDS2, BDS3 and Galileo inter-system biases and their influence on RTK positioning. Meas Sci Technol 31(1):015009. https://doi.org/10.1088/1361-6501/ab4209

Montenbruck O, Hauschild A, Steigenberger P, Hugentobler U, Teunissen P, Nakamura S (2013) Initial assessment of the COMPASS/BeiDou-2 regional navigation satellite system. GPS Solut 17(2):211–222. https://doi.org/10.1007/s10291-012-0272-x

Odijk D, Teunissen PJG (2012) Characterization of between-receiver GPS-Galileo inter-system biases and their effect on mixed ambiguity resolution. GPS Solut 17(4):521–533. https://doi.org/10.1007/s10291-012-0298-0

Odijk D, Nadarajah N, Zaminpardaz S, Teunissen PJG (2016) GPS, Galileo, QZSS and IRNSS differential ISBs: estimation and application. GPS Solut 21(2):439–450. https://doi.org/10.1007/s10291-016-0536-y

Odolinski R, Teunissen PJG (2017a) Low-cost, 4-system, precise GNSS positioning: a GPS, Galileo, BDS and QZSS ionosphere-weighted RTK analysis. Meas Sci Technol 28(12):125801. https://doi.org/10.1088/1361-6501/aa92eb

Odolinski R, Teunissen PJG (2017b) Low-cost, high-precision, single-frequency GPS–BDS RTK positioning. GPS Solut 21(3):1315–1330. https://doi.org/10.1007/s10291-017-0613-x

Odolinski R, Teunissen PJG, Odijk D (2014a) Combined BDS, Galileo, QZSS and GPS single-frequency RTK. GPS Solut 19(1):151–163. https://doi.org/10.1007/s10291-014-0376-6

Odolinski R, Teunissen PJG, Odijk D (2014b) First combined COMPASS/BeiDou-2 and GPS positioning results in Australia. Part II: single- and multiple-frequency single-baseline RTK positioning. J Spat Sci 59(1):25–46. https://doi.org/10.1080/14498596.2013.866913

Odolinski R, Teunissen PJG, Odijk D (2015) Combined GPS + BDS for short to long baseline RTK positioning. Meas Sci Technol 26(4):045801. https://doi.org/10.1088/0957-0233/26/4/045801

Pan L, Guo F (2018) Real-time tropospheric delay retrieval with GPS, GLONASS, Galileo and BDS Data. Sci Rep 8(1):1–17. https://doi.org/10.1038/s41598-018-35155-3

Paziewski J, Wielgosz P (2014) Accounting for Galileo-GPS inter-system biases in precise satellite positioning. J Geodesy 89(1):81–93. https://doi.org/10.1007/s00190-014-0763-3

Psychas D, Verhagen S, Liu X, Memarzadeh Y, Visser H (2019) Assessment of ionospheric corrections for PPP-RTK using regional ionosphere modelling. Meas Sci Technol 30(1):014001. https://doi.org/10.1088/1361-6501/aaefe5

Sanz J, Juan JM, Rovira-Garcia A, Gonzalez-Casado G (2017) GPS differential code biases determination: methodology and analysis. GPS Solut 21(4):1549–1561. https://doi.org/10.1007/s10291-017-0634-5

Sardon E, Rius A, Zarraoa N (1994) Estimation of the transmitter and receiver differential biases and the ionospheric total electron-content from global positioning system observations. Radio Sci 29(03):577–586. https://doi.org/10.1029/94rs00449

Teunissen PJG (1995) The least-squares ambiguity decorrelation adjustment: a method for fast GPS integer ambiguity estimation. J Geodesy 70:65–82. https://doi.org/10.1007/bf00863419

Teunissen PJG (2018) Distributional theory for the DIA method. J Geodesy 92(1):59–80. https://doi.org/10.1007/s00190-017-1045-7

Tian Y, Ge M, Neitzel F, Zhu J (2017) Particle filter-based estimation of inter-system phase bias for real-time integer ambiguity resolution. GPS Solut 21(3):949–961

Tu R, Zhang P, Zhang R, Fan L, Liu J, Xi Lu (2019) Multiple GNSS inter-system biases in precise time transfer. Meas Sci Technol 30(11):115003. https://doi.org/10.1088/1361-6501/ab32b3

Verhasselt K, Defraigne P (2019) Multi-GNSS time transfer based on the CGGTTS. Metrologia 56(6):065003. https://doi.org/10.1088/1681-7575/ab3ed7

Wang K, Khodabandeh A, Teunissen PJG (2018) Five-frequency Galileo long-baseline ambiguity resolution with multipath mitigation. GPS Solut 22(3):1–14. https://doi.org/10.1007/s10291-018-0738-6

Wang M, Wang J, Dong D, Meng L, Chen J, Wang A, Cui H (2019) Performance of BDS-3: satellite visibility and dilution of precision. GPS Solut 23(2):56. https://doi.org/10.1007/s10291-019-0847-x

Yang Y, Li J, Wang A, Xu J, He H, Guo H, Shen J, Dai X (2014) Preliminary assessment of the navigation and positioning performance of BeiDou regional navigation satellite system. Sci China Earth Sci 57(1):144–152. https://doi.org/10.1007/s11430-013-4769-0

Yang Y, Xu Y, Li J, Yang C (2018) Progress and performance evaluation of BeiDou global navigation satellite system: data analysis based on BDS-3 demonstration system. Sci China Earth Sci 61(5):614–624. https://doi.org/10.1007/s11430-017-9186-9

Yang Y, Gao W, Guo S, Mao Y, Yang Y (2019) Introduction to BeiDou-3 navigation satellite system. Navigation 66(1):7–18. https://doi.org/10.1002/navi.291

Yang Y, Mao Y, Sun B (2020) Basic performance and future developments of BeiDou global navigation satellite system. Satell Navig 1(1):1. https://doi.org/10.1186/s43020-019-0006-0

Yuan Y, Mi X, Zhang B (2020) Initial assessment of single-and dual-frequency BDS-3 RTK positioning. Satell Navig 1(2):31. https://doi.org/10.1186/s43020-020-00031-x

Zha J, Zhang B, Yuan Y, Zhang X, Li M (2019) Use of modified carrier-to-code leveling to analyze temperature dependence of multi-GNSS receiver DCB and to retrieve ionospheric TEC. GPS Solut 23(4):103. https://doi.org/10.1007/s10291-019-0895-2

Zhang B, Teunissen PJG (2015) Characterization of multi-GNSS between-receiver differential code biases using zero and short baselines. Sci Bull 60(21):1840–1849. https://doi.org/10.1007/s11434-015-0911-z

Zhang B, Teunissen PJG, Yuan Y (2016) On the short-term temporal variations of GNSS receiver differential phase biases. J Geodesy 91(5):563–572. https://doi.org/10.1007/s00190-016-0983-9

Zhang B, Chen Y, Yuan Y (2018) PPP-RTK based on undifferenced and uncombined observations: theoretical and practical aspects. J Geodesy 93(7):1011–1024. https://doi.org/10.1007/s00190-018-1220-5

Xiaolong Mi is a Ph.D. candidate at the Innovation Academy for Precision Measurement Science and Technology, Chinese Academy of Sciences, China, and Curtin University, Australia. His research focuses on high-precision GNSS positioning, multi-GNSS inter-operability, and software development, especially in the receiver-related biases estimation and application.

Chuanzhen Sheng has been a senior engineer at the State Key Laboratory of Satellite Navigation System and Equipment Technology since 2015. His research interests include GNSS/LEO orbit determination, GNSS Time Transfer, Real-time Kinematic Positioning, Precise Point Positioning, and GNSS Deformation.

Ahmed El-Mowafy is an Associate Professor in Curtin University, Australia. His research areas include precise positioning and navigation using GNSS, integrity monitoring, and estimation theory. He is a member of the IGS MGEX working group, chair of the IAG study group Integrity Monitoring for Precise Positioning, sets on the Editorial Board of five journals, and published more than 150 research articles.

Baocheng Zhang is a professor at the Innovation Academy for Precision Measurement Science and Technology, Chinese Academy of Sciences. His research focuses on modeling multiple global navigation satellite systems for integer ambiguity resolution-enabled precise point positioning (PPP-RTK) applications.

5 UDUC GNSS Time Transfer considering Time-varying Receiver Code Biases

5.1 Introduction

The realization of GNSS time transfer depends on a premise and an assumption. The premise is the precise calibration of the receiver code bias, and the assumption is that the receiver code bias remains stable (Defraigne et al., 2021). It should be noted that the receiver code bias in GNSS time transfer should be more accurately expressed as the receiver-end code bias, because it is composed of the delay generated by the GNSS receiver, antenna, external clock and cables connecting these devices (Leute, 2018). Currently, absolute and relative calibration methods satisfy the requirements of receiver code bias calibration for GNSS time transfer (Esteban et al., 2010; Lewandowski et al., 1987; Overney et al., 1997; Plumb et al., 2005). As a result, the key to the success of GNSS time transfer is that the time-invariant assumption of the biases is guaranteed.

Nevertheless, research has indicated that short-term variations in receiver code bias exist and are closely linked to environmental factors, particularly temperature (Mi et al., 2020; Petit et al., 2022; Ray and Senior, 2001; Rieck et al., 2003). Consequently, to minimize the impact of these short-term variations on GNSS time transfer, time laboratories typically utilize the following measures: establishing a near-constant temperature to control the GNSS receiver environment, selecting antennas that are minimally affected by environmental factors, and choosing cables with good temperature stability. These strategies effectively mitigate significant short-term variations in receiver code bias and ensure the accuracy of GNSS time transfer. However, long-term trends in receiver code bias remain a challenge for which there are currently no viable solutions (Petit and Defraigne, 2023; Zhang et al., 2015). This chapter will explore the impact of receiver code bias variations on GNSS time transfer. A solution is proposed that involves modifying the model to describe the receiver code bias variations, rather than attempting to control each bias component, so that it no longer affects GNSS time transfer.

This chapter presents a novel time transfer model that considers time-varying receiver code biases, building upon the UDUC PPP time transfer model. Using this model, the chapter investigates the characteristics of receiver code bias variations and their impact on time transfer.

5.2 Full-rank GNSS Time Transfer Model for Terrestrial Applications

In this section, a new GNSS time transfer model considering time-varying receiver code biases is presented. As a starting point to develop this model, the UDUC GNSS equations are first given as follows,

$$\begin{aligned} p^s_{r,j}(i) &= \rho^s_r(i) + dt_r(i) + d_{r,j} + \tau^s_r(i) + \mu_j I^s_{r,j}(i) - dt^s - d^s_{,j} + \varepsilon^s_{p,j} \\ \phi^s_{r,j}(i) &= \rho^s_r(i) + dt_r(i) + \delta_{r,j} + \tau^s_r(i) - \mu_j I^s_{r,j}(i) - dt^s - \delta^s_{,j} + \lambda_j N^s_{r,j} + \varepsilon^s_{\phi,j} \end{aligned} \tag{5.1}$$

where r, s, j and i represent the receiver, satellite, frequency, and epoch, respectively. $p^s_{r,j}(i)$ and $\phi^s_{r,j}(i)$ are the UDUC GNSS code and phase observations, respectively. $\rho^s_r(i)$ is the satellite-receiver range, $dt_r(i)$ is the receiver clock offset and $\tau^s_r(i)$ is the tropospheric delay. $d_{r,j}$ and $\delta_{r,j}$ are the code and phase biases at the receiver-end, and their counterpart $d^s_{,j}$ and $\delta^s_{,j}$ are those at the satellite-end. $I^s_{r,j}(i)$ is the ionospheric delay and $\mu_j = \lambda^2_j / \lambda^2_1$ is its coefficient where λ_j is the wavelength. dt^s is the satellite clock and $N^s_{r,j}$ is the phase ambiguity. $\varepsilon^s_{p,j}$ and $\varepsilon^s_{\phi,j}$ are the code and phase observation noise and miss-modelled random effects.

In the PPP time transfer model, the precise satellite clocks $d\tilde{t}^s = dt^s + d^s_{,IF}$ based on IF combination, where $d^s_{,IF} = \frac{\mu_2}{\mu_2-\mu_1} d^s_{,1} - \frac{\mu_1}{\mu_2-\mu_1} d^s_{,2}$, are directly corrected in GNSS code and phase observations. The tropospheric delay is usually expressed as the sum of the dry and wet delays $\tau^s_r = (\tau_d)^s_r + m^s_r \tau_r$, where $(\tau_d)^s_r$ is the dry part and usually pre-corrected by empirical models. $m^s_r \tau_r$ is the wet tropospheric delay, where m^s_r is the known mapping function and τ_r is the unknown tropospheric zenith wet delay (ZWD). Both Chapter 3 and Chapter 4 have addressed the rank deficiencies observed in the UDUC GNSS equations. Thus, the classical full-rank UDUC PPP can be directly given as follows,

$$\begin{aligned} \tilde{p}^s_{r,j}(i) &= \rho^s_r(i) + d\tilde{t}_r(i) + m^s_r \tau_r(i) + \mu_j \tilde{I}^s_{r,j}(i) - \tilde{d}^s_{r,j} + \varepsilon^s_{p,j} \\ \tilde{\phi}^s_{r,j}(i) &= \rho^s_r(i) + d\tilde{t}_r(i) + m^s_r \tau_r(i) - \mu_j \tilde{I}^s_{r,j}(i) - \tilde{\delta}^s_{r,j} + \varepsilon^s_{\phi,j} \end{aligned} \tag{5.2}$$

where $\tilde{p}^s_{r,j}(i) = p^s_{r,j}(i) + d\tilde{t}^s - (\tau_d)^s_r$ and $\tilde{\phi}^s_{r,j}(i) = p^s_{r,j}(i) + d\tilde{t}^s - (\tau_d)^s_r$, respectively. The estimable unknowns and their interpretations are given in Table 1, where $d_{r,GF} = \frac{1}{\mu_2-\mu_1}(d_{r,2} - d_{r,1})$, $d^s_{GF} = \frac{1}{\mu_2-\mu_1}(d^s_{,2} - d^s_{,1})$ and $d_{r,IF} = \frac{\mu_2}{\mu_2-\mu_1} d_{r,1} - \frac{\mu_1}{\mu_2-\mu_1} d_{r,2}$ (GF: geometry-free).

Table 1 Estimable unknowns and their interpretations in classical UDUC PPP together with the *S*-basis used

Estimable parameter	Notation and interpretation
Receiver clock offset	$d\tilde{t}_r(i) = dt_r(i) + d_{r,IF}$
Ionospheric delay	$\tilde{I}^s_r(i) = I^s_r(i) + d_{r,GF} - d^s_{,GF}$
Satellite code bias	$\tilde{d}^s_{r,j} = d^s_{,j} - d^s_{,IF} - \mu_j d^s_{,GF} - d_{r,j} + d_{r,IF} + \mu_j d_{r,GF}$, $j \geq 3$
Satellite phase bias	$\tilde{\delta}^s_{r,j} = \delta^s_{,j} - d^s_{,IF} + \mu_j d^s_{,GF} - \lambda_j N^s_{r,j} - \delta_{r,j} + d_{r,IF} - \mu_j d_{r,GF}$, $j \geq 1$
S-basis	$d_{r,j}$, $\delta_{r,j}$, $d_{r,IF}$, $N^s_{r,j}$, $d_{r,GF}$, $d^s_{,GF}$

Particular attention should be paid to the receiver clock offset $d\tilde{t}_r(i) = dt_r(i) + d_{r,IF}$, where $d_{r,IF}$ is usually assumed to be time-invariant. However, in principle, $d_{r,j}$ may be time-varying. If $d_{r,j}$ is time-varying, then $d_{r,IF}$ will be time-varying, which will affect time transfer. Taking $d_{r,j}(i)$ as the time-varying receiver code bias, it should be estimated in the model. However, in this situation, some additional *S*-basis elements are needed to be selected to eliminate the rank deficiency caused by the introduction of $d_{r,j}(i)$. This rank deficiency is solved by selecting the *S*-basis from the first epoch, and after it is eliminated, the full-rank GNSS time transfer model considering time-varying receiver code biases (defined as TVRCB model in what follows) can be given as follows,

$$\begin{aligned}
\tilde{p}^s_{r,j}(i) &= \rho^s_r(i) + d\tilde{\tilde{t}}_r(i) + \tilde{d}_{r,j}(i) + m^s_r \tau_r(i) + \mu_j \tilde{\tilde{I}}^s_{r,j}(i) - \tilde{\tilde{d}}^s_{r,j} + \varepsilon^s_{p,j} \\
\tilde{\phi}^s_{r,j}(i) &= \rho^s_r(i) + d\tilde{\tilde{t}}_r(i) + m^s_r \tau_r(i) - \mu_j \tilde{\tilde{I}}^s_{r,j}(i) - \tilde{\tilde{\delta}}^s_{r,j} + \varepsilon^s_{\phi,j}
\end{aligned} \tag{5.3}$$

where $\tilde{d}_{r,j}(i) = d_{r,j}(i) - d_{r,j}(1)$ with $i \geq 2$. This implies that the estimation of $d_{r,j}(i)$ is not possible, whereas $\tilde{d}_{r,j}(i)$ can be estimated with respect to the first epoch. The receiver clock offset, ionospheric delay, satellite code and phase biases are only related to the receiver code biases of the first epoch, thus are free from the impact of time-varying receiver code biases. The estimable forms of the remaining parameters within the TVRCB model are presented in Table 2.

Table 2 Estimable unknowns and their interpretations in the TVRCB model in Equation (5.3) together with additional *S*-basis

Estimable parameter	Notation and interpretation
Receiver clock offset	$d\tilde{\tilde{t}}_r(i) = dt_r(i) + d_{r,IF}(1)$
Ionospheric delay	$\tilde{\tilde{I}}_r^s(i) = I_r^s(i) + d_{r,GF}(1) - d_{,GF}^s$
Satellite code bias	$\tilde{\tilde{d}}_{r,j}^s = d_{,j}^s - d_{,IF}^s - \mu_j d_{,GF}^s - d_{r,j}(1) + d_{r,IF}(1) + \mu_j d_{r,GF}(1)$, $j \geq 3$
Satellite phase bias	$\tilde{\tilde{\delta}}_{r,j}^s = \delta_{,j}^s - d_{,IF}^s + \mu_j d_{,GF}^s - \lambda_j N_{r,j}^s - \delta_{r,j} + d_{r,IF}(1) - \mu_j d_{r,GF}(1)$, $j \geq 1$
S-basis	$d_{r,j}(1)$, $d_{r,IF}(1)$, $d_{r,GF}(1)$

At present, the time transfer community is actively engaged in determining the effects of code biases originating from the receiver-end on GNSS time transfer. Applying the new model proposed in this chapter presents a potential solution, as it encompasses the variation of the receiver-end code biases within $\tilde{d}_{r,j}(i)$.

5.3 Time-varying Characteristics of GNSS Receiver Code Biases

To investigate the variations of receiver code bias and their impact on GNSS time transfer, a data collection exercise was conducted involving two time laboratories. The first is the Innovation Academy for Precision Measurement Science and Technology (APM), Chinese Academy of Sciences, and the second is the Physikalisch-Technische Bundesanstalt (PTB). The specifications of the GNSS data gathered during this study are outlined in Table 3. At the APM laboratory, two receivers were employed, namely APM1 and APM3, synchronized with a common H-maser clock. Similarly, at the PTB laboratory, the receivers PTBB and PT10 were synchronized with the same H-maser clock. Throughout the period spanning from October 12 to November 16, 2022, GPS observations from both the L1 and L2 frequencies of these receivers were collected.

The same data processing strategy was employed for both models, except for the incorporation of receiver code biases as white noise in the TVRCB model. To ensure a seamless convergence process, a bidirectional Kalman filter was implemented (Liu and Zhang, 2021). Receiver clock and ionospheric delay were estimated as white noise. The dry component of tropospheric delay was corrected using the UNB3m model (Leandro et al. 2008), while the wet component was estimated as a random walk (Hadas et al. 2017). The stochastic model utilized an elevation-dependent weighting function (Shen et al., 2009), with phase and code standard deviations of 0.003 m and 0.3 m, respectively. Precise satellite orbit and clock products were provided by the International GNSS Service (IGS), and the P1-C1 Differential code bias (DCB) used was sourced from the Centre for Orbit Determination in Europe (CODE). The Detection, Identification, and Adaptation (DIA) procedure was used to detect and eliminate the effect of outliers (Teunissen, 2018).

Table 3 A general overview of GNSS data considered in this research

Station	Institute	Clock Type	Receiver Type	Antenna Type	Location
APM1	APM	H-maser	TRIMBLE ALLOY	TRM5791.00	30.53°N, 114.36°E
APM3			SEPT POLARX5	TRM159800.00	
PTBB	PTB	H-maser	SEPT POLARX5TR	LEIAR25.R4	52.30°N, 110.46°E
PT10			JAVAD TRE_G3T	NAX3G + C	

This study aims to examine the variations in receiver code bias utilizing the TVRCB model and investigate their influences on GNSS time transfer. Figure 1 provides a visual representation of the variations in receiver code bias for both L1 and L2 frequencies computed using the proposed method of the receiver APM1 on Days of Year (DOYs) 285-320, 2022. Two main conclusions can be drawn from the figure. Firstly, the time-dependent nature of receiver code biases is substantial and necessitates consideration in GNSS applications susceptible to these biases, such as time transfer and ionospheric monitoring. Notably, the receiver code bias for both L1 and L2 frequencies demonstrates temporal variability. Secondly, the variations in receiver code biases closely correlate with the carrier frequency. Specifically, the receiver code bias for L1 experiences a declining trend over time, whereas the bias for L2 showcases irregular variations.

Further supporting these conclusions, Figure 2 presents the variations in receiver code biases for the receiver APM3. It is evident that both L1 and L2 frequencies exhibit significant time-varying characteristics in their receiver code biases. Additionally, while the biases for L1 and L2 demonstrate a similar trend, disparity exists in their magnitudes.

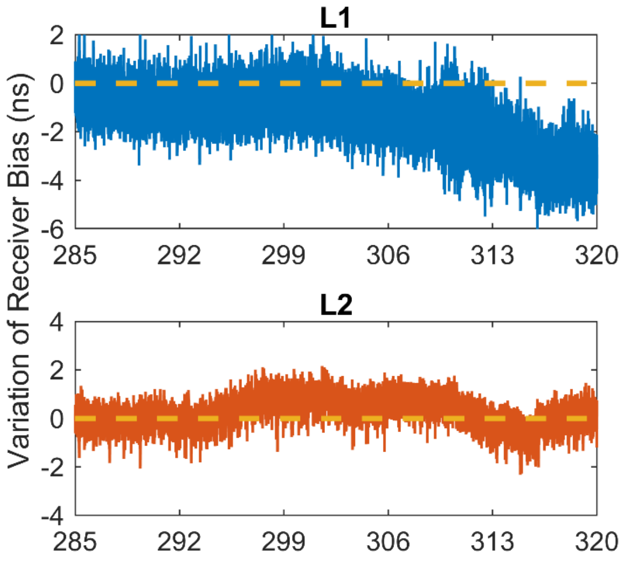

Figure 1 Variations of receiver code biases of L1 and L2 for receiver APM1 on Days of Year (DOYs) 285-320, 2022

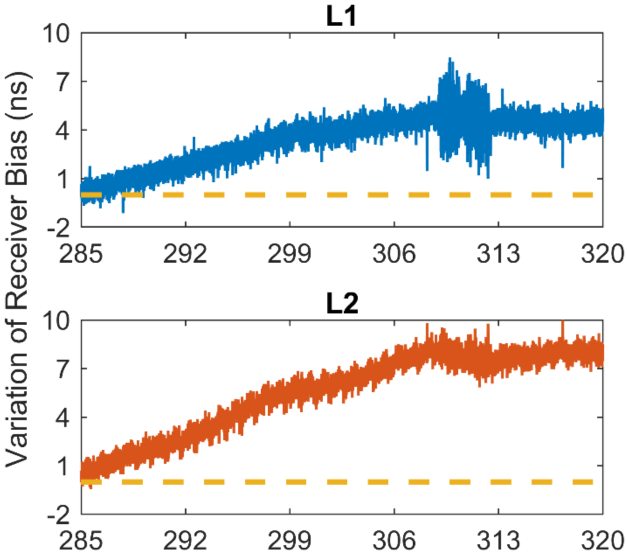

Figure 2 Variations of receiver code biases of L1 and L2 for receiver APM3 on DOYs 285-320, 2022

In addition to the conclusions mentioned above, Figures 3 and 4 depict the estimated variations in receiver code bias for two receivers, PTBB and PT10, respectively. While both devices exhibit similar long-term patterns in their receiver code biases, there are noticeable differences in their short-term fluctuations. These findings highlight the importance for the time community to consider the significant influence of both long-term and short-term variation characteristics of receiver code bias on GNSS time transfer. Understanding these variations becomes crucial to account for their impact on time transfer applications accurately.

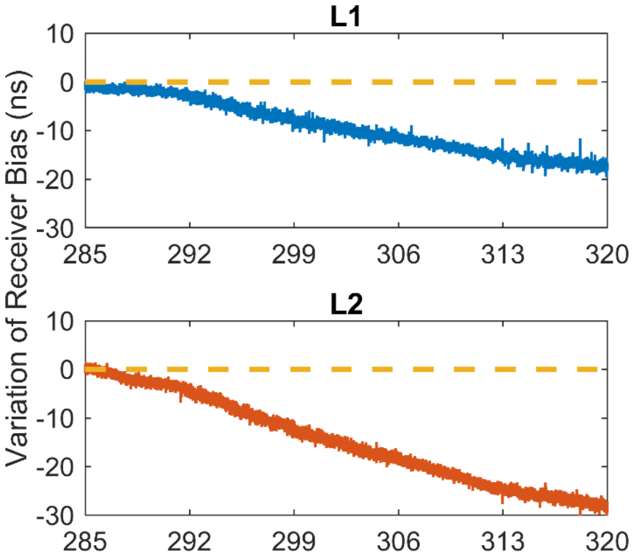

Figure 3 Variations of receiver code biases of L1 and L2 for receiver PTBB on DOYs 285-320, 2022

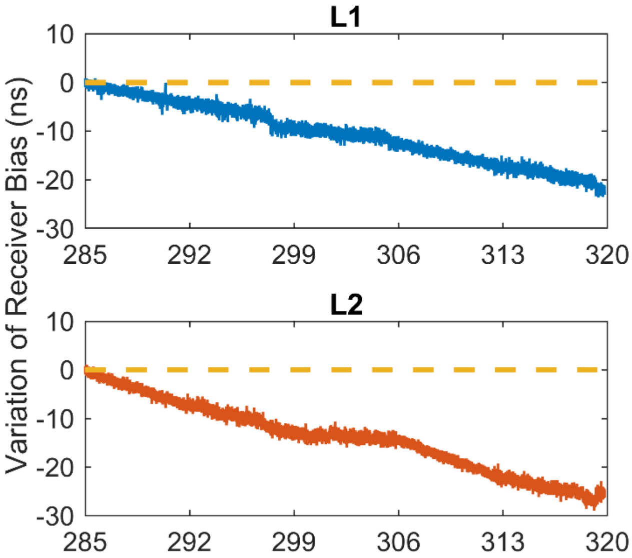

Figure 4 Variations of receiver code biases of L1 and L2 for receiver PT10 on DOYs 285-320, 2022

It is essential to highlight that in GNSS time transfer, the receiver clock offset estimation incorporates the IF receiver code bias, which requires special attention. Figures 1 to 4 provide insights into the variations of receiver code bias for each frequency across four receivers, and Figures 5 and 6 focus on the time-varying characteristics of the IF receiver code bias. These figures reveal that while the receiver code bias for each frequency may exhibit significant time variations, the variation in the IF receiver code bias might not be as pronounced due to potential correlations between the two frequency biases in certain receiver type.

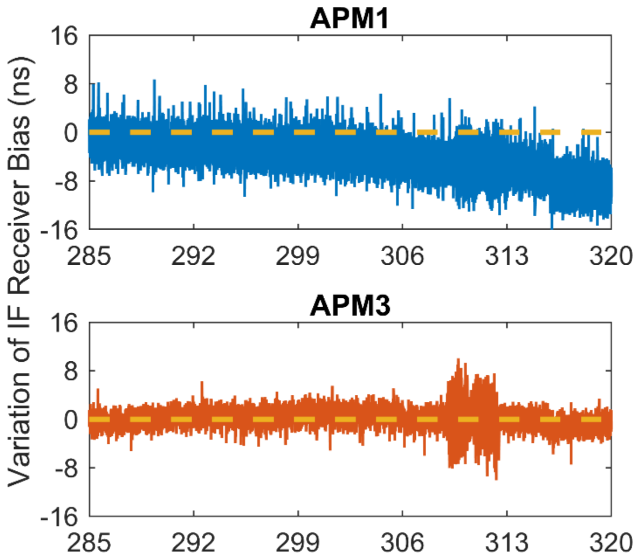

Fig. 5 Variations of IF receiver code bias for receivers APM1 and APM3, respectively, on DOYs 285-320, 2022

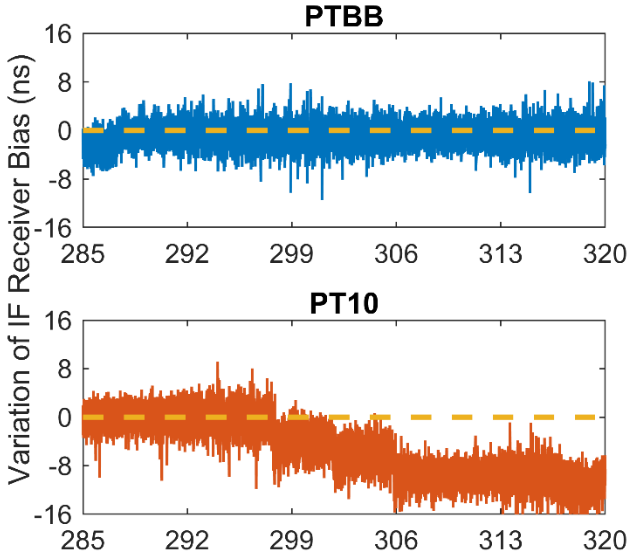

Fig. 6 Variations of IF receiver code bias for receivers PTBB and PT10, respectively, on DOYs 285-320, 2022

For instance, by comparing Figure 1 with Figure 5, one can see that for receiver APM1, the variation in L1 is more prominent compared to that in L2. This suggests that the variation tend in the IF receiver code bias aligns more closely with the variation observed in the receiver code bias for L1. On the other hand, when considering Figures 2 and 5, the receiver APM3 code bias for both the L1 and L2 displays a similar trend, resulting in a less noticeable variation in the IF receiver code bias. Similar conclusions can be drawn from the findings of PTBB and PT10.

In summary, it is evident that receiver code bias exhibits time-varying characteristics, and it would be inappropriate to treat it as a time-invariant parameter in the context of time transfer. Consequently, the following section of the study will analyze the impact of these time-varying characteristics of receiver code biases on GNSS time transfer.

5.4 Impacts of Time-varying Receiver Code Biases on GNSS Time Transfer

The primary objective of investigating time-varying receiver code biases is maximizing GNSS time transfer performance. In this study, the potential impact of these time-varying biases on GNSS time transfer is explored using two models: the UDUC PPP model and the TVRCB model.

Figure 7 shows the time difference obtained from APM1-APM3 utilizing both the UDUC PPP and TVRCB models discussed earlier. APM1 and APM3 are synchronized with the same H-maser clock, which eliminates the influence of the atomic clock itself, providing an ideal setup to investigate the influence of receiver code bias variations on GNSS time transfer. In this common clock scenario, the performance of GNSS time transfer relies solely on the estimated IF receiver code bias.

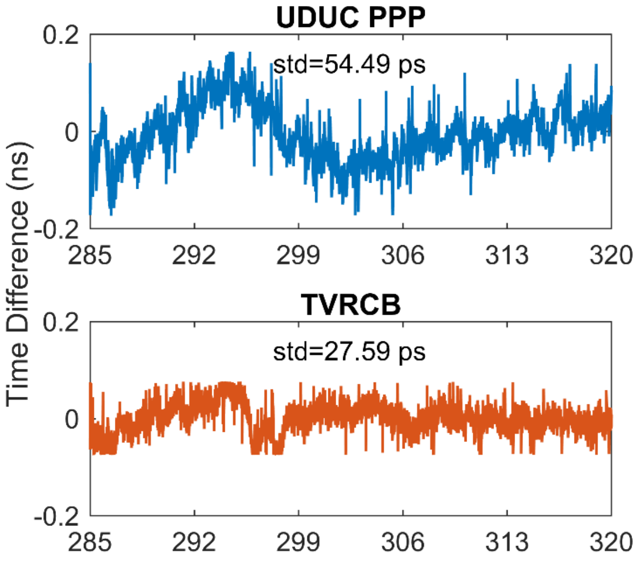

Figure 7 Time difference between receivers APM1 and APM3 with the UDUC PPP and TVRCB models on DOYs 285-320, 2022

When the UDUC PPP model is employed, the time difference exhibits significant time variation, which diminishes the performance of GNSS time transfer. However, when the proposed TVRCB model, which accounts for receiver code bias variations, is utilized, the time difference demonstrates improved stability. The standard deviation of the time difference for the UDUC PPP model and the TVRCB model is measured at 54.49 ps and 27.59 ps, respectively, indicating a notable enhancement of 49.3% when utilizing the TVRCB model. These results affirm that incorporating receiver code bias variations into the model, as done in the TVRCB approach, is advantageous for GNSS time transfer. By considering the time-varying characteristics of receiver code biases, the proposed TVRCB model outperforms the UDUC PPP model, emphasizing the importance of accounting for these variations to enhance the performance of GNSS time transfer.

Figure 8 illustrates the modified Allan deviation (MDEV) of the time differences between APM1 and APM3, which leads to two important conclusions. Firstly, the short-term stability of the UDUC PPP model is superior to that of the TVRCB model. For instance, the frequency stability for an averaging time of 120 s using the UDUC PPP and TVRCB models is 5.15×10^{-14} and 9.60×10^{-14}, respectively. This is attributed to the TVRCB's estimation of the time-varying receiver code bias, which increases the noise of the parameter estimation and reduces the short-term stability. Secondly, due to the incorporation of time variation of the receiver code bias, the TVRCB exhibits distinct advantages for the long-term stability. For example, the frequency stability for an averaging time of one day for the UDUC PPP and TVRCB models is 3.57×10^{-16} and 2.86×10^{-16}, respectively. This represents a 19.9% improvement in the frequency stability using the TVRCB model compared to the UDUC PPP model, thus emphasizing the benefits of considering receiver code bias variations.

The second experiment involves the PTBB and PT10 receivers, utilizing the same H-maser clock. Figure 9 illustrates that the performance improvement achieved by the TVRCB model compared to the UDUC PPP model for PTBB-PT10 is not as pronounced as observed for APM1-APM3. This disparity can be attributed to the fact that the variations in receiver code bias for PTBB-PT10, as depicted in Figures 5 and 6, are not as significant as those observed for the receivers APM1-APM3.

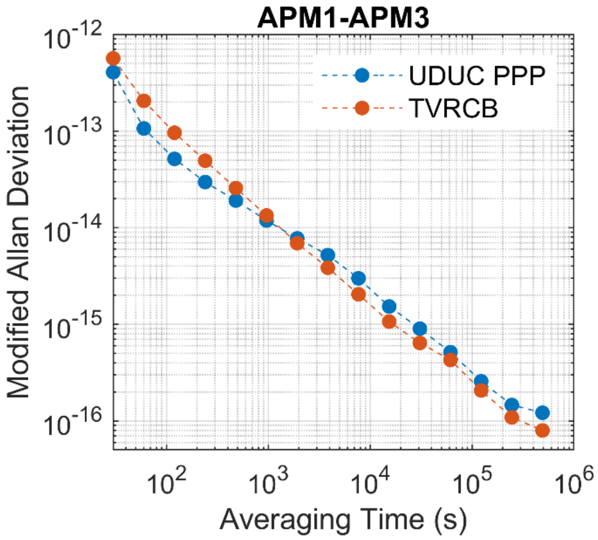

Figure 8 MDEV of the APM1-APM3 with the UDUC PPP and TVRCB models

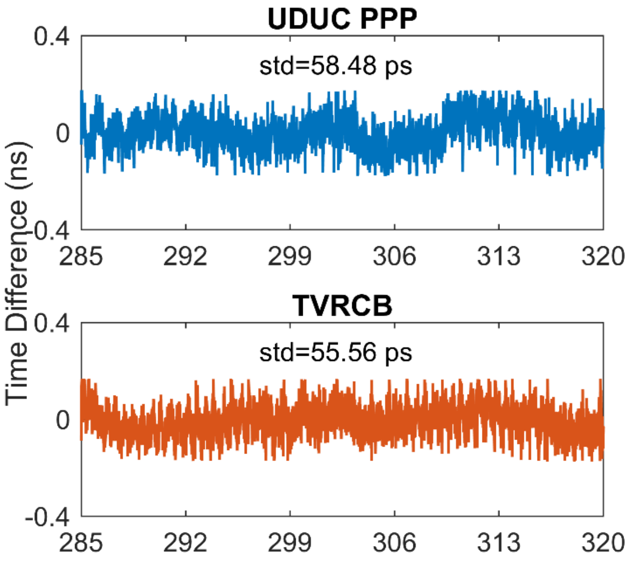

Figure 9 Time difference between receivers PTBB and PT10 with the two models on DOYs 285-320, 2022

The corresponding standard deviation of the time difference for the UDUC PPP and TVRCB models is 58.48 ps and 55.56 ps, respectively, indicating a relatively minor improvement. Further supporting these findings, Figure 10 presents the MDEV of the two models for the receivers PTBB-PT10. From the figure one can see firstly, the short-term stability of the TVRCB model is inferior to that of the UDUC PPP model due to the additional estimation of receiver code bias variations. For instance, the frequency stability for an averaging time of 240 s is 17.5% lower in the TVRCB model than the UDUC PPP model. Secondly, the performance of long-term frequency stability experiences significant improvement when variations in receiver code bias are considered. The frequency stability for an averaging time at one day for the two models is 3.89×10^{-16} and 2.50×10^{-16}, respectively, showing an improvement of 35.7%.

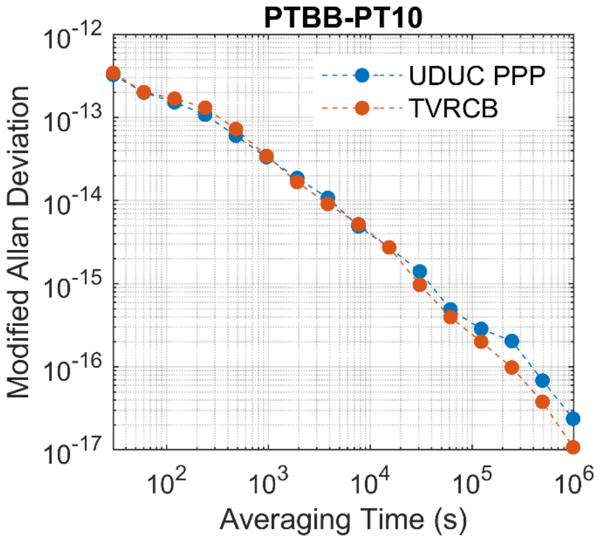

Figure 10 MDEV of the PTBB-PT10 with the UDUC PPP and TVRCB models

5.5 Chapter Summary

The GNSS time transfer relies on the assumption that receiver code bias remains time-invariant, which is challenging to achieve. The time community has recognized the significance of considering receiver code bias variations. However, the existing solution of separately controlling receiver, antenna, external clock and cable biases is complex and expensive. Therefore, in this study, a new GNSS time transfer model based on the traditional UDUC PPP model is proposed, where receiver code bias variations are estimated within the model to mitigate their impact on time transfer. The proposed method estimates the receiver code bias variations caused by the receiver, antenna, and cable, which is simple and low-cost and does not require complex external environments and hardware conditions.

Experimental results obtained from the APM and PTB laboratories were utilized to validate the proposed model and explore the effects of receiver code bias variations on GNSS time transfer. The significant variations in receiver code bias and their strong frequency dependence are confirmed, which must be accounted for in GNSS time transfer. However, it is found that the parameter estimation noise becomes more significant in the TVRCB model compared to the UDUC PPP model, resulting in reduced short-term stability. Nevertheless, test results show that long-term stability has been significantly improved after considering receiver code bias variations.

This study presents a novel and innovative approach to effectively mitigate receiver code bias variations in GNSS time transfer, which has been validated through the utilization of common-clock time links. In contrast to conventional complex schemes that are employed to control receiver code bias variations, the proposed approach exclusively resolves the detrimental effects caused by these variations at the algorithmic level. This pioneering method offers essential technical support for the future development of GNSS time transfer. However, it is essential to note that achieving a significant improvement in GNSS time transfer performance requires addressing several challenges, including applying high-precision optical clocks, synchronization estimation of satellite clocks, and accounting for receiver code bias variations. The thesis addresses the impact of these challenges on GNSS time transfer at the algorithmic level and proposes solutions in different chapters. With the anticipated widespread use of high-precision optical clocks in the future, the solutions proposed in this thesis are expected to contribute significantly to the advancement of the next generation time reference.

6 UDUC Precise Orbit Determination of LEO Satellites

The precise orbit determination (POD) of low Earth orbit (LEO) satellite is a fundamental requirement for various space science applications. In this regard, this chapter aims to facilitate the successful implementation of space applications for GNSS time transfer in subsequent chapters by examining the limitations of the current LEO POD methods and proposing a new POD method that is well-suited for both absolute and relative POD based on modelling undifferenced and uncombined (UDUC) observations. The research findings of this chapter are presented in the following publication:

Mi, X., Allahvirdi-Zadeh, A., El-Mowafy, A., Huang, Z., Wang, K., Zhang, B., & Yuan, Y. (2023). Absolute and relative POD of LEO satellites in formation flying: Undifferenced and uncombined approach. Advances in Space Research, 72(4), 1070-1080. https://doi.org/10.1016/j.asr.2023.05.024

Available online at www.sciencedirect.com

ScienceDirect

Advances in Space Research 72 (2023) 1070–1080

ADVANCES IN SPACE RESEARCH
(a COSPAR publication)

www.elsevier.com/locate/asr

Absolute and relative POD of LEO satellites in formation flying: Undifferenced and uncombined approach

Xiaolong Mi [a], Amir Allahvirdi-Zadeh [a], Ahmed El-Mowafy [a], Zhiyong Huang [c], Kan Wang [d,e], Baocheng Zhang [b,f,*], Yunbin Yuan [b]

[a] School of Earth and Planetary Sciences, Curtin University, Perth, Australia
[b] State Key Laboratory of Geodesy and Earth's Dynamics, Innovation Academy for Precision Measurement Science and Technology, Chinese Academy of Sciences, Wuhan, China
[c] Institute of Geospatial Information, Information Engineering University, China
[d] National Time Service Center, Chinese Academy of Sciences, Xi'an, China
[e] University of Chinese Academy of Sciences, Beijing, China
[f] State Key Laboratory of Satellite Navigation System and Equipment Technology, the 54th Research Institute of China Electronics Technology Group Corporation, Shijiazhuang 050081, China

Received 7 February 2023; received in revised form 9 May 2023; accepted 13 May 2023
Available online 19 May 2023

Abstract

Absolute or relative precise orbit determination (POD) is an essential prerequisite for many low earth orbit (LEO) missions. The POD of LEO satellites typically relays on processing the onboard global navigation satellite system (GNSS) measurements. The absolute POD is usually based on an ionosphere-free (IF) combination, and currently, integer ambiguity resolution (IAR) can be achieved only when external GNSS satellite phase bias (SPB) products are used. The use of these products is not flexible in multi-frequency/multi-constellation scenarios and is difficult to achieve in real-time missions. For relative POD, the double-differenced (DD) with IAR is the most general method. However, the differencing process amplifies observation noise and loses the opportunity to impose dynamic constraints on some eliminated parameters. In this contribution, based on the use of undifferenced and uncombined (UDUC) observations, a new model for both absolute and relative POD is proposed. In this model, the ambiguities of common-view satellites are constructed into DD form, thus IAR can be achieved without any external SPB products. Working with the UDUC observations, multi-frequency scenarios can be easily applied, and residuals can be separated for each frequency. In addition, with precise GNSS satellite clock/orbit products, both the absolute and relative orbits can be derived, which supports absolute and relative LEO POD. Based on onboard GPS observations of T-A and T-B satellites in formation flying, the performance of the UDUC POD model with DD ambiguity was evaluated. With the UDUC algorithm and IAR, the proposed model presented a consistency of 2.8–3.8 cm in 3D with the reference orbits, and the orbit difference was reduced by 16.3% and 10.6% for T-A and T-B compared with the IF-based POD, respectively. In addition, the relative orbit of the two satellites derived from the proposed model showed a consistency of 1.1–1.5 mm, which proved the feasibility of the UDUC POD model with DD ambiguity for formation flying missions.

Keywords: Low Earth Orbit (LEO); Precise Orbit Determination (POD); Formation flying; Global Navigation Satellite System (GNSS); Integer Ambiguity Resolution (IAR); Undifferenced and Uncombined (UDUC)

---

* Corresponding author.
E-mail addresses: xiaolong_mi@asch.whigg.ac.cn (X. Mi), amir.allahvirdizadeh@curtin.edu.au (A. Allahvirdi-Zadeh), A.El-Mowafy@curtin.edu.au (A. El-Mowafy), geo_hzy@126.com (Z. Huang), wangkan@ntsc.ac.cn (K. Wang), b.zhang@whigg.ac.cn (B. Zhang), yybgps@whigg.ac.cn (Y. Yuan).

https://doi.org/10.1016/j.asr.2023.05.024
0273-1177/© 2023 COSPAR. Published by Elsevier B.V.

1. Introduction

Low Earth Orbit (LEO) satellites are those with orbital altitudes generally between a few hundred kilometers and 1500 km, which enables earth and space exploration with high-precision and high spatial–temporal resolution. Accurate orbital information in an absolute or relative mode is an essential prerequisite for many LEO missions (Montenbruck et al., 2009; Bandyopadhyay et al., 2016). The global navigation satellite system (GNSS) and the dynamics of LEO satellites have been used in the precise orbit determination (POD) algorithms. The kinematic and reduced-dynamic approaches are the two main POD methods developed during the past decades (Allahvirdi-Zadeh et al., 2021a, Allende-Alba et al., 2017; Montenbruck et al., 2018; Yunck et al., 1994). Compared to the reduced-dynamic method which exploits extensive dynamic models to estimate orbit perturbations, the kinematic POD is based on precise positioning using GNSS observations without considering any dynamic model (Allahvirdi-Zadeh et al., 2021b; Li et al., 2019c). Currently, there are several hundreds of LEO satellites, including nanosatellites and CubeSats flying in the LEO region. This number will increase in the coming years with more satellites launched for, e.g., aiding GNSS in Positioning, Navigation, and Timing (PNT) applications (Li et al., 2019a; Li et al., 2019b; El-Mowafy et al., 2022). In this sense, absolute and relative POD of LEO constellations are particularly essential mainly in (near) real-time.

Due to the introduction of precise satellite orbit and clock products, kinematic POD uses the concept of precise point positioning (PPP) (Bertiger et al, 2010; Zumberge et al., 1997) to obtain the state solution of a single LEO satellite. It is widely used in the absolute POD of LEO satellites (Hauschild et al., 2016), mainly when the orbits are required to not be affected by dynamic models. However, general kinematic POD usually utilizes the ionosphere-free (IF) combination, which has three disadvantages. Firstly, the IF combination causes a waste of observation information as only one independent parameter is eliminated at the expense of using more observational information (Teunissen, 2020). Secondly, as we explain in the paper, it is not conducive to the expansion of multi-frequency scenarios (Odijk et al., 2016). Thirdly, the ambiguities lose their integer characteristic in the IF model, which is not restored unless by applying external corrections, and limits the performance of the LEO POD. The integer ambiguity resolution (IAR) is needed for realizing high-precision GNSS positioning (Teunissen, 2001). There are some methods to achieve the POD with IAR, which are mainly based on the use of external satellite phase bias (SPB) products (Laurichesse et al., 2009; Ge et al., 2008; Collins, 2008). However, these methods are still based on the IF combination and are thus limited by its drawbacks (Odijk et al., 2016; Teunissen and Khodabandeh, 2015).

In addition to the absolute POD, accurate knowledge of relative states (position and velocity) and the baselines between LEO satellites are required in formation flying missions, as well as docking and rendezvous in space (Bandyopadhyay et al., 2016; Gill et al., 2007). To achieve high-precision relative state solutions, the double-differenced (DD) model with IAR is favored to remove highly correlated parameters and recover the integer nature of the ambiguities (Jäggi et al., 2012; Yi et al., 2022). However, this approach also has some drawbacks. Firstly, the DD model requires strict common-view satellites, which is not guaranteed for high-speed LEO satellites flying at different altitudes in the complex space environment. Secondly, the assumption of the differencing is that the eliminated parameters, such as receiver biases, do not have any time links (Zhang et al., 2019; Odijk et al., 2017). However, this is not the case in actual scenarios (Allahvirdi-Zadeh et al., 2022). The differencing process thus loses the opportunity to impose dynamic constraints on the eliminated parameters (Zhang et al., 2022). Thirdly, the noise of the DD observations is doubled compared to the original observations, which is unfavorable for high-precision relative navigation in formation flying missions, and this has to be considered when modelling their stochastic properties, e.g. in their covariance matrices. There are some remedies for these drawbacks that are implemented for the real-time kinematic (RTK) positioning application on the ground by constructing a single-differenced (SD) model using the S-system theory (Odolinski et al., 2015b; Mi et al., 2019). In this case, the stability of the receiver code and phase biases can be used to increase the strength of the model (Mi et al., 2020). However, the SD model still ignores the stability of code and phase biases at the GNSS end. In addition, the observation noise is amplified during the construction of the SD model compared to the undifferenced (UD) observations.

An alternative approach for the GNSS positioning is based on the undifferenced and uncombined (UDUC) GNSS observation equations (Zhang et al., 2011). In the UDUC approach, neither (single or double) differences are taken nor combinations are formed in the observation domain (Teunissen and Khodabandeh, 2015). The advantages of UDUC formulation have been recognized in geodesy and GNSS for a long time (Lindlohr and Wells, 1985; De Jonge, 1998; Lannes and Prieur, 2013). With uncombined formulation, one can extend the observation equations to arbitrary frequencies, and the ionospheric delays also remain in the observation equations, which can be estimated for use in environmental studies (Zha et al., 2021). Working with the undifferenced formulation allows all the parameters (after necessary re-formulation) to remain available for possible further model strengthening (Khodabandeh and Teunissen, 2015; Psychas et al., 2022). In addition, the UDUC observation equations allow the use of the simplest variance matrix without amplifying the observation noise. However, rank deficiencies need to be considered in the UDUC observation equations since the unbiased estimation of all parameters is impossible (Teunissen, 1985). The application of UDUC method in

LEO POD has been initially explored and has demonstrated its superiority compared with existing methods in various studies (Zehentner and Mayer-Gürr 2016; Suesser-Rechberger et al., 2022).

In this contribution, a new POD model based on the UDUC observations is developed. After removing the rank deficiencies, the ambiguities are presented in the DD form to facilitate the IAR. With the introduction of precise GNSS satellite orbit and clock products, both absolute and relative POD can be achieved using the proposed model. The paper aims to study the benefits of the UDUC formulation and IAR for both absolute and relative POD. In the next section, the UDUC POD model with DD ambiguity is first developed. Next, the proposed model is verified using T-A and T-B LEO satellites in both absolute and relative POD cases. In the last section, the findings are summarized and the conclusions are given.

2. Methodology

In this section, based on the raw GNSS observations, a full-rank UDUC POD model with DD ambiguity will be constructed with the application of the *S*-system theory (Teunissen 1985; Odijk et al., 2016). It will be shown how the model applies to the absolute and relative POD of LEO satellites.

2.1. UDUC GNSS observation equations for LEO satellite

As the starting point of developing the model, we first give the equations for raw GNSS code and phase observations of the LEO satellite, which read,

$$\begin{aligned} p^{s}_{r,j} &= \rho^{s}_{r} + dt_{r} - dt^{s} + \mu_{j} I^{s}_{r} + d_{r,j} - d^{s}_{,j} + \varepsilon^{s}_{p,j} \\ \phi^{s}_{r,j} &= \rho^{s}_{r} + dt_{r} - dt^{s} - \mu_{j} I^{s}_{r} + \lambda_{j} N^{s}_{r,j} + \delta_{r,j} - \delta^{s}_{,j} + \varepsilon^{s}_{\phi,j} \end{aligned} \tag{1}$$

where $p^{s}_{r,j}$ and $\phi^{s}_{r,j}$ are the raw code and phase observables with GNSS satellite s, LEO satellite r and frequency j, respectively.ρ^{s}_{r} is the GNSS-LEO satellite range, which includes the antenna calibration of phase center offset (PCO) and variations (PCV) for code and phase, and phase wind up for the phase. dt_{r} and dt^{s} are the LEO and GNSS satellite clock offsets, respectively.I^{s}_{r} and $\mu_{j} = \lambda^{2}_{j}/\lambda^{2}_{1}$($\lambda_{j}$ is the wavelength of frequency j) are the ionospheric delay on the first frequency and its coefficient.$N^{s}_{r,j}$ is the phase ambiguity. $d_{r,j}$ and $d^{s}_{,j}$ are the LEO and GNSS satellite code biases, respectively, and their counterpart $\delta_{r,j}$ and $\delta^{s}_{,j}$ are the LEO and GNSS satellite phase biases. $\varepsilon^{s}_{p,j}$ and $\varepsilon^{s}_{\phi,j}$ denote the code and phase observation noises and miss-modeled effects including multipath.

2.2. Uncombined (UC) POD model

Due to the existence of the following rank deficiencies, the unknowns in Eq. (1) are difficult to be estimated individually. Therefore, as the first step in constructing the full-rank model, it is necessary to identify these rank deficiencies using the *S*-system theory. With m GNSS satellites and f frequencies tracked at each epoch, eight types of rank deficiencies with one LEO satellite are identified (Odijk et al., 2016; Mi et al. 2023), in the corresponding class:

1. Between the LEO and GNSS satellite clocks of size 1;
2. Between the LEO and GNSS satellite code biases of size f;
3. Between the LEO and GNSS satellite phase biases of size f;
4. Between the LEO satellite clock, code biases and phase biases of size 1;
5. Between the GNSS satellite clocks, code biases and phase biases of size m;
6. Between the GNSS satellite phase biases and ambiguities of size $f \times m$;
7. Between the ionospheric delays, LEO satellite code and phase biases of size 1;
8. Between the ionospheric delays, GNSS satellite code and phase biases of size m.

where the size means the number of rank deficiencies.

Let's review how the classical IF model for the kinematic POD is formed from Eq. (1) and what are the drawbacks of such a model. To achieve precise kinematic POD of LEO satellites, precise GNSS satellite orbits and clocks are necessary. When using precise satellite clock products, the rank deficiencies of types 1 and 5 no longer exist. $\widetilde{dt}^{s} = dt^{s} + d^{s}_{,IF}$ is the precise satellite clock provided by the International GNSS Service (IGS), where $d^{s}_{,IF} = \frac{\mu_{2}}{\mu_{2}-\mu_{1}} d^{s}_{,1} - \frac{\mu_{1}}{\mu_{2}-\mu_{1}} d^{s}_{,2}$. For classical PPP based on the IF combination, the seventh and eighth types of rank deficiencies do not need to be considered either. After solving the remaining four rank deficiencies (No. 2, 3, 4, and 6), the full-rank model of the IF POD model can be expressed as:

$$\begin{aligned} \tilde{p}^{s}_{r,IF} &= \rho^{s}_{r,j} + \widetilde{dt}_{r} + \varepsilon^{s}_{p,IF} \\ \tilde{\phi}^{s}_{r,IF} &= \rho^{s}_{r,j} + \widetilde{dt}_{r} - \tilde{\delta}^{s}_{r,IF} + \varepsilon^{s}_{\phi,IF} \end{aligned} \tag{2}$$

where $\tilde{p}^{s}_{r,IF} = p^{s}_{r,IF} + \widetilde{dt}^{s}$ and $\tilde{\phi}^{s}_{r,IF} = \phi^{s}_{r,IF} + \widetilde{dt}^{s}$, respectively. $\widetilde{dt}_{r} = dt_{r} + d_{r,IF}$ is the estimable LEO satellite clock offset, where $d_{r,IF}$ is the IF LEO code bias. $\tilde{\delta}^{s}_{r,IF} = \delta_{r,IF} - \delta^{s}_{,IF} - d_{r,IF} + \lambda_{IF} N^{s}_{r,IF}$ is the estimable phase ambiguity. As presented in Eq. (2), although the ionospheric delays are eliminated, the observational noise is amplified at the same time. Taking the dual-frequency case as an example, the IF combination is formed in code and phase observations, respectively, but only an independent parameter of the ionosphere delay is eliminated, resulting in a waste of observational information. This is critical for the onboard receivers with a limited number of channels tracking GNSS satellites. In addition, in multi-frequency scenarios, multiple IF combinations can be formed, but this approach has two drawbacks. The first is wasting observational information, and the second is obscuring the possible correlations between the combined observations (Teunissen, 2020). Therefore, the IF combination is not the optimal choice for multi-frequency multi-constellation GNSS data processing.

To provide a solution to such limitations, we form the full-rank model for the UC observation (Zha et al., 2021). With precise satellite clock products, we are free from the first and the fifth types of rank deficiency. These deficiency types are described in the section "***Uncombined (UC) POD model***" in the paper. To address the second and the third types of rank deficiency, the LEO code biases ($d_{r,j}$) and phase biases ($\delta_{r,j}$) are chosen as the S-basis, respectively. The rank deficiency (of size 1) between the LEO satellite clock, code biases and phase biases can be eliminated by fixing the IF code bias of the LEO satellite as an S-basis. For the rank deficiencies between the ionospheric delays, LEO satellite code and phase biases and between the ionospheric delays, GNSS satellite code and phase biases are usually eliminated by fixing the geometry-free (GF) code bias of the LEO satellite and GNSS satellite as the S-basis, respectively. After solving those rank deficiencies, the full-rank UC POD model can be expressed as (Zehentner and Mayer-Gürr, 2016),

$$\begin{aligned} \overset{\sim s}{p}_{r,j} &= \rho_r^s + \widetilde{dt}_r + \mu_j \overset{\sim s}{I}_r - \overset{\sim s}{d}_{r,j} + \varepsilon_{p,j}^s \\ \overset{\sim s}{\phi}_{r,j} &= \rho_r^s + \widetilde{dt}_r - \mu_j \overset{\sim s}{I}_r - \overset{\sim s}{\delta}_{r,j} + \varepsilon_{\phi,j}^s \end{aligned} \tag{3}$$

where $\overset{\sim s}{p}_{r,j} = p_{r,j}^s + \overset{\sim s}{dt}$ and $\overset{\sim s}{\phi}_{r,j} = \phi_{r,j}^s + \overset{\sim s}{dt}$ are code and phase observables with satellite clock corrected.$\overset{\sim s}{I}_r = I_r^s + d_{r,GF} - d_{,GF}^s$ is the estimable ionospheric delay. $d_{r,GF} = \frac{1}{\mu_2 - \mu_1}(d_{r,2} - d_{r,1})$ and $d_{,GF}^s = \frac{1}{\mu_2 - \mu_1}(d_{,2}^s - d_{,1}^s)$ denote the GF code bias of LEO and GNSS satellites, respectively. $\overset{\sim s}{d}_{r,j} = d_{,j}^s - d_{,IF}^s - \mu_j d_{,GF}^s - d_{r,j} + d_{r,IF} + \mu_j d_{r,GF}$ is the combined GNSS and LEO satellite code bias with $j \geqslant 3$, which shows the flexibility of the UC POD model for multi-frequency expansion. $\overset{\sim s}{\delta}_{r,j} = \delta_{,j}^s - d_{,IF}^s + \mu_j d_{,GF}^s - \lambda_j N_{r,j}^s - \delta_{r,j} + d_{r,IF} - \mu_j d_{r,GF}$ is the combined GNSS and LEO satellite phase bias, which also absorbs the ambiguity parameters. In addition, it can be seen from Eq. (3) that the UC POD model retains the original observation noise and facilitates the analysis of residuals at each frequency; something that is not possible for the IF POD model.

2.3. UDUC POD model with DD ambiguity

Concerning the absolute POD for LEO constellations, there are two points that cannot be ignored. First, the phase ambiguities are present in the float form in the UC POD model, which limits the POD performance. Second, the properties of the common-view GNSS satellites in the LEO constellation are ignored. With the help of these common-view satellites, the joint POD of the LEO constellation can be realized, which can improve computational efficiency compared with the satellite-by-satellite POD. In addition, DD ambiguities with integer characteristics can also be constructed with the help of the common-view satellites. In the relative POD, the DD model is widely used because the model does not have any rank deficiency. However, the DD model only obtains relative states and requires strict common-view GNSS satellites. Possible non-common-view satellite observations are wasted in such cases.

Considering the above points, we present here a model that can serve both the absolute and relative POD based on the UC POD model by taking advantage of the characteristics of common-view GNSS satellites. Satellites A and B are assumed in a LEO constellation, so that the model can be easily extended to other multi-satellite cases. For the common-view GNSS satellites, the satellite code and phase biases $d_{,j}^s - d_{,IF}^s - \mu_j d_{,GF}^s$ and $\delta_{,j}^s - d_{,IF}^s + \mu_j d_{,GF}^s$ are the same for the LEO satellites A and B. Taking $\overset{\sim s}{d}_{A,j}$ and $\overset{\sim s}{\delta}_{A,j}$ as the S-basis, the parameters to be estimated can be reduced. In addition, the ambiguities can be constructed in the DD form. In this case, the UDUC POD model with DD ambiguity can be constructed as follows,

$$\begin{aligned} \overset{\sim s}{p}_{A,j} &= \rho_A^s + \widetilde{dt}_A + \mu_j \overset{\sim s}{I}_A - \overset{\sim s}{d}_{A,j} + \varepsilon_{p,j}^s \\ \overset{\sim s}{\phi}_{A,j} &= \rho_A^s + \widetilde{dt}_A - \mu_j \overset{\sim s}{I}_A - \overset{\sim s}{\delta}_{A,j} + \varepsilon_{\phi,j}^s \\ \overset{\sim s}{p}_{B,j} &= \rho_B^s + \widetilde{dt}_B + \mu_j \overset{\sim s}{I}_B - \overset{\sim s}{d}_{A,j} + \tilde{d}_{AB,j} + \varepsilon_{p,j}^s \\ \overset{\sim s}{\phi}_{B,j} &= \rho_B^s + \widetilde{dt}_B - \mu_j \overset{\sim s}{I}_B - \overset{\sim s}{\delta}_{A,j} + \tilde{\delta}_{AB,j} + \lambda_j N_{AB,j}^{1s} + \varepsilon_{\phi,j}^s \end{aligned} \tag{4}$$

where $\tilde{d}_{AB,j} = d_{B,j} - d_{A,j} - d_{AB,IF} - \mu_j d_{AB,GF}$ is the between-LEO code bias when $j \geqslant 3$ and $\tilde{\delta}_{AB,j} = \delta_{B,j} - \delta_{A,j} - d_{AB,IF} + \mu_j d_{AB,GF} + \lambda_j N_{AB,j}^1$ is the between-LEO phase bias with $j \geqslant 1$. $N_{AB,j}^{1s} = N_{AB,j}^s - N_{AB,j}^1$ is the DD ambiguity. Kalman filter is used in the UDUC model with DD ambiguity, where $\tilde{d}_{AB,j}$,$\tilde{\delta}_{AB,j}$,$\overset{\sim s}{d}_{A,j}$,$\overset{\sim s}{\delta}_{A,j}$ and $N_{AB,j}^{1s}$ are estimated as time-invariant parameters.

The UDUC model with DD ambiguity has the following advantages:

1. The model can estimate the absolute orbit of each LEO satellite as well as the relative state between LEO satellites, thus can serve both absolute and relative POD.
2. The ambiguities are in the DD form, thus IAR can be performed without external SPB products.
3. Joint POD of a LEO constellation reduces the number of estimated parameters, which can improve computational efficiency.
4. Code and phase biases at both LEO and GNSS-end remained for further model strengthening.
5. For those GNSS satellites which are non-common-view, they also contribute to POD with the UC POD model.

The model, however, has two extreme cases. Firstly, when the distance between the LEO satellites is long such that there are no common-view GNSS satellites at all, this will be equivalent to having two LEO satellites performing the UC POD model separately. Although this method can be applied to long baselines in theory, it might be difficult to solve the IAR due to the length of the baseline being too long in practice, which will affect the accuracy of the POD. Secondly, when the common-view GNSS satellites of the two LEO satellites are the same, which is equivalent to the relative POD based on the UD model. It should be mentioned that in the second case, the UD model also has advantages over the traditional DD model since it can better utilize the stability of LEO and GNSS satellite biases to improve the model strength.

Eq. (4) can be defined as the ionosphere-float UDUC POD model with DD ambiguity, as no constraint is assumed between I_A^s and I_B^s in this situation. However, when the distance between the two LEO satellites in formation flying is between 10 km and 200 km, the model strength can be improved by imposing SD ionospheric constraints with pseudo-observables (Odijk, 2000; Odijk, 2002). Adding those observables enables a-priori reasonable information on the ionospheric delay. In this case, the ionosphere-weighted UDUC POD model with DD ambiguity can be constructed as follow,

$$\begin{aligned}
\tilde{p}_{A,j}^{s} &= \rho_A^s + d\tilde{t}_A + \mu_j \tilde{I}_A^s - \tilde{d}_{A,j}^{s} + \varepsilon_{p,j}^s \\
\tilde{\phi}_{A,j}^{s} &= \rho_A^s + d\tilde{t}_A - \mu_j \tilde{I}_A^s - \tilde{\delta}_{A,j}^{s} + \varepsilon_{\phi,j}^s \\
\tilde{p}_{B,j}^{s} &= \rho_B^s + d\tilde{t}_B + \mu_j \tilde{I}_A^s + \mu_j I_{AB}^s + \mu_j d_{AB,GF} - \tilde{d}_{A,j}^{s} + \tilde{d}_{AB,j} + \varepsilon_{p,j}^s \\
\tilde{\phi}_{B,j}^{s} &= \rho_B^s + d\tilde{t}_B - \mu_j \tilde{I}_A^s - \mu_j I_{AB}^s - \mu_j d_{AB,GF} - \tilde{\delta}_{A,j}^{s} + \tilde{\delta}_{AB,j} + \lambda_j N_{AB,j}^{1s} \\
&\quad + \varepsilon_{\phi,j}^s \\
\bar{I}_{AB}^s &= I_{AB}^s + \varepsilon_{AB}^s
\end{aligned} \tag{5}$$

where $\bar{I}_{AB}^{s}$ and I_{AB}^s is the between-LEO SD ionospheric delay and its pseudo-observables. ε_{AB}^s is the random observation noise of the between-LEO SD ionospheric delay. With the between-LEO differential code biases (DCB) $d_{AB,GF}$, the ionospheric delay of LEO satellite B does not need to be estimated in the model, consequently, the model strength improves.

In addition, if the distance between LEO satellites is less than 10 km, it is safe to assume $I_{AB}^s = 0$ (Odolinski et al., 2015a). Thus, the ionosphere-fixed UDUC POD model with DD ambiguity can be written as,

$$\begin{aligned}
\tilde{p}_{A,j}^{s} &= \rho_A^s + d\tilde{t}_A + \mu_j \tilde{I}_A^{s} - \tilde{d}_{A,j}^{s} + \varepsilon_{p,j}^s \\
\tilde{\phi}_{A,j}^{s} &= \rho_A^s + d\tilde{t}_A - \mu_j \tilde{I}_A^{s} - \tilde{\delta}_{A,j}^{s} + \varepsilon_{\phi,j}^s \\
\tilde{p}_{B,j}^{s} &= \rho_B^s + d\tilde{t}_B + \mu_j \tilde{I}_A^{s} + \mu_j d_{AB,GF} - \tilde{d}_{A,j}^{s} + \tilde{d}_{AB,j} + \varepsilon_{p,j}^s \\
\tilde{\phi}_{B,j}^{s} &= \rho_B^s + d\tilde{t}_B - \mu_j \tilde{I}_A^{s} - \mu_j d_{AB,GF} - \tilde{\delta}_{A,j}^{s} + \tilde{\delta}_{AB,j} + \lambda_j N_{AB,j}^{1s} + \varepsilon_{\phi,j}^s
\end{aligned} \tag{6}$$

where the interpretation of the estimated parameters is the same as in Eq. (5).

3. Results

This section will first introduce the LEO satellites involved in this experiment. The data processing strategy of LEO will be given, and the results of absolute and relative POD will be shown on this basis.

3.1. LEO data and processing strategy

The satellites used in our experiments are two LEO satellites T-A and T-B, working in a formation flying (Lou et al., 2020). T-A and T-B orbit the Earth at 527 km altitude in an orbital plane with an inclination of 97.5°, completing one revolution in roughly 95 min (Yi et al., 2021a; Zhang et al., 2021). The relevant characteristics of the mission are summarized in Table 1.

To validate the feasibility and effectiveness of the UDUC POD model with DD ambiguity, we test using the onboard GPS data of T-A and T-B satellites from September 2nd to 8th, 2021. GPS L1 and L2 observations with a sampling rate of 10 s were used in our study. The IGS final precise GPS orbits and clocks products were used (Johnston et al., 2017), and GPS P1-C1 DCB was corrected using the monthly DCBs published by the Centre for Orbit Determination in Europe (CODE) (Dach et al., 2016). Considering that the distance between T-A and T-B is usually within two kilometers (Zhang et al., 2021), the ionosphere-fixed UDUC POD model with DD ambiguity was adopted. The main data processing strategies for the UDUC POD model with DD ambiguity are summarized in Table 2.

3.2. POD performance of the UDUC POD model with DD ambiguity

Comparing the orbit solutions with precise reference orbits is a simple and effective means of evaluating the LEO POD model. In this section, the kinematic orbits generated using the UDUC POD model with DD ambiguity are compared with the reference orbits provided courtesy of the operating team of the mission of T-A and T-B.

Table 1
An overview of the mission.

Item	Index
Satellites	T-A and T-B
Orbit	Sun-synchronous
Altitude	527 km
Inclination	97.5°
Period	95 min
GNSS system tracked	GPS and BDS-3
Measurement	Code, Phase and Doppler
Sample interval	1 s

Table 2
Main data processing strategies in the study.

Item	Strategy
Observation	GPS L1 + L2
GPS antenna offset	PCO and PCV are corrected with IGS igs14.atx (Rebischung and Schmid, 2016)
LEO antenna offset	PCO is corrected with the value from the data provider
LEO attitude	Quaternions from onboard star trackers
SPB	Estimated as time-constants in a continuous arc
Between-LEO phase biases	Estimated as time-constants
Between-LEO DCB	Estimated as a time-constant
Slant ionospheric delays	Estimated as white noise
Parameter estimator	Kalman filter
IAR and validation	LAMBDA (Teunissen, 1995) with ratio test (Verhagen and Teunissen, 2013)
Outlier detection and elimination	Detection, identification, and adaptation (DIA) procedure (Teunissen, 2018)

The reference orbits of the two satellites are generated using a reduced-dynamic model in post-processed batch least-squares adjustment. IAR is performed for the reference orbits with the SD method (Yi et al., 2021; Zhang et al., 2021). To show the performance improvement with the use of our model compared to the classical POD model, the orbits of the classical kinematic IF POD are calculated using Bernese GNSS software V5.4 (Dach and Walser 2015). The kinematic orbits generated by Bernese GNSS Software are ambiguity-fixed solutions using the phase bias products provided by the CODE (Schaer et al., 2021).

Fig. 1 shows the orbit differences of the kinematic IF POD and UDUC POD with DD ambiguity solutions for T-A with respect to the reference orbit on the day of year (DOY) 248 (September 5th), 2021. There is a gap in the results for nearly two hours due to multiple satellite maneuvers during this period with some orbital data missing. Compared with the IF POD, the orbits calculated by the UDUC POD with DD ambiguity are more consistent with the reference orbit. The root mean square (RMS) values of the orbit differences in three directions for the IF POD are 2.7 cm, 2.6 cm and 2.6 cm and that for the UDUC POD with DD ambiguity are 2.0 cm, 2.2 cm and 2.3 cm. The reduction of the orbit differences of the proposed model is thus 25.9%, 15.4% and 11.5% compared to the IF POD, respectively. The UDUC POD with DD ambiguity performs better than the IF POD for the following reasons. Firstly, IAR is achieved for the UDUC POD with DD ambiguity, which guarantees high-precision orbit solutions. Secondly, ionospheric constraints are considered in the UDUC POD with DD ambiguity, enabling instantaneous IAR to speed up the solution convergence process. Fig. 2 is analogous to Fig. 1 but illustrates the results for T-B. Unlike T-A, T-B does not have any maneuvers on this day. From the results, it can also be seen that the UDUC POD with DD ambiguity performs better than the IF

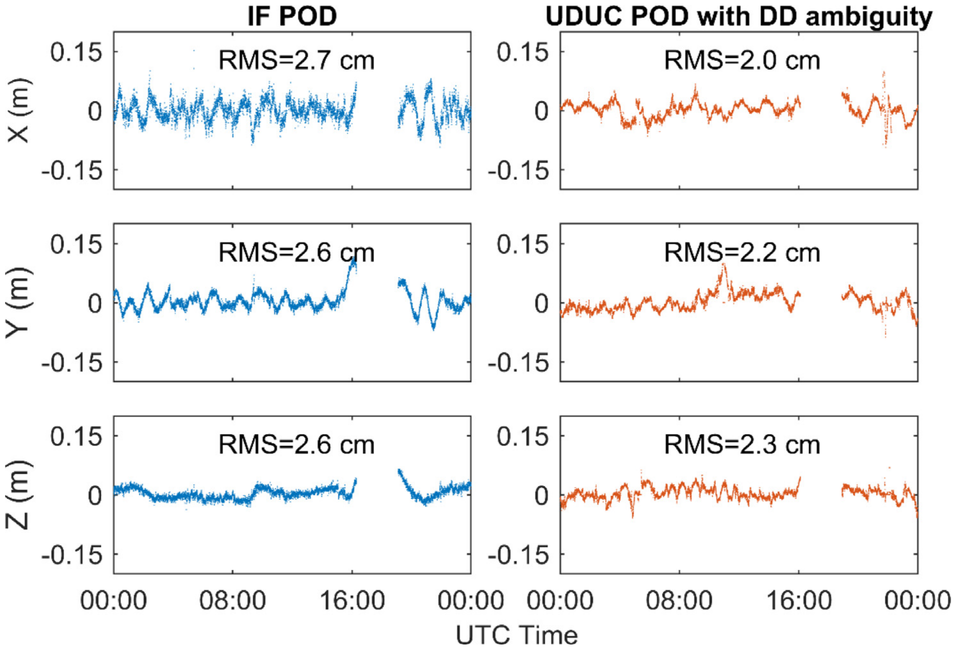

Fig. 1. Orbit differences of the IF POD and UDUC POD with DD ambiguity of T-A with respect to the reference orbit on DOY 248 (September 5th), 2021.

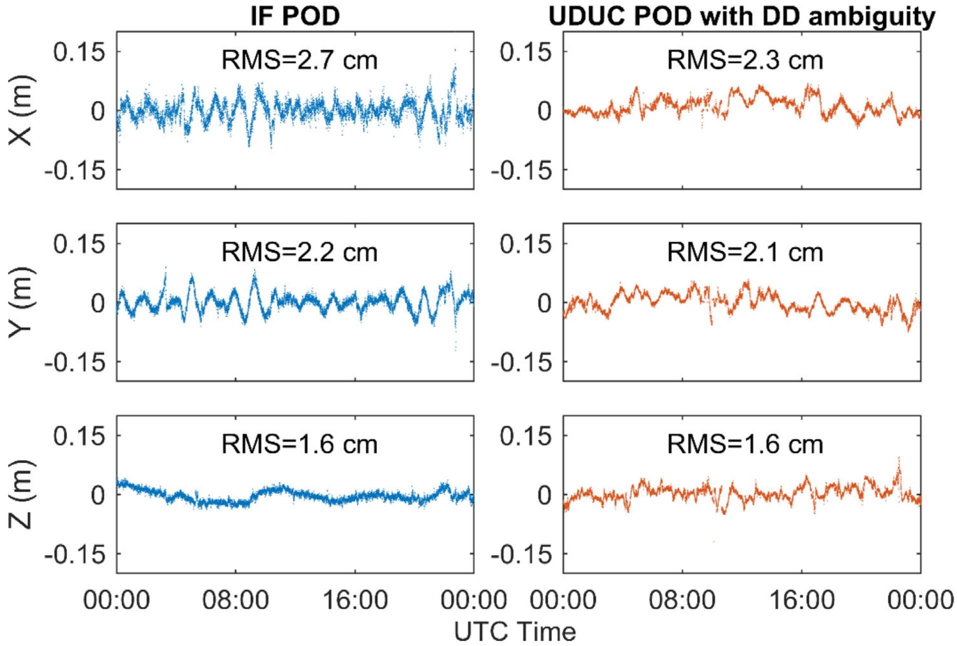

Fig. 2. Orbit differences of the IF POD and UDUC POD with DD ambiguity of T-B with respect to the reference orbit on DOY 248 (September 5th), 2021.

POD from the RMS of orbit differences with the reference orbit. The RMS of orbit differences for two models in three directions are 2.7 cm, 2.2 cm and 1.6 cm and 2.3 cm, 2.1 cm and 1.6 cm, respectively. Also note that the Bernese GNSS Software results in the left panel of Fig. 1 are processed based on batch least-squares adjustment, which can only be achieved in near-real-time due to the processing time of a few minutes up to more than 10 min, depending on the computational efficiency. The UDUC results from the right panel of Fig. 1 are processed with a Kalman filter, which can be achieved almost in real-time with much shorter delays.

The POD results of T-A and T-B covering one week in the test period are shown in Fig. 3 and Fig. 4 with box-whisker diagrams for the IF POD and UDUC POD with DD ambiguity. In a box-whiskers diagram, the maximum and minimum values are displayed. In addition, the first and third quartiles are indicated by the top and bottom edges of each box, while the median is marked as the centerline of the box. The RMS values of the orbit differences

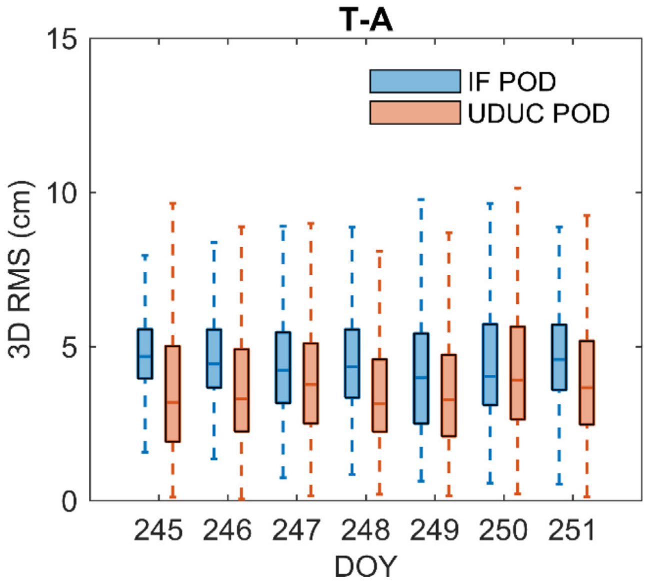

Fig. 3. Daily 3D RMS of orbit differences of the IF POD and UDUC POD with DD ambiguity with respect to the reference orbits for T-A on DOYs 245–251 (September 2nd to 8th), 2021.

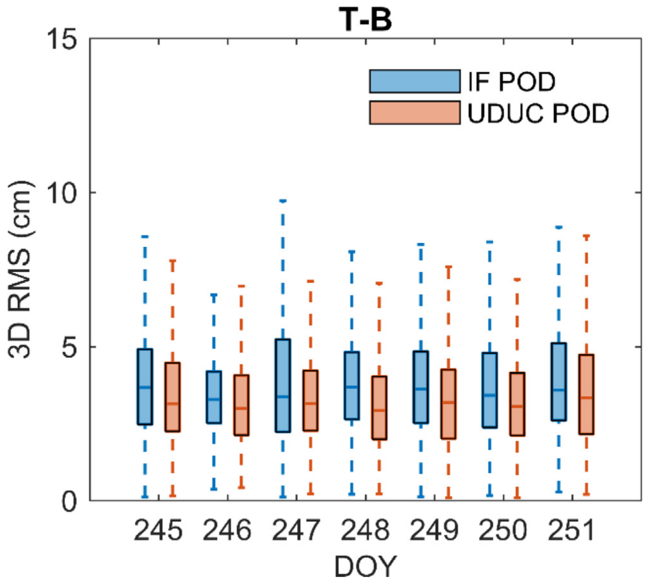

Fig. 4. Daily 3D RMS of orbit differences of the IF POD and UDUC POD with DD ambiguity with respect to the reference orbits for T-B on DOYs 245–251 (September 2nd to 8th), 2021.

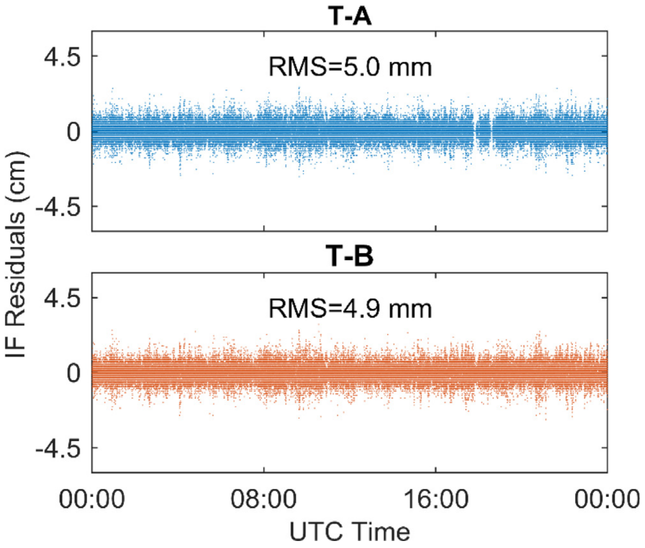

Fig. 5. IF phase residuals of the IF POD for T-A and T-B on DOY 247 (September 4th), 2021.

with respect to the reference orbit is displayed. The median absolute errors amount to between 3.4 cm and 4.6 cm for T-A with the IF POD. When using the UDUC POD with DD ambiguity, corresponding values of 2.9 cm to 3.8 cm were obtained for the testing period. For T-B, the median of the absolute errors of the IF POD are from 3.0 cm to 3.6 cm and of the UDUC POD with DD ambiguity are between 2.8 cm and 3.1 cm. The average percentage of reduction in the orbit differences in 3D of the proposed model is 16.3% and 10.6% for T-A and T-B, respectively, compared with the IF POD. This comparison verifies the advantages of the UDUC POD with DD ambiguity.

As an alternative indicator, phase residuals are usually used to assess the internal precision of orbit solutions. As we mentioned earlier, another advantage of the UDUC POD with DD ambiguity is that the original observation noise is preserved and the residuals at each frequency can be separated. However, the IF POD can only output the combined phase residuals and cannot distinguish the contributions of different frequencies. Take DOY 247, 2021 as an example, Fig. 5 presents the IF phase residuals of the IF POD. The phase residuals fluctuate randomly around the mean for both T-A and T-B. In addition, the RMS of IF phase residuals for T-A and T-B are 5.0 mm and 4.9 mm, respectively.

However, when the UDUC POD with DD ambiguity is used, the phase residuals of L1 and L2 can be separated. Fig. 6 shows the phase residuals of L1 and L2 separately for T-A and T-B, respectively, from which two conclusions can be drawn. Firstly, with the UDUC POD with DD ambiguity, smaller residuals can be obtained compared with the IF POD. Taking T-A as an example, the phase residuals for L1 and L2 are 1.8 mm and 1.7 mm, respectively, which is smaller than the IF residuals obtained from the IF POD. The reasons are as follows. Firstly, the original observation noise is preserved without amplification in the UDUC method. Secondly, the phase residuals are further reduced with successful IAR. In addition, for T-A and T-B, the phase residuals of L2 are always smaller than that of L1, which indicates that the L2 observations are more accurate than that of L1, hence, they can play an important role in POD.

With the UDUC POD with DD ambiguity, the orbits of each LEO satellite can be obtained. In addition, relative POD can also be achieved with this method. Fig. 7 depicts the results compared to the reference baseline for seven days. The reference baseline between T-A and T-B is generated based on the DD model with IAR. The median absolute errors amount to 1.1–1.5 mm in 3D for the week (September 2nd to 8th), respectively. The above results show that the UDUC POD with DD ambiguity can

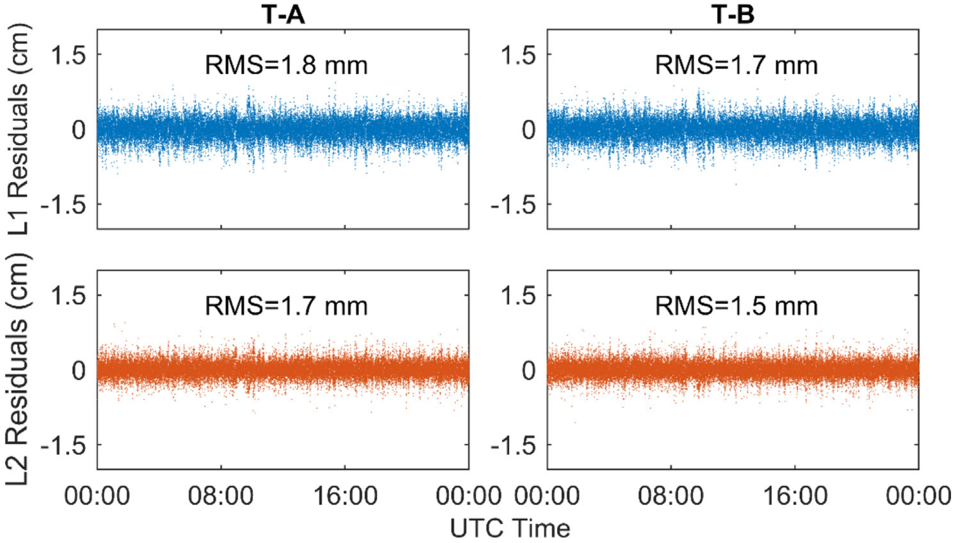

Fig. 6. L1 and L2 phase residuals of the UDUC POD with DD ambiguity for T-A and T-B on DOY 247 (September 4th), 2021.

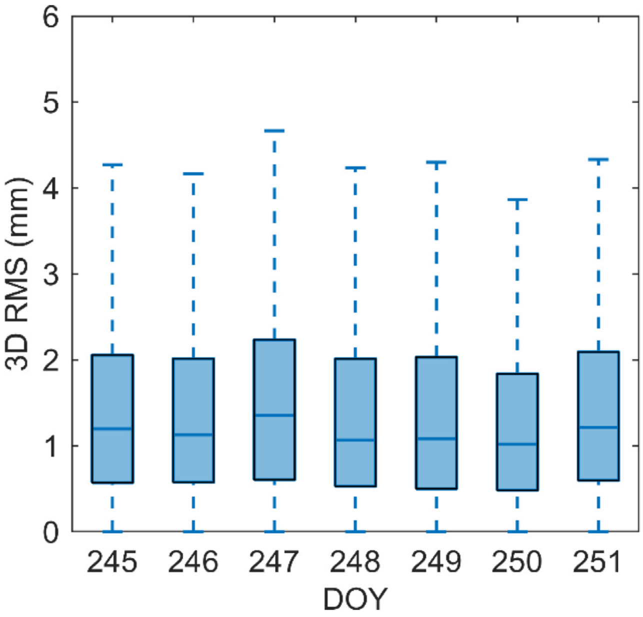

Fig. 7. 3D Differences of the baseline solutions between the UDUC POD with DD ambiguity and the reference for T-A and T-B on DOYs 245–251 (September 2nd to 8th), 2021.

achieve millimeter-level relative POD, which can be used for formation flying, space docking and rendezvous missions.

4. Conclusions

In this contribution, we developed a model based on the UDUC observations that can be used for absolute and relative LEO POD, namely the UDUC POD model with DD ambiguity. This model has the following characteristics, making it well-suited for different LEO satellite missions including formation flying:

1. The model is based on the UDUC observations, which can be flexibly used in multi-frequency scenarios and the original observation noise is not amplified as in the difference modes.
2. DD ambiguities are formed with common-view GNSS satellites, enabling IAR for high-precision LEO POD without any SPB products.
3. All the parameters, such as code and phase biases of LEO and GNSS satellites, remain available for possible further model strengthening.
4. With the use of precise products, the non-common-view GNSS satellites can also be used, and both absolute and relative POD can be achieved.
5. Phase residuals of each frequency can be separated, which is useful for exploring and analysing the contribution of observations with different frequencies.

Based on onboard GPS data from two LEO satellites for formation flying, the performance of the proposed UDUC POD model with DD ambiguity was evaluated. In addition, classical kinematic IF POD was generated to demonstrate the benefits of the proposed model. The orbits generated by the IF POD and the UDUC POD with DD ambiguity for the two LEO satellites were compared with the reference orbits. The experimental results showed that compared with the IF POD, the differences between the UDUC POD with DD ambiguity solution and the reference orbit were smaller. This result illustrates that the UDUC algorithms and IAR were beneficial for LEO POD. The phase residuals of L1 and L2 were obtained with the proposed model, which are much smaller than the IF phase residuals with the IF POD, which showed the advantages of the UDUC model with DD ambiguity. By comparing the computed distance from the estimated two LEO satellite positions with their reference baseline, the ability of the UDUC POD with DD ambiguity solution to achieve millimeter-level relative POD was demonstrated, proving that the model could be used for formation flying missions, as well as space docking and rendezvous applications.

This study shows the potential of the UDUC algorithms with IAR for absolute and relative LEO POD. The current research is only focused on onboard GPS observations without any dynamic modeling. However, if dynamic models can be introduced, the UDUC POD model with DD ambiguity will hopefully serve real-time LEO POD with IAR. Thus, our future work will consider the reduced-dynamic POD based on the use of this model.

Declaration of Competing Interest

The authors declare that they have no known competing financial interests or personal relationships that could have appeared to influence the work reported in this paper.

Acknowledgments

This work was partially funded by the Australian Research Council Discovery Project (Grant No. DP 190102444), the National Natural Science Foundation of China (Grant No. 42022025) and the National Time Service Center, Chinese Academy of Sciences (CAS) (No. E167SC14). Baocheng Zhang is supported by the CAS Pioneer Hundred Talents Program. We thank the IGS for providing precise orbit and clock products.

References

Allahvirdi-Zadeh, A., Wang, K., El-Mowafy, A., 2021a. POD of small LEO satellites based on precise real-time MADOCA and SBAS-aided PPP corrections. GPS Solut. 25, 1–14. https://doi.org/10.1007/s10291-020-01078-8.

Allahvirdi-Zadeh, A., Wang, K., El-Mowafy, A., 2021b. Precise orbit determination of LEO satellites based on undifferenced GNSS observations. J. Surv. Eng. 148 (1). https://doi.org/10.1061/(ASCE)SU.1943-5428.0000382 03121001.

Allahvirdi-Zadeh, A., Awange, J., El-Mowafy, A., Ding, T., Wang, K., 2022. Stability of CubeSat clocks and their impacts on GNSS radio occultation. Remote Sens. (Basel) 14 (2), 1–26. https://doi.org/10.3390/rs14020362.

Allende-Alba, G., Montenbruck, O., Jäggi, A., Arnold, D., Zangerl, F., 2017. Reduced-dynamic and kinematic baseline determination for the

Swarm mission. GPS Solut. 21, 1275–1284. https://doi.org/10.1007/s10291-017-0611-z.

Bandyopadhyay, S., Foust, R., Subramanian, G.P., Chung, S.J., Hadaegh, F.Y., 2016. Review of formation flying and constellation missions using nanosatellites. J. Spacecr. Rocket. 53 (3), 567–578. https://doi.org/10.2514/1.A33291.

Bertiger, W., Desai, S.D., Haines, B., Harvey, N., Moore, A.W., Owen, S., Weiss, J.P., 2010. Single receiver phase ambiguity resolution with GPS data. J. Geod. 84, 327–337. https://doi.org/10.1007/s00190-010-0371-9.

Collins, P., 2008. Isolating and estimating undifferenced GPS integer ambiguities. In Proceedings of the 2008 National Technical Meeting of The Institute of Navigation, (720-732).

Dach, R., Walser, P., 2015. Bernese GNSS Software Version 5.2. https://doi.org/10.7892/boris.72297.

Dach, R., Schaer, S., Arnold, D., Orliac, E., Prange, L., Susnik, A., Villiger, A., Jäggi, A., 2016. CODE final product series for the IGS. https://doi.org/10.7892/boris.75876.4

De Jonge, P.J., 1998. A processing strategy for the application of the GPS in networks. Publicatons Geod. 46.

El-Mowafy, A., Wang, K., 2022. The potential of LEO mega-constellations in aiding GNSS to enable positioning in challenging environments. In XXVII FIG Congress, 1-11.

Ge, M., Gendt, G., Rothacher, M.A., Shi, C., Liu, J., 2008. Resolution of GPS carrier-phase ambiguities in precise point positioning (PPP) with daily observations. J. Geod. 82 (7), 389–399. https://doi.org/10.1007/s00190-007-0187-4.

Gill, E., D'Amico, S., Montenbruck, O., 2007. Autonomous formation flying for the PRISMA mission. J. Spacecr. Rocket. 44 (3), 671–681. https://doi.org/10.2514/1.23015.

Hauschild, A., Tegedor, J., Montenbruck, O., Visser, H., Markgraf, M., 2016. Precise onboard orbit determination for LEO satellites with real-time orbit and clock corrections. In Proceedings of the 29th International Technical Meeting of the Satellite Division of The Institute of Navigation (ION GNSS+ 2016) (3715-3723). https://doi.org/10.33012/2016.14717.

Jäggi, A., Montenbruck, O., Moon, Y., Wermuth, M., König, R., Michalak, G., Bock, H., Bodenmann, D., 2012. Inter-agency comparison of TanDEM-X baseline solutions. Adv. Space Res. 50 (2), 260–271. https://doi.org/10.1016/j.asr.2012.03.027.

Johnston, G., Riddell, A., Hausler, G., 2017. The International GNSS Service. Springer Handbk. Global Navig. Satell. Syst. 967–982. https://doi.org/10.1007/978-3-319-42928-1_33.

Khodabandeh, A., Teunissen, P.J.G., 2015. An analytical study of PPP-RTK corrections: precision, correlation and user-impact. J. Geod. 89, 1109–1132. https://doi.org/10.1007/s00190-015-0838-9.

Lannes, A., Prieur, J.L., 2013. Calibration of the clock-phase biases of GNSS networks: the closure-ambiguity approach. J. Geod. 87, 709–731. https://doi.org/10.1007/s00190-013-0641-4.

Laurichesse, D., Mercier, F., Berthias, J.P., Broca, P., Cerri, L., 2009. Integer ambiguity resolution on undifferenced GPS phase measurements and its application to PPP and satellite precise orbit determination. Navigation 56 (2), 135–149. https://doi.org/10.1002/j.2161-4296.2009.tb01750.x.

Li, B., Ge, H., Ge, M., Nie, L., Shen, Y., Schuh, H., 2019a. LEO enhanced Global Navigation Satellite System (LeGNSS) for real-time precise positioning services. Adv. Space Res. 63 (1), 73–93. https://doi.org/10.1016/j.asr.2018.08.017.

Li, X., Ma, F., Li, X., Lv, H., Bian, L., Jiang, Z., Zhang, X., 2019b. LEO constellation-augmented multi-GNSS for rapid PPP convergence. J. Geod. 93, 749–764. https://doi.org/10.1007/s00190-018-1195-2.

Li, X., Wu, J., Zhang, K., Li, X., Xiong, Y., Zhang, Q., 2019c. Real-time kinematic precise orbit determination for LEO satellites using zero-differenced ambiguity resolution. Remote Sens. (Basel) 11 (23), 1–21. https://doi.org/10.3390/rs11232815.

Lindlohr, W., Wells, D., 1985. GPS design using undifferenced carrier beat phase observations. Manuscr. Geodaet. 10 (4), 255–295.

Lou, L., Liu, Z., Zhang, H., Qian, F., Huang, Y., 2020. TH-2 satellite engineering design and implementation. Acta Geod. Cartogr. Sin. 49, 1252–1264. https://doi.org/10.11947/j.AGCS.2020.20200175.

Mi, X., Zhang, B., Yuan, Y., 2019. Multi-GNSS inter-system biases: estimability analysis and impact on RTK positioning. GPS Solut. 23. https://doi.org/10.1007/s10291-019-0873-8 81.

Mi, X., Zhang, B., Odolinski, R., Yuan, Y., 2020. On the temperature sensitivity of multi-GNSS intra-and inter-system biases and the impact on RTK positioning. GPS Solut. 24, 1–14. https://doi.org/10.1007/s10291-020-01027-5.

Mi, X., Zhang, B., El-Mowafy, A., Wang, K., Yuan, Y., 2023. On the potential of undifferenced and uncombined GNSS time and frequency transfer with integer ambiguity resolution and satellite clocks estimated. GPS Solut. 27 (1). https://doi.org/10.1007/s10291-022-01363-8 25.

Montenbruck, O., Garcia-Fernandez, M., Yoon, Y., Schön, S., Jäggi, A., 2009. Antenna phase center calibration for precise positioning of LEO satellites. GPS Solut. 13, 23–34. https://doi.org/10.1007/s10291-008-0094-z.

Montenbruck, O., Hackel, S., van den Ijssel, J., Arnold, D., 2018. Reduced dynamic and kinematic precise orbit determination for the Swarm mission from 4 years of GPS tracking. GPS Solut. 22 (3). https://doi.org/10.1007/s10291-018-0746-6 79.

Odijk, D., 2000. Improving ambiguity resolution by applying ionosphere corrections from a permanent GPS array. Earth Planets Space 52, 675–680. https://doi.org/10.1186/BF03352262.

Odijk, D., 2002. Fast precise GPS positioning in the presence of ionospheric delays. Publications Geod. 52.

Odijk, D., Zhang, B., Khodabandeh, A., Odolinski, R., Teunissen, P.J.G., 2016. On the estimability of parameters in undifferenced, uncombined GNSS network and PPP-RTK user models by means of *S*-system theory. J. Geod. 90 (1), 15–44. https://doi.org/10.1007/s00190-015-0854-9.

Odijk, D., Khodabandeh, A., Nadarajah, N., Choudhury, M., Zhang, B., Li, W., Teunissen, P.J.G., 2017. PPP-RTK by means of *S*-system theory: Australian network and user demonstration. J. Spat. Sci. 62 (1), 3–27. https://doi.org/10.1080/14498596.2016.1261373.

Odolinski, R., Teunissen, P.J.G., Odijk, D., 2015a. Combined BDS, Galileo, QZSS and GPS single-frequency RTK. GPS Solut. 19, 151–163. https://doi.org/10.1007/s10291-014-0376-6.

Odolinski, R., Teunissen, P.J.G., Odijk, D., 2015b. Combined GPS+ BDS for short to long baseline RTK positioning. Meas. Sci. Technol. 26 (4). https://doi.org/10.1088/0957-0233/26/4/045801 045801.

Psychas, D., Khodabandeh, A., Teunissen, P.J.G., 2022. Impact and mitigation of neglecting PPP-RTK correctional uncertainty. GPS Solut. 26 (1). https://doi.org/10.1007/s10291-021-01214-y 33.

Rebischung, P., Schmid, R., 2016. IGS14/igs14. atx: a new framework for the IGS products. In AGU fall meeting 2016.

Schaer, S., Villiger, A., Arnold, D., Dach, R., Prange, L., Jäggi, A., 2021. The CODE ambiguity-fixed clock and phase bias analysis products: generation, properties, and performance. J. Geod. 95. https://doi.org/10.1007/s00190-021-01521-9 81.

Suesser-Rechberger, B., Krauss, S., Strasser, S., Mayer-Guerr, T., 2022. Improved precise kinematic LEO orbits based on the raw observation approach. Adv. Space Res. 69 (10), 3559–3570. https://doi.org/10.1016/j.asr.2022.03.014.

Teunissen, P.J.G., 1985. Zero order design: generalized inverses, adjustment, the datum problem and S-transformations (11–55). Springer, Berlin Heidelberg.

Teunissen, P.J.G., 1995. The least-square ambiguity decorrelation adjustment: a method for fast GPS integer ambiguity estimation. J. Geod. 70 (1), 65–82. https://doi.org/10.1007/BF00863419.

Teunissen, P.J.G., 2001. Integer estimation in the presence of biases. J. Geod. 75, 399–407. https://doi.org/10.1007/s001900100191.

Teunissen, P.J.G., 2018. Distributional theory for the DIA method. J. Geod. 92 (1), 59–80. https://doi.org/10.1007/s00190-017-1045-7.

Teunissen, P.J.G., 2020. GNSS precise point positioning. position, navigation, and timing technologies in the 21st century: integrated satellite navigation. Sensor Syst. Civ. Appl. 1, 503–528. https://doi.org/10.1002/9781119458449.ch20.

Teunissen, P.J.G., Khodabandeh, A., 2015. Review and principles of PPP-RTK methods. J. Geod. 89 (3), 217–240. https://doi.org/10.1007/s00190-014-0771-3.

Verhagen, S., Teunissen, P.J.G., 2013. The ratio test for future GNSS ambiguity resolution. GPS Solut. 17, 535–548. https://doi.org/10.1007/s10291-012-0299-z.

Yi, B., Gu, D., Shao, K., Ju, B., Zhang, H., Qin, X., Duan, X., Huang, Z., 2021. Precise relative orbit determination for Chinese TH-2 satellite formation using onboard GPS and BDS2 observations. Remote Sens. (Basel) 13 (21). https://doi.org/10.3390/rs13214487 4487.

Yi, B., Gu, D., Ju, B., Shao, K., Zhang, H., 2022. Enhanced baseline determination for formation flying LEOs by relative corrections of phase center and code residual variations. Chin. J. Aeronaut. 35 (2), 185–194. https://doi.org/10.1016/j.cja.2021.03.016.

Yunck, T., Bertiger, W., Wu, S., Bar-Sever, Y., Christensen, E., Haines, B., Lichten, S., Muellerschoen, R., Vigue, Y., Willis, P., 1994. First assessment of GPS-based reduced dynamic orbit determination on TOPEX/Poseidon. Geophys. Res. Lett. 21 (7), 541–544. https://doi.org/10.1029/94GL00010.

Zehentner, N., Mayer-Gürr, T., 2016. Precise orbit determination based on raw GPS measurements. J. Geod. 90, 275–286. https://doi.org/10.1007/s00190-015-0872-7.

Zha, J., Zhang, B., Liu, T., Hou, P., 2021. Ionosphere-weighted undifferenced and uncombined PPP-RTK: theoretical models and experimental results. GPS Solut. 25 (4). https://doi.org/10.1007/s10291-021-01169-0 135.

Zhang, B., Chen, Y., Yuan, Y., 2019. PPP-RTK based on undifferenced and uncombined observations: theoretical and practical aspects. J. Geod. 93, 1011–1024. https://doi.org/10.1007/s00190-018-1220-5.

Zhang, H., Gu, D., Ju, B., Shao, K., Yi, B., Duan, X., Huang, Z., 2021. Precise orbit determination and Maneuver assessment for TH-2 satellites using spaceborne GPS and BDS2 observations. Remote Sens. (Basel) 13 (24). https://doi.org/10.3390/rs13245002 5002.

Zhang, B., Teunissen, P.J.G., Odijk, D., 2011. A novel un-differenced PPP-RTK concept. J. Navig. 64 (S1), S180–S191. https://doi.org/10.1017/S0373463311000361.

Zhang, B., Hou, P., Zha, J., Liu, T., 2022. PPP–RTK functional models formulated with undifferenced and uncombined GNSS observations. Satell. Navig. 3 (1). https://doi.org/10.1186/s43020-022-00064-4 3.

Zumberge, J., Heflin, M., Jefferson, D., Watkins, M., Webb, F., 1997. Precise point positioning for the efficient and robust analysis of GPS data from large networks. J. Geophys. Res. Solid Earth 102 (B3), 5005–5017. https://doi.org/10.1029/96JB03860.

7 LEO-Based GNSS Time Transfer Using the UDUC approach

7.1 Introduction

Precise orbit determination (POD) is essential in low-earth orbit (LEO) satellite missions. However, alongside POD, the aspect of timing also assumes a critical role in various LEO satellite missions, as highlighted by researchers (Cacciapuoti and Salomon, 2009; Guo et al., 2022). These missions require accurate timekeeping, such as time stamping of altimetry measurements, synchronization of payloads for formation-flying satellites, and constellation-wide network synchronization (Nie et al., 2007). In addition, precise time information is crucial for LEO satellites serving applications such as remote sensing and communication. Furthermore, accurate information about the orbit and time of LEO satellites is a prerequisite for positioning, navigation, and timing (PNT) services from LEO constellations, which is an active research area.

Spaceborne timing applications present more complex challenges than terrestrial timing applications. Firstly, the high-speed movement of the spaceborne GNSS receiver antenna makes precise timing and real-time POD inseparable. This is because the instantaneous position of LEO satellites, particularly their radial component, is related to the estimable receiver clock offset (Kunzi and Montenbruck, 2022). Addressing the challenge of POD for LEO satellites is discussed in Chapter 6. Secondly, the space environment for LEO satellites is highly complex, which can lead to significant variations in receiver hardware delay. However, the method in Chapter 5 can adequately compensate for the influence of those variations on LEO POD and time synchronization, thus offering a viable solution to this challenge.

This chapter first introduces GNSS time transfer models considering time-varying receiver code biases for LEO satellites. The models used are similar to that presented in Chapter 5. Based on the proposed models, the chapter characterizes the achievable accuracy and precision of real-time GNSS time transfer between LEO satellites that are equipped with external clocks. Furthermore, the potential of LEO-based GNSS time transfer based on time links with the same clock is investigated.

7.2 Full-rank GNSS Time Transfer Model for Spaceborne Applications

In the previous chapters, the various types of rank deficiencies in the UDUC GNSS observations and the *S*-basis chosen to eliminate them are explained in detail. The critical difference between spaceborne and terrestrial applications of the UDUC GNSS lies in whether the tropospheric delay needs to be considered. Consequently, this chapter presents the full-rank GNSS time transfer model of spaceborne applications without the need for further derivation.

If the receiver code biases are assumed to be constant, then the classical UDUC PPP time transfer for LEO satellites, based on Equation (5.2), can be expressed as

$$\begin{aligned} \tilde{\tilde{p}}_{r,j}^{s}(i) &= \tilde{\rho}_{r}^{s}(i) + d\tilde{t}_{r}(i) + \mu_{j}\tilde{I}_{r,j}^{s}(i) - \tilde{d}_{r,j}^{s} + \varepsilon_{p,j}^{s} \\ \tilde{\tilde{\phi}}_{r,j}^{s}(i) &= \tilde{\rho}_{r}^{s}(i) + d\tilde{t}_{r}(i) - \mu_{j}\tilde{I}_{r,j}^{s}(i) - \tilde{\delta}_{r,j}^{s} + \varepsilon_{\phi,j}^{s} \end{aligned} \tag{7.1}$$

where $\tilde{\tilde{p}}_{r,j}^{s}(i) = p_{r,j}^{s}(i) + d\tilde{t}^{s}$ and $\tilde{\tilde{\phi}}_{r,j}^{s}(i) = p_{r,j}^{s}(i) + d\tilde{t}^{s}$ with $d\tilde{t}^{s} = dt^{s} + d_{,IF}^{s}$ the precise satellite clock, respectively. $\tilde{\rho}_{r}^{s}(i)$ is the GNSS-LEO satellite range, which includes the calibrated values for the antenna phase centre offset (PCO) and variations (PCV) for code and phase observations, and the phase wind up for the phase observations. $d\tilde{t}_{r}(i) = dt_{r}(i) + d_{r,IF}$ is the estimable receiver clock offset and $\tilde{I}_{r,j}^{s}(i) = I_{r,j}^{s}(i) + d_{r,GF} - d_{,GF}^{s}$ is the estimable ionospheric delay. The remaining parameters and their meanings are the same to those defined in Equation (5.2).

If the receiver code biases are assumed to be variable, then the full-rank UDUC PPP time transfer model considering time-varying receiver biases for LEO satellites reads,

$$\begin{aligned} \tilde{\tilde{p}}_{r,j}^{s}(i) &= \tilde{\rho}_{r}^{s}(i) + d\tilde{\tilde{t}}_{r}(i) + \tilde{d}_{r,j}(i) + \mu_{j}\tilde{\tilde{I}}_{r,j}^{s}(i) - \tilde{\tilde{d}}_{r,j}^{s} + \varepsilon_{p,j}^{s} \\ \tilde{\tilde{\phi}}_{r,j}^{s}(i) &= \tilde{\rho}_{r}^{s}(i) + d\tilde{\tilde{t}}_{r}(i) - \mu_{j}\tilde{\tilde{I}}_{r,j}^{s}(i) - \tilde{\tilde{\delta}}_{r,j}^{s} + \varepsilon_{\phi,j}^{s} \end{aligned} \tag{7.2}$$

where $\tilde{d}_{r,j}(i) = d_{r,j}(i) - d_{r,j}(1)$ is the variation of receiver code bias with $i \geq 2$. $d\tilde{\tilde{t}}_{r}(i) = dt_{r}(i) + d_{r,IF}(1)$ and $\tilde{\tilde{I}}_{r}^{s}(i) = I_{r}^{s}(i) + d_{r,GF}(1) - d_{,GF}^{s}$ are the estimable receiver clock offset and ionospheric delay, respectively. The remaining parameters and their meanings are the same as in Equation (5.3).

However, as discussed in previous chapters, it should be noted that the concept of IAR is not applicable in Equations (7.1) and (7.2), thereby, making phase observations underutilized. Consequently, to make full use of phase observations and facilitate the study of GNSS time transfer in space, the POD model introduced in Chapter 6 is expanded.

In situations where time-varying receiver code biases are not considered, Equations (4), (5), and (6) from Chapter 6 can be directly utilized for GNSS time transfer for long, medium, and short baselines in space. These models above can cater for both POD and time transfer applications and are therefore referred to as the traditional UDUC POD and time transfer model with DD ambiguity for ionosphere-fixed, -medium, and -float, respectively. However, when considering time-varying receiver code biases, these biases can be estimated within the model employing the methodology proposed in Chapter 5.

When the time-varying receiver code biases are considered, the ionosphere-float UDUC POD and time transfer model with DD ambiguity can be constructed based on Equation (4) in Chapter 6 as follows,

$$\begin{aligned}
\tilde{\tilde{p}}^s_{A,j}(i) &= \tilde{\rho}^s_A(i) + d\tilde{\tilde{t}}_A(i) + \tilde{d}_{A,j}(i) + \mu_j \tilde{\tilde{I}}^s_{A,j}(i) - \tilde{\tilde{d}}^s_{A,j} + \varepsilon^s_{p,j} \\
\tilde{\tilde{\phi}}^s_{A,j}(i) &= \tilde{\rho}^s_A(i) + d\tilde{\tilde{t}}_A(i) - \mu_j \tilde{\tilde{I}}^s_{A,j}(i) - \tilde{\tilde{\delta}}^s_{A,j} + \varepsilon^s_{\phi,j} \\
\tilde{\tilde{p}}^s_{B,j}(i) &= \tilde{\rho}^s_B(i) + d\tilde{\tilde{t}}_B(i) + \tilde{d}_{B,j}(i) + \mu_j \tilde{\tilde{I}}^s_B(i) - \tilde{\tilde{d}}^s_{A,j} + \tilde{\tilde{d}}_{AB,j} + \varepsilon^s_{p,j} \\
\tilde{\tilde{\phi}}^s_{B,j}(i) &= \tilde{\rho}^s_B(i) + d\tilde{\tilde{t}}_B(i) - \mu_j \tilde{\tilde{I}}^s_B(i) - \tilde{\tilde{\delta}}^s_{A,j} + \tilde{\tilde{\delta}}_{AB,j} + \lambda_j N^{1s}_{AB,j} + \varepsilon^s_{\phi,j}
\end{aligned} \tag{7.3}$$

where $\tilde{\tilde{d}}_{AB,j} = d_{B,j}(1) - d_{A,j}(1) - d_{AB,IF}(1) - \mu_j d_{AB,GF}(1)$ is the estimable between-LEO code bias with $j \geq 3$ and $\tilde{\tilde{\delta}}_{AB,j} = \delta_{B,j} - \delta_{A,j} - d_{AB,IF}(1) + \mu_j d_{AB,GF}(1) + \lambda_j N^1_{AB,j}$ is the between-LEO phase bias with $j \geq 1$.

When the time-varying receiver code biases are considered for medium baselines, the ionosphere-weighted UDUC POD and time transfer model with DD ambiguity can be given as follow,

$$\begin{aligned}
\tilde{\tilde{p}}^s_{A,j}(i) &= \tilde{\rho}^s_A(i) + d\tilde{\tilde{t}}_A(i) + \tilde{d}_{A,j}(i) + \mu_j \tilde{\tilde{I}}^s_{A,j}(i) - \tilde{\tilde{d}}^s_{A,j} + \varepsilon^s_{p,j} \\
\tilde{\tilde{\phi}}^s_{A,j}(i) &= \tilde{\rho}^s_A(i) + d\tilde{\tilde{t}}_A(i) - \mu_j \tilde{\tilde{I}}^s_{A,j}(i) - \tilde{\tilde{\delta}}^s_{A,j} + \varepsilon^s_{\phi,j} \\
\tilde{\tilde{p}}^s_{B,j}(i) &= \tilde{\rho}^s_B(i) + d\tilde{\tilde{t}}_B(i) + \tilde{d}_{B,j}(i) + \mu_j \tilde{\tilde{I}}^s_B(i) + \mu_j d_{AB,GF}(1) - \tilde{\tilde{d}}^s_{A,j} + \tilde{\tilde{d}}_{AB,j} + \varepsilon^s_{p,j} \\
\tilde{\tilde{\phi}}^s_{B,j}(i) &= \tilde{\rho}^s_B(i) + d\tilde{\tilde{t}}_B(i) - \mu_j \tilde{\tilde{I}}^s_B(i) - \mu_j d_{AB,GF}(1) - \tilde{\tilde{\delta}}^s_{A,j} + \tilde{\tilde{\delta}}_{AB,j} + \lambda_j N^{1s}_{AB,j} + \varepsilon^s_{\phi,j} \\
\overline{I}^s_{AB}(i) &= I^s_{AB}(i) + \varepsilon^s_{AB}
\end{aligned} \tag{7.4}$$

where $\overline{I}^s_{AB}(i)$ and $I^s_{AB}(i)$ is the between-LEO SD ionospheric delay and its pseudo-observables with ε^s_{AB} the random observation noise. $d_{AB,GF}(1)$ is the LEO between-satellite DCB, which reduces the estimable parameters in the model and thus improves the model strength.

When the time-varying receiver code biases are considered for short baselines, the ionosphere-fixed UDUC POD and time transfer model with DD ambiguity reads,

$$\begin{aligned}
&\tilde{\tilde{p}}^{s}_{A,j}(i) = \tilde{\rho}^{s}_{A}(i) + d\tilde{\tilde{t}}_{A}(i) + \tilde{d}_{A,j}(i) + \mu_j \tilde{\tilde{I}}^{s}_{A,j}(i) - \tilde{\tilde{d}}^{s}_{A,j} + \varepsilon^{s}_{p,j} \\
&\tilde{\tilde{\phi}}^{s}_{A,j}(i) = \tilde{\rho}^{s}_{A}(i) + d\tilde{\tilde{t}}_{A}(i) - \mu_j \tilde{\tilde{I}}^{s}_{A,j}(i) - \tilde{\tilde{\delta}}^{s}_{A,j} + \varepsilon^{s}_{\phi,j} \\
&\tilde{\tilde{p}}^{s}_{B,j}(i) = \tilde{\rho}^{s}_{B}(i) + d\tilde{\tilde{t}}_{B}(i) + \tilde{d}_{B,j}(i) + \mu_j \tilde{\tilde{I}}^{s}_{B}(i) + \mu_j d_{AB,GF}(1) - \tilde{\tilde{d}}^{s}_{A,j} + \tilde{\tilde{d}}_{AB,j} + \varepsilon^{s}_{p,j} \\
&\tilde{\tilde{\phi}}^{s}_{B,j}(i) = \tilde{\rho}^{s}_{B}(i) + d\tilde{\tilde{t}}_{B}(i) - \mu_j \tilde{\tilde{I}}^{s}_{B}(i) - \mu_j d_{AB,GF}(1) - \tilde{\tilde{\delta}}^{s}_{A,j} + \tilde{\tilde{\delta}}_{AB,j} + \lambda_j N^{1s}_{AB,j} + \varepsilon^{s}_{\phi,j}
\end{aligned} \tag{7.5}$$

where the interpretation of the estimated parameters is the same as in Equation (7.4).

7.3 LEO-based GNSS Time Transfer Performance

In this study, the performance evaluation of LEO-based GNSS time transfer is conducted using real LEO data. The dataset used is the same as the one presented in Chapter 6. Specifically, two LEO satellites, T-A and T-B, are equipped with external rubidium clocks with frequency stability of 1×10^{-14}, which serve as a time reference for time synchronization in space.

The study begins by investigating the time transfer performance between T-A and T-B using the ionosphere-fixed UDUC POD and time transfer model with DD ambiguity (refer to Equation 7.5). The short baseline between T-A and T-B allows for accurate modelling of ionospheric effects. The processing strategies used in this phase are consistent with those outlined in Chapter 6 (see Table 2), with the estimation of receiver code bias variations.

Figure 1 presents the time difference results of the T-A/T-B time link, with the mean values subtracted. The time difference falls within a 20 ns range, indicating that the performance of the spaceborne clocks carried by T-A and T-B is inferior to that of the clocks carried by GNSS satellites. The standard deviation of epoch difference for this time link is 2.02 ns.

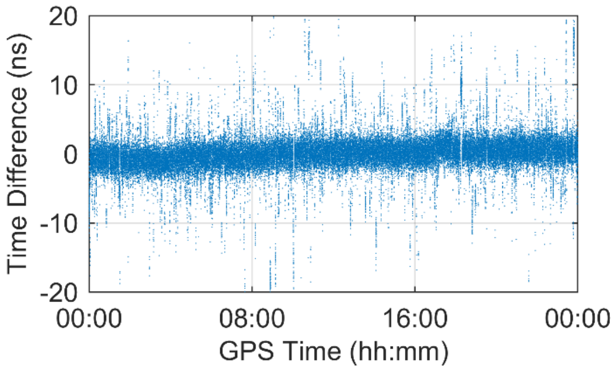

Figure 1 Time difference between the LEO receivers T-A and T-B with different clocks on DOY 248, 2021

Figure 2 displays the MDEV of the time link over a week, allowing for examination of frequency stability. For example, when considering the results at a one-day average time, the

MDEV of the proposed model is 2.21×10^{-14}. This analysis reveals that the performance of LEO-based GNSS time transfer between T-A and T-B is constrained by the quality of the onboard clocks. Consequently, adopting of higher-precision atomic clocks, such as optical clocks with time accuracy reaching the picosecond level along with frequency stability surpassing 1×10^{-18} , offers an inevitable progression to achieve high-precision time synchronization in space.

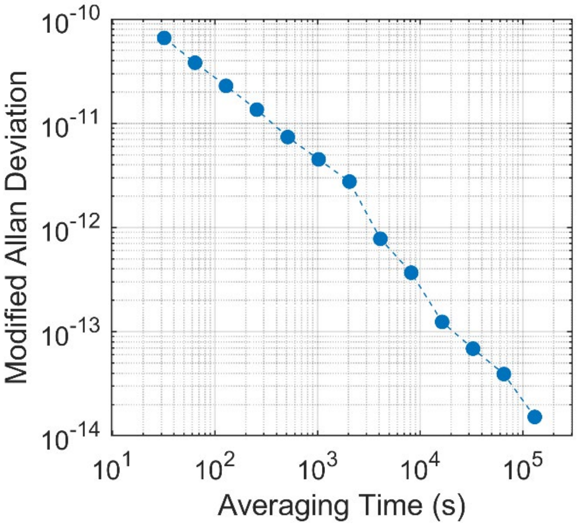

Figure 2 MDEV of the T-A-T-B with the ionosphere-fixed UDUC POD and time transfer model with DD ambiguity

While the results of time transfer between T-A and T-B demonstrate the performance of time synchronization between two LEO satellites, it is essential to recognize that this performance does not represent the upper limit of LEO-based GNSS time transfer in space. The complex space environment requires careful consideration, as conclusions drawn from terrestrial GNSS time transfer cannot be directly extrapolated. Therefore, it is crucial to thoroughly explore the potential performance of space-time reference maintenance using LEO-based GNSS data, especially for future applications in LEO-based Positioning, Navigation, and Timing (PNT) systems.

To investigate the potential of LEO-based GNSS for space-time reference maintenance, a set of GNSS receivers linked to the same atomic clock on the same LEO satellite, which is immune to the performance of the atomic clock is favoured. Fortunately, T-A carries two GNSS receivers (referred to as T-A1 and T-A2) linked to the same rubidium clock with uncertain of 1×10^{-14}, as does T-B (designated as T-B1 and T-B2). The T-A and T-B satellites provide an ideal experimental setup for this purpose. Leveraging the short baselines formed by T-A1/T-

A2 and T-B1/T-B2, the same model and data processing strategy employed in the T-A and T-B experiments are applied.

Figure 3 illustrates the time difference obtained for the short time link T-A1/T-A2 using the proposed model. This time link reflects the potential performance of GNSS time transfer in space-time reference maintenance, as it is linked to the same rubidium clock. The standard deviation of the time difference using the proposed model is 10.67 ps, indicating that GNSS time transfer in space can achieve performance similar to that on the ground when IAR is achieved, and time-varying receiver code bias is accounted for. Furthermore, Figure 4 depicts the MDEV of the time difference for T-A1/T-A2. With the achievement of IAR, the frequency stability of the proposed model reaches 5.2×10^{-17} at an averaging time of one day.

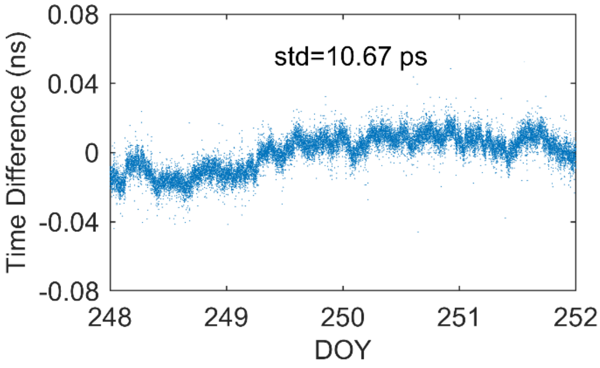

Figure 3 Time difference between the LEO receivers T-A1 and T-A2 with the same clock on DOYs 248-251, 2021

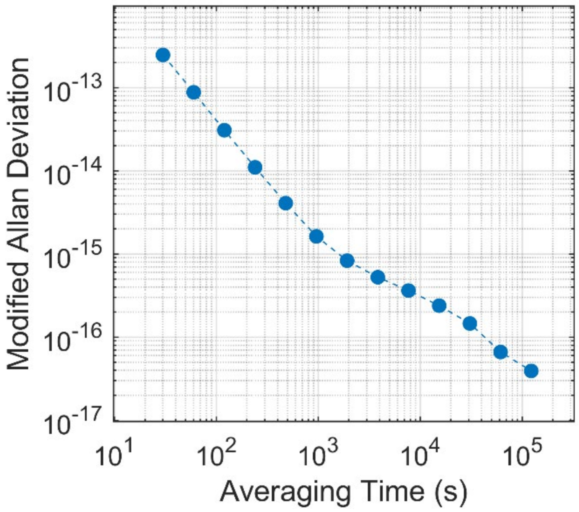

Figure 4 MDEV of the T-A1/T-A2 with the ionosphere-fixed UDUC POD and time transfer model with DD ambiguity

Figures 5 and 6 present analogous results to Figures 3 and 4 but focus on the time link T-B1/T-B2. The result of this time link is better compared with the T-A1/T-A2. The results for this time link are superior compared to T-A1/T-A2. This finding aligns with the results of POD in Chapter 6, as T-B did not experience frequent manoeuvres during this period. When a LEO satellite executes a maneuver, it alters its velocity, thereby potentially inducing a shift in the frequency of the satellite's clock. Consequently, this shift can introduce errors in the time transfer process. The magnitude of these errors is contingent upon various factors, including the nature and duration of the maneuver, as well as the accuracy of the satellite's clock. The standard deviation of the time difference for T-B1/T-B2 is 5.79 ps, confirming that LEO-based GNSS time transfer can achieve picosecond-level accuracy. With the proposed model, the frequency stability of T-B1/T-B2 reaches 3.5×10^{-17} at an averaging time of one day.

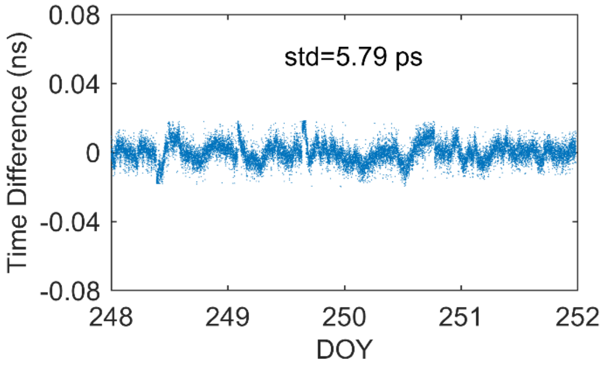

Figure 5 Time difference between the LEO receivers T-B1 and T-B2 with the same clock on DOYs 248-251, 2021

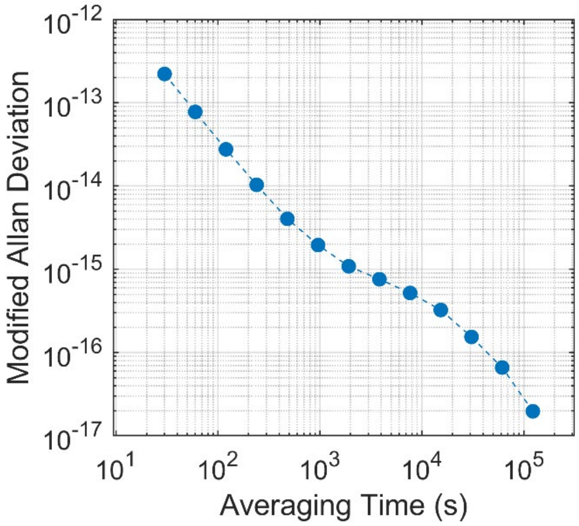

Figure 6 MDEV of the T-B1/T-B2 with the ionosphere-fixed UDUC POD and time transfer model with DD ambiguity

The experiments yield two significant conclusions. Firstly, GNSS enables picosecond-level space-time transfer. Additionally, LEO-based GNSS exhibits the potential for achieving frequency transfer within the sub-10^{-16} range for averaging times within one day.

7.4 Chapter Summary

High-precision time synchronization of LEO satellites is crucial for their space science applications. However, space time transfer applications differ from terrestrial time transfer applications, as they are closely intertwined with POD. In Chapter 6, the challenge of POD has been addressed. However, the space environment imposes limitations on the accuracy and reliability of space time transfer applications compared to their terrestrial counterparts. Based on the previous chapters, this chapter proposes models suitable for LEO POD and time transfer considering IAR and time-varying variations of receiver code bias.

The performance of GNSS time transfer in space is assessed using real data from GNSS receivers on LEO satellites. The experiments affirm that the performance of LEO-based GNSS time transfer is constrained by the capabilities of the clocks carried by LEO satellites. Consequently, the potential of LEO-based GNSS time transfer is explored based on common-clock GNSS receivers on LEO satellites. The experimental results indicate that GNSS onboard LEO satellites could potentially achieve 10^{-17} range frequency transfer once ultra-precise clocks with uncertainty of 1×10^{-18} and beyond become available.

This chapter verifies that LEO-based GNSS can achieve superior frequency stability in space, surpassing 10^{-16}. This achievement is anticipated to be a vital technical support for future space-time reference maintenance. It again underscores the significant advantages of the UDUC approach, IAR, and the consideration of receiver code bias variations for time transfer. However, as mentioned in the introduction, numerous technical challenges still require resolution in practice. These challenges necessitate further investigation into the maintenance of space-time reference in the future.

8 Conclusions and Recommendations

8.1 Summary of the Thesis Outcomes

Time transfer (synchronization) is a critical aspect of scientific research and industrial applications. GNSS has emerged as a competitive method for time transfer due to its high accuracy and cost-effectiveness. However, the advent of high-precision optical clocks (Fortier and Baumann, 2019) with time accuracy reaching the picosecond level along with frequency stability surpassing 1×10^{-18} has raised the bar for the accuracy and reliability of time transfer techniques, necessitating improvements in GNSS models and algorithms to maintain GNSS's leading position in time transfer.

The thesis investigates the limitations of current GNSS time transfer techniques and proposes viable solutions. Firstly, classical GNSS time transfer relies on the IF combination and dual-frequency observations, which lack flexibility in multi-frequency scenarios. Secondly, traditional GNSS time transfer methods do not achieve IAR, which diminishes the significance of phase observations. Although IPPP with IAR has been introduced, it is still constrained by the drawbacks of the IF combination. Thirdly, external precise satellite clock products are usually required for time transfer, which introduces dependencies on these products. However, the impact of satellite clock products on time transfer and methods to mitigate this impact have not been explored. Lastly, the estimable receiver clock assumes the receiver code bias to be time-invariant, yet significant time variations in the receiver code bias may exist and requires proper modelling and treatment.

To address these limitations, the thesis proposes using the UDUC approach, which offers a promising method for multi-frequency multi-constellation GNSS time transfer. By leveraging the UDUC approach, IAR is achieved by constructing of integer estimable phase DD ambiguities, aided by common-view satellites. The thesis presents UDUC GNSS time transfer models with IAR for short, medium, and long baselines, accounting for ionospheric delays under different baseline conditions. The proposed models demonstrate improved frequency stability compared to traditional UDUC PPP, ranging from 25% to 60% and 9% to 30% for short and medium baselines, respectively. Furthermore, the proposed model shows 10% to 25% greater stability than UDUC PPP for averaging times exceeding one day in long-baseline scenarios.

The thesis also addresses the limitations related to the accuracy of precise satellite clock products. While these products' accuracy surpasses that of existing microwave atomic clocks, they must be considered when using high-precision optical clocks. To mitigate their impact, the thesis proposes a UDUC model with IAR and satellite clocks estimated, eliminating the influence of the external precise satellite clock products. The proposed model exhibits a 10% to 40% improvement over the model with satellite clocks estimated. Moreover, the thesis demonstrates the potential for GPS, Galileo, and BDS-3 to achieve frequency transfer in the low-mid10^{-17} range for averaging times within one day.

The IF receiver code bias is always included in the estimable receiver clock and should be calibrated beforehand. Thus, the implementation of GNSS time transfer relies on the time-invariant assumption of the IF receiver code bias. However, in practice, this is not the case. The time variations of different types of between-receiver biases are confirmed based on short baselines in this thesis. This drives the consideration of time-varying receiver code biases in the time transfer. To compensate for the influence of receiver code biases on GNSS time transfer, the TVRCB model has been proposed in this thesis, in which the variations of receiver code bias relative to the first epoch can be estimated by selecting an additional *S*-basis. Experiments based on the TVRCB model show that the receiver bias of a single receiver may have noticeable time-varying variations and the time variations are related to frequency. The influence of time-varying receiver code biases on GNSS time transfer can be effectively accounted for using the TVRCB model, and long-term frequency stability can be improved by 20%-50%.

Onboard time synchronization is an essential requirement for LEO missions and their applications. For GNSS-based time synchronization, the POD of the satellites needs to be performed, and ultimately, the quality of the POD determines the timing accuracy achievable from GNSS measurements. The current mainstream POD method is based on IF PPP, so it is limited by the disadvantages of the IF combination. In addition, absolute and relative POD are usually performed separately in a LEO constellation, which significantly reduces data processing efficiency. Considering the above drawbacks, the UDUC GNSS POD model with DD ambiguity has been proposed in this thesis, which can be compatible with absolute and relative POD requirements. The proposed model presented a consistency of 2.8–3.8 cm in 3D in absolute POD mode and showed a consistency with the reference orbits of 1.1–1.5 mm in the relative POD model, which can provide a high-precision orbit for time synchronization.

Unlike terrestrial timing applications that benefit from the static position of the receiving GNSS antenna, spaceborne time synchronization is closely related to real-time kinematic POD. Due to the complexity of the space environment, spaceborne timing applications face more complex challenges than ground timing applications. Although the problem of POD is appropriately solved by the method proposed in this thesis, the complexity of the space environment also determines that the conclusion from terrestrial timing is difficult to apply directly for spaceborne timing. The performance of spaceborne GNSS time transfer is explored in this thesis using the UDUC method, and considering IAR, satellite clock synchronization estimation, and time-varying receiver code biases. The experimental results show that GNSS onboard LEO satellites could potentially achieve sub-10^{-16} range frequency transfer, providing a preliminary verification for establishing LEO-based space-time reference in the future.

8.2 Recommendations and Future Work

The thesis highlights the potential of GNSS in achieving picosecond time transfer and sub-10^{-16} frequency transfer. However, there are still challenges that need to be addressed to achieve global time synchronization and maintain time references.

For terrestrial timing applications, it is essential to incorporate high-precision atmospheric delay corrections to enable fast IAR. One possible solution is to generate these corrections either network-wide or partition-wise. Furthermore, expanding the non-common-view model is crucial for terrestrial timing applications, particularly under long-baseline conditions where the number of common-view satellites is limited. To achieve the generation of GNSS satellite clock products with picosecond-scale accuracy, it is highly recommended to employ a GNSS receiver network equipped with optical clocks. Moreover, it is advisable to extend the UDUC model to encompass multi-frequency multi-constellation scenarios, with a specific emphasis on investigating inter-system biases (ISB) for the fusion of multiple constellations.

In spaceborne timing applications, it is necessary to address the challenges faced in terrestrial timing as a prerequisite, but further research is still needed. Firstly, understanding the factors that drive variations in receiver code biases and analysing them in different LEO missions would provide valuable insights. Secondly, investigating the synchronization estimation of precise orbits and timing, as well as studying their interplay, is recommended. Thirdly, exploring the potential of using multiple antennas on LEO satellites for real-time attitude determination, orbit determination, and time synchronization is worth investigating. Lastly, it is crucial to explore the GNSS time transfer performance of LEO constellations and assess the feasibility of using GNSS for maintaining space-time references in future LEO PNT applications.

When the orbit and time synchronization of LEO constellations are accurately determined, applying these findings to PNT applications becomes a significant concern. Research on effectively combining LEO satellites with GNSS to serve high-precision PNT will be a crucial area of focus in future space science. Designing signal systems, models, and algorithms aligned with LEO satellites will be critical areas of investigation in subsequent research.

References

This Chapter provides the references for Chapters 1, 5, and 7 only. The additional references for Chapters 2-4, 6 are listed at the end of the enclosed papers.

Adhikari, P., Hooshyar, H., Fitsik, R., Vanfretti, L. (2021). Precision timing and communication networking experiments in a real-time power grid hardware-in-the-loop laboratory. Sustainable Energy Grids & Networks, 28, 100549. https://doi.org/10.1016/j.segan.2021.100549.

Allahvirdi-Zadeh, A., Wang, K., El-Mowafy, A. (2021). POD of small LEO satellites based on precise real-time MADOCA and SBAS-aided PPP corrections. GPS Solutions, 25, 1-14. https://doi.org/10.1007/s10291-020-01078-8.

Allan, D., Weiss, M. (1980). Accurate time and frequency transfer during common-view of a GPS satellite. In: 34th Annual Symposium on Frequency Control, 334-346. https://doi.org/10.1109/FREQ.1980.200424.

Arms, S., Galbreath, J., Townsend, C., Churchill, D., Corneau, B., Ketcham, R., Phan, N. (2009). Energy Harvesting Wireless Sensors and Networked Timing Synchronization for Aircraft Structural Health Monitoring. In: 2009 1st International Conference on Wireless Communication, Vehicular Technology, Information Theory and Aerospace & Electronic Systems Technology, 16-20. https://doi.org/10.1109/Wirelessvitae.2009.5172414.

Bruyninx, C., Defraigne, P., Sleewaegen, J. (1999). Time and Frequency Transfer Using GPS Codes and Carrier Phases: Onsite Experiments. GPS Solutions, 3, 1-10. https://doi.org/10.1007/Pl00012772.

Cacciapuoti, L., Salomon, C. (2009). Space clocks and fundamental tests: The ACES experiment. European Physical Journal-Special Topics, 172, 57-68. https://doi.org/10.1140/epjst/e2009-01041-7.

Chen, Y., Yuan, Y., Zhang, B., Liu, T., Ding, W., Ai, Q. (2018). A modified mix-differenced approach for estimating multi-GNSS real-time satellite clock offsets. GPS Solutions, 22, 1-10. https://doi.org/10.1007/s10291-018-0739-5.

Chou, C., Hume, D., Rosenband, T., Wineland, D. (2010). Optical Clocks and Relativity. Science, 329, 1630-1633. https://doi.org/10.1126/science.1192720.

Cliche, J., Shillue, B. (2006). Precision timing control for radioastronomy - Maintaining femtosecond synchronization in the atacama large millimeter array. IEEE Control Systems Magazine, 26, 19-26. https://doi.org/10.1109/Mcs.2006.1580149.

Collins, P. (2008). Isolating and Estimating Undifferenced GPS Integer Ambiguities. In: Proceedings of the 2008 National Technical Meeting of the Institute of Navigation, 720-732.

Defraigne, P., Aerts, W., Harmegnies, A., Petit, G., Rovera, D., Uhrich, P. (2013). Advances in Multi-GNSS Time Transfer. In: 2013 Joint European Frequency and Time Forum & International Frequency Control Symposium (EFTF/IFCS), 508-512. https://doi.org/10.1109/EFTF-IFC.2013.6702126.

Defraigne, P., Petit, G. (2003). Time transfer to TAI using geodetic receivers. Metrologia, 40, 184-188. https://doi.org/10.1088/0026-1394/40/4/307.

Defraigne, P., Petit, G. (2015). CGGTTS-Version 2E: an extended standard for GNSS Time Transfer. Metrologia, 52, G1. https://doi.org/10.1088/0026-1394/52/6/G1.

Defraigne, P., Pinat, E., Bertrand, B., Uhrich, P., Chupin, B., Riedel, F. (2021). Stability of Hardware Delays of GNSS Signals. In: 2021 Joint Conference of the European Frequency and Time Forum and IEEE International Frequency Control Symposium (EFTF/IFCS), 1-5. https://doi.org/10.1109/EFTF/IFCS52194.2021.9604324.

Esteban, H., Palacio, J., Galindo, F., Feldmann, T., Bauch, A., Piester, D. (2010). Improved GPS-Based Time Link Calibration Involving ROA and PTB. IEEE Transactions on Ultrasonics Ferroelectrics and Frequency Control, 57, 714-720. https://doi.org/10.1109/Tuffc.2010.1469.

Fortier, T., & Baumann, E. (2019). 20 years of developments in optical frequency comb technology and applications. Communications Physics, 2(1), 153. https://doi.org/10.1038/s42005-019-0249-y.

Ge, M., Gendt, G., Rothacher, M., Shi, C., Liu, J. (2008). Resolution of GPS carrier-phase ambiguities in Precise Point Positioning (PPP) with daily observations. Journal of Geodesy, 82, 389-399. https://doi.org/10.1007/s00190-007-0187-4.

Guo, J., Geng, J. (2018). GPS satellite clock determination in case of inter-frequency clock biases for triple-frequency precise point positioning. Journal of Geodesy, 92, 1133-1142. https://doi.org/10.1007/s00190-017-1106-y.

Guo, Y., Gao, S., Bai, Y., Pan, Z., Liu, Y., Lu, X., Zhang, S. (2022). A New Space-to-Ground Microwave-Based Two-Way Time Synchronization Method for Next-Generation Space Atomic Clocks. Remote Sensing, 14, 528. https://doi.org/10.3390/rs14030528.

Hadas, T., Teferle, F., Kazmierski, K., Hordyniec, P., Bosy, J. (2017). Optimum stochastic modeling for GNSS tropospheric delay estimation in real-time. GPS Solutions, 21, 1069-1081. https://doi.org/10.1007/s10291-016-0595-0.

Huang, G., Zhang, Q., Xu, G. (2014). Real-time clock offset prediction with an improved model. GPS Solutions, 18, 95-104. https://doi.org/10.1007/s10291-013-0313-0.

Jiang, Z. (2008). Towards a TWSTFT network time transfer. Metrologia, 45, S6-S11. https://doi.org/10.1088/0026-1394/45/6/S02.

Khodabandeh, A., Teunissen, P. (2016). PPP-RTK and inter-system biases: the ISB look-up table as a means to support multi-system PPP-RTK. Journal of Geodesy, 90, 837-851. https://doi.org/10.1007/s00190-016-0914-9.

Kodet, J., Panek, P., Prochazka, I. (2016). Two-way time transfer via optical fiber providing subpicosecond precision and high temperature stability. Metrologia, 53, 18-26. https://doi.org/10.1088/0026-1394/53/1/18.

Kunzi, F., Montenbruck, O. (2022). Precise Onboard Time Synchronization for LEO Satellites. NAVIGATION: Journal of the Institute of Navigation, 69. https://doi.org/10.33012/navi.531.

Lannes, A., Prieur, J. (2013). Calibration of the clock-phase biases of GNSS networks: the closure-ambiguity approach. Journal of Geodesy, 87, 709-731. https://doi.org/10.1007/s00190-013-0641-4.

Larson, K., Levine, J. (1999). Carrier-phase time transfer. IEEE Transactions on Ultrasonics Ferroelectrics and Frequency Control, 46, 1001-1012. https://doi.org/10.1109/58.775667.

Laurichesse, D., Mercier, F., BERTHIAS, J., Broca, P., Cerri, L. (2009). Integer ambiguity resolution on undifferenced GPS phase measurements and its application to PPP and satellite precise orbit determination. Navigation, 56, 135-149. https://doi.org/10.1002/j.2161-4296.2009.tb01750.x

Leandro, R., Langley, R., Santos, M. (2008). UNB3m_pack: a neutral atmosphere delay package for radiometric space techniques. GPS Solutions, 12, 65-70. https://doi.org/10.1007/s10291-007-0077-5.

Lee, S., Schutz, B., Lee, C., Yang, S. (2008). A study on the Common-View and All-in-View GPS time transfer using carrier-phase measurements. Metrologia, 45, 156-167. https://doi.org/10.1088/0026-1394/45/2/005.

Lesage, P., Ayi, T. (1984). Characterization of frequency stability: analysis of the modified Allan variance and properties of its estimate. IEEE transactions on instrumentation and measurement, 33, 332-336. https://doi.org/10.1109/TIM.1984.4315235.

Leute, J. (2018). Characterization and evaluation of GPS PPP techniques for optical clock comparisons. Doctoral dissertation, Leibniz University Hannover. https://doi.org/10.15488/3301.

Levine, J. (2008). A review of time and frequency transfer methods. Metrologia, 45, S162-S174. https://doi.org/10.1088/0026-1394/45/6/S22.

Lewandowski, W., Petit, G., Thomas, C. (1993). Precision and Accuracy of GPS Time Transfer. IEEE Transactions on Instrumentation and Measurement, 42, 474-479. https://doi.org/10.1109/19.278607.

Lewandowski, W., Weiss, M., Davis, D. (1987). A Calibration of GPS Equipment at Time and Frequency Standards Laboratories in the USA and Europe. Metrologia, 24, 181-186. https://doi.org/10.1088/0026-1394/24/4/005.

Li, B., Ge, H., Ge, M., Nie, L., Shen, Y., Schuh, H. (2019a). LEO enhanced Global Navigation Satellite System (LeGNSS) for real-time precise positioning services. Advances in Space Research, 63, 73-93. https://doi.org/10.1016/j.asr.2018.08.017.

Li, X., Ma, F., Li, X., Lv, H., Bian, L., Jiang, Z., Zhang, X. (2019b). LEO constellation-augmented multi-GNSS for rapid PPP convergence. Journal of Geodesy, 93, 749-764. https://doi.org/10.1007/s00190-018-1195-2.

Liu, T., Zhang, B. (2021) Estimation of code observation-specific biases (OSBs) for the modernized multi-frequency and multi-GNSS signals: an undifferenced and uncombined approach. Journal of Geodesy, 95, 1–20. https://doi.org/10.1007/s00190-021-01549-x.

Lisdat, C., Grosche, G., Quintin, N., Shi, C., Raupach, S., Grebing, C., Nicolodi, D., Stefani, F., Al-Masoudi, A., Dorscher, S., Hafner, S., Robyr, J., Chiodo, N., Bilicki, S., Bookjans, E., Koczwara, A., Koke, S., Kuhl, A., Wiotte, F., Meynadier, F., Camisard, E., Abgrall, M., Lours, M., Legero, T., Schnatz, H., Sterr, U., Denker, H., Chardonnet, C., Le Coq, Y., Santarelli, G., Amy-Klein, A., Le Targat, R., Lodewyck, J., Lopez, O., Pottie, P. (2016). A clock network for geodesy and fundamental science. Nature Communications, 7, 12443. https://doi.org/10.1038/ncomms12443.

Mi, X., Sheng, C., El-Mowafy, A., Zhang, B. (2021). Characteristics of receiver-related biases between BDS-3 and BDS-2 for five frequencies including inter-system biases, differential code biases, and differential phase biases. GPS Solutions, 25, 113. https://doi.org/10.1007/s10291-021-01151-w.

Mi, X., Zhang, B., El-Mowafy, A., Wang, K., Yuan, Y. (2023). Undifferenced and uncombined GNSS time and frequency transfer with integer ambiguity resolution. Journal of Geodesy*,* 97, 13. https://doi.org/10.1007/s00190-022-01689-8.

Mi, X., Zhang, B., Odolinski, R., Yuan, Y. (2020). On the temperature sensitivity of multi-GNSS intra- and inter-system biases and the impact on RTK positioning. GPS Solutions*,* 24, 1-14. https://doi.org/10.1007/s10291-020-01027-5.

Montenbruck, O., Garcia-Fernandez, M., Yoon, Y., Schon, S., Jaggi, A. (2009). Antenna phase center calibration for precise positioning of LEO satellites. GPS Solutions*,* 13, 23-34. https://doi.org/10.1007/s10291-008-0094-z.

Montenbruck, O., Hackel, S., van den Ijssel, J., Arnold, D. (2018). Reduced dynamic and kinematic precise orbit determination for the Swarm mission from 4 years of GPS tracking. GPS Solutions*,* 22, 79. https://doi.org/10.1007/s10291-018-0746-6.

Nie, G., Wu, F., Zhang, K., Zhu, B. (2007). Research on LEO satellites time synchronization with GPS receivers onboard. In: 2007 IEEE International Frequency Control Symposium-Jointly with the 21st European Frequency and Time Forum, 896-900. https://doi.org/10.1109/FREQ.2007.4319208.

Nussbaumer, H. (1982). The Fast Fourier Transform. In: Fast Fourier Transform and Convolution Algorithms. Springer Series in Information Sciences, vol 2. Springer, Berlin, Heidelberg. https://doi.org/10.1007/978-3-642-81897-4_4.

Odijk, D., Zhang, B., Khodabandeh, A., Odolinski, R., Teunissen, P. (2016). On the estimability of parameters in undifferenced, uncombined GNSS network and PPP-RTK user models by means of *S*-system theory. Journal of Geodesy*,* 90, 15-44. https://doi.org/10.1007/s00190-015-0854-9.

Overney, F., Schildknecht, T., Beutler, G., Prost, L., Feller, U. (1997). GPS time transfer using geodetic receivers: Middle-term stability and temperature dependence of the signal delays. In: 11th European Frequency and Time Forum, 504-508.

Petit, G., Defraigne, P. (2023). Calibration of GNSS stations for UTC. Metrologia*,* 60, 025009. https://doi.org/10.1088/1681-7575/acbd52.

Petit, G., Jiang, Z. (2008). GPS all in view time transfer for TAI computation. Metrologia*,* 45, 35-45. https://doi.org/10.1088/0026-1394/45/1/006.

Petit, G., Kanj, A., Harmegnies, A., Loyer, S., Delporte, J., Mercier, F., Perosanz, F. (2014). GPS frequency transfer with IPPP. In: 2014 European Frequency and Time Forum (EFTF), 451-454. https://doi.org/10.1109/EFTF.2014.7331533.

Petit, G., Leute, J., Loyer, S., Perosanz, F. (2017). Sub 10(-16) frequency transfer with IPPP: Recent results. In: 2017 Joint Conference of the European Frequency and Time Forum and IEEE International Frequency Control Symposium (EFTF/IFCS), 784-787. https://doi.org/10.1109/FCS.2017.8089035.

Petit, G., Meynadier, F., Harmegnies, A., Parra, C. (2022). Continuous IPPP links for UTC. Metrologia, 59, 045007. https://doi.org/10.1088/1681-7575/ac7687.

Piester, D., Bauch, A., Breakiron, L., Matsakis, D., Blanzano, B., Koudelka, O. (2008). Time transfer with nanosecond accuracy for the realization of International Atomic Time. Metrologia, 45, 185-198. https://doi.org/10.1088/0026-1394/45/2/008.

Plumb, J., Larson, K., White, J., Powers, E. (2005). Absolute calibration of a geodetic time transfer system. IEEE Transactions on Ultrasonics Ferroelectrics and Frequency Control, 52, 1904-1911. https://doi.org/10.1109/Tuffc.2005.1561658.

Ray, J., Senior, K. (2001). Temperature sensitivity of timing measurements using Dorne Margolin antennas. GPS Solutions, 5, 24-30. https://doi.org/10.1007/PL00012873.

Rieck, C., Jarlemark, P., Jaldehag, K., Johansson, J. (2003). Thermal influence on the receiver chain of GPS carrier phase equipment for time and frequency transfer. In: Proceedings of the 2003 IEEE International Frequency Control Symposium & PDA Exhibition Jointly with 17th European Frequency and Time Forum, 326-331. https://doi.org/10.1109/FREQ.2003.1275110.

Riley, W. (2008). Handbook of Frequency Stability Analysis, NIST Special Publications. https://safe.nrao.edu/wiki/pub/Main/ToddHunter/nist1065.pdf.

Samain, E., Vrancken, P., Guillemot, P., Fridelance, P., Exertier, P. (2014). Time transfer by laser link (T2L2): characterization and calibration of the flight instrument. Metrologia, 51, 503-515. https://doi.org/10.1088/0026-1394/51/5/503.

Shen, Y., Li, B., Xu, G. (2009). Simplified equivalent multiple baseline solutions with elevation-dependent weights. GPS Solutions, 13, 165-171. https://doi.org/10.1007/s10291-008-0109-9.

Shi, C., Guo, S., Gu, S., Yang, X., Gong, X., Deng, Z., Ge, M., Schuh, H. (2019). Multi-GNSS satellite clock estimation constrained with oscillator noise model in the existence of data discontinuity. Journal of Geodesy, 93, 515-528. https://doi.org/10.1007/s00190-018-1178-3.

Teunissen, P. (1985). Zero Order Design: Generalized Inverses, Adjustment, the Datum Problem and S-Transformations. In: Grafarend, E.W., Sansò, F. (eds) Optimization and

Design of Geodetic Networks. Springer, Berlin, Heidelberg. https://doi.org/10.1007/978-3-642-70659-2_3.

Teunissen, P. (2018). Distributional theory for the DIA method. Journal of Geodesy*,* 92, 59-80. https://doi.org/10.1007/s00190-017-1045-7.

Tu, R., Zhang, P., Zhang, R., Liu, J., Lu, X. (2019). Modeling and performance analysis of precise time transfer based on BDS triple-frequency un-combined observations. Journal of Geodesy*,* 93, 837-847. https://doi.org/10.1007/s00190-018-1206-3.

Zhang, V., Parker, T., Yao, J. (2015). Long-Term Uncertainty in Time Transfer Using GPS and TWSTFT Techniques. In: 2015 Joint Conference of the IEEE International Frequency Control Symposium & the European Frequency and Time Forum, 723-727. https://doi.org/10.1109/FCS.2015.7138943.

Appendix A: Copyright Permission Statements

I have obtained, where necessary, permission from the copyright owners to use any third-party copyright material reproduced in the thesis or to use any of my own published work (e.g., journal articles) in which the copyright is held by another party (e.g., publisher, co-author). The permissions are all provided below.

Xiaolong Mi

The following paper is published in **Journal of Geodesy** under the open access license provided below. The CC BY license allows me, as the author, to retain the copyright while licensing the use of the paper to Springer as the publisher. Others may use the paper's content, either in full or in part, without seeking permission from the Springer or the author, provided that proper attribution is given to the original author.

- **Mi, X.**, Zhang, B., El-Mowafy, A., Wang, K., & Yuan, Y. (2023). Undifferenced and uncombined GNSS time and frequency transfer with integer ambiguity resolution. Journal of Geodesy, 97(2), 13. https://doi.org/10.1007/s00190-022-01689-8

Attribution:

The following papers are published in **GPS Solutions** under the open access license provided below. The CC BY license allows me, as the author, to retain the copyright while licensing the use of the papers to Springer as the publisher. Others may use the paper's content, either in full or in part, without seeking permission from the Springer or the author, provided that proper attribution is given to the original author.

- **Mi, X.**, Zhang, B., El-Mowafy, A., Wang, K., & Yuan, Y. (2023). On the potential of undifferenced and uncombined GNSS time and frequency transfer with integer ambiguity resolution and satellite clocks estimated. GPS Solutions, 27(1), 25. https://doi.org/10.1007/s10291-022-01363-8
- **Mi, X.**, Sheng, C., El-Mowafy, A., & Zhang, B. (2021). Characteristics of receiver-related biases between BDS-3 and BDS-2 for five frequencies including inter-system biases, differential code biases, and differential phase biases. GPS Solutions, 25(3), 113. https://doi.org/10.1007/s10291-021-01151-w

Attribution:

The following paper is published in **Advances in Space Research** under the open access license provided below. The CC BY license allows me, as the author, to retain the copyright while licensing the use of the paper to Elsevier as the publisher. Others may use the paper's content, either in full or in part, without seeking permission from the Elsevier or the author, provided that proper attribution is given to the original author.

- **Mi, X.,** Allahvirdi-Zadeh, A., El-Mowafy, A., Huang, Z., Wang, K., Zhang, B., & Yuan, Y. (2023). Absolute and relative POD of LEO satellites in formation flying: Undifferenced and uncombined approach. Advances in Space Research, 72(4), 1070-1080. https://doi.org/10.1016/j.asr.2023.05.024

Attribution:

Appendix B: Statement of Contributions by Co-Authors

This thesis presents 4 first-author papers that are published in journals. The authors' contributions to these papers are provided in this appendix.

I, Xiaolong Mi, collaborated with Prof. Baocheng Zhang and Prof. Ahmed El-Mowafy to conceive and develop the ideas presented in the following paper. As the first author, I took responsibility for drafting the manuscript, deriving the analytical expressions, and providing the numerical results. In the case of co-authorship, Prof. Kan Wang, and Prof. Yunbin Yuan provided their comments to improve the manuscripts for submission. Mi, X., Zhang, B., El-Mowafy, A., Wang, K., & Yuan, Y. (2023). Undifferenced and uncombined GNSS time and frequency transfer with integer ambiguity resolution. Journal of Geodesy, 97(2), 13. https://doi.org/10.1007/s00190-022-01689-8

Xiaolong Mi ________________________________

I, as a Co-Author, endorse that this level of contributions by the candidate indicated above is appropriate.

Baocheng Zhang ________________________________

Ahmed El-Mowafy ________________________________

Kan Wang ________________________________

Yunbin Yuan ________________________________

I, Xiaolong Mi, proposed the ideas presented of the following paper with Professor Baocheng Zhang, with guidance from Prof. Ahmed El-Mowafy. As the first author, I took responsibility for drafting the manuscript, deriving the analytical expressions, and providing the numerical results. In the case of co-authorship, Prof. Ahmed El-Mowafy, Prof. Kan Wang, and Prof. Yunbin Yuan provided their comments to improve the manuscripts for submission. Mi, X., Zhang, B., El-Mowafy, A., Wang, K., & Yuan, Y. (2023). On the potential of undifferenced and uncombined GNSS time and frequency transfer with integer ambiguity resolution and satellite clocks estimated. GPS Solutions, 27(1), 25. https://doi.org/10.1007/s10291-022-01363-8

Xiaolong Mi ________________________________

I, as a Co-Author, endorse that this level of contributions by the candidate indicated above is appropriate.

Baocheng Zhang ________________________________

Ahmed El-Mowafy ________________________________

Kan Wang ________________________________

Yunbin Yuan ________________________________

For the following paper, I, Xiaolong Mi, designed the work by consulting Prof. Baocheng Zhang and Prof. Ahmed El-Mowafy. I processed the data and analysed the results and wrote the manuscript. Dr. Chuanzhen Sheng provided his comments to improve the manuscripts for submission. Mi, X., Sheng, C., El-Mowafy, A., & Zhang, B. (2021). Characteristics of receiver-related biases between BDS-3 and BDS-2 for five frequencies including inter-system biases, differential code biases, and differential phase biases. GPS Solutions, 25(3), 113. https://doi.org/10.1007/s10291-021-01151-w

Xiaolong Mi ______________________________

I, as a Co-Author, endorse that this level of contributions by the candidate indicated above is appropriate.

Chuanzhen Sheng ______________________________

Ahmed El-Mowafy ______________________________

Baocheng Zhang ______________________________

For the following paper, I, Xiaolong Mi, designed the work by consulting Prof. Ahmed El-Mowafy and Prof. Baocheng Zhang. I processed the and analysed the results and wrote the manuscript. Dr. Amir Allahvirdizadeh, Mr. Zhiyong Huang and Prof. Yunbin Yuan provided their comments to improve the manuscripts for submission. Mi, X., Allahvirdi-Zadeh, A., El-Mowafy, A., Huang, Z., Wang, K., Zhang, B., & Yuan, Y. (2023). Absolute and relative POD of LEO satellites in formation flying: Undifferenced and uncombined approach. Advances in Space Research, 72(4), 1070-1080. https://doi.org/10.1016/j.asr.2023.05.024

Xiaolong Mi ____

I, as a Co-Author, endorse that this level of contributions by the candidate indicated above is appropriate.

Amir Allahvirdizadeh ____

Ahmed El-Mowafy ____

Zhiyong Huang ____

Kan Wang ____

Baocheng Zhang ____

Yunbin Yuan ____